Play nice or pay the price

How local interactions shape a microbial community

Los, R.

DOI
10.4233/uuid:d42917bf-d1c0-4294-935e-2fba8b9c5cf6

Publication date
2025

Document Version
Final published version

Citation (APA)
Los, R. (2025). *Play nice or pay the price: How local interactions shape a microbial community*. [Dissertation (TU Delft), Delft University of Technology]. https://doi.org/10.4233/uuid:d42917bf-d1c0-4294-935e-2fba8b9c5cf6

Important note
To cite this publication, please use the final published version (if applicable).
Please check the document version above.

PLAY NICE OR PAY THE PRICE

HOW LOCAL INTERACTIONS SHAPE A MICROBIAL COMMUNITY

PLAY NICE OR PAY THE PRICE

HOW LOCAL INTERACTIONS SHAPE A MICROBIAL COMMUNITY

Dissertation

for the purpose of obtaining the degree of doctor,
at Delft University of Technology,
by the authority of the Rector Magnificus prof. dr. ir. T.H.J.J. van der Hagen,
chair of the Board for Doctorates,
to be defended publicly on,
Friday 10 January 2025 at 15:00 o'clock

by

Rachel LOS

Master of Science in Nanobioloby, Erasmus Medical Centre & Delft University of Technology, born in Utrecht, Nederland.

This dissertation has been approved by the promotors.

Composition of the doctoral committee:

Rector Magnificus,	voorzitter
Dr. T. Idema,	Technische Universiteit Delft, promotor
Dr. S.M. Depken,	Technische Universiteit Delft, copromotor

Independent members:

Prof. Dr. S.J. Tans	Technische Universiteit Delft
Prof. Dr. K. Drescher	University of Basel
Dr. S. Jabbari Farouji	University of Amsterdam
Dr. B.P. Tighe	Technische Universiteit Delft
Prof. Dr. S.J.J. Brouns	Technische Universiteit Delft, reserve member

Other members:

Dr. R.J. van Tatenhove-Pel
Technische Universiteit Delft

Keywords: microbial communities, cross-feeding, individual-based simulations, metabolic interactions, costly cooperation

Printed by: Gildeprint

Front & Back: Ink prints by Rachel Los

Casimir PhD Series, Delft-Leiden 2025

ISBN 978-94-6496-317-5

An electronic version of this dissertation is available at
http://repository.tudelft.nl/.

CONTENTS

SUMMARY

Microorganisms often live in dense, surface-attached communities called biofilms. These biofilms exist in diverse environments, from the inside of your gut and the surfaces of your teeth, to the roots of your house plants and the inside of your coffee machine. These biofilms, composed of various bacteria, fungi, and viruses encased in a self-produced extracellular matrix, exhibit complex behaviours. They also play a dual role in human health and industry, contributing to persistent infections and antibiotic resistance while being crucial for digestion and industrial applications like wastewater treatment. Understanding biofilm formation and function is essential for decreasing their detrimental effects and increasing their potential in biotechnology.

In this thesis, I use individual-based modelling of spherocylindrical particles to learn something about the effects of spatial structure on their mechanical and social interactions.

In **chapter 2** we explore the aggregation dynamics of blue-light switchable adhesive *E. coli* in solution. We aim to understand experimental results that bacteria aggregate more and formed bigger clusters under pulsating light. We simulate a system of particles undergoing Brownian motion, where the cell-cell adhesion can be periodically turned on and off and compare and match our simulations to the experimental data. We show how tuning the light off-period to the decay time of the adhesion leads to increased clustering. We conclude that partial disassembly of the aggregates leads to more effective clustering. In addition, our co-authors show that this increased clustering leads to increased biofilm formation in a laboratory setting. Moreover, it can be used to increase productivity in a bioreactor.

We use what we learnt about cell-cell interactions to simulate growing surface-attached systems in **chapter 3**. We motivate some choices about the interactions between cells and the interaction with the surface. We then show how varying the strengths of these interactions can lead to different microcolony architectures.

We then use this model of growing microcolonies to study cooperator interactions in a spatially structured environment. Where the mechanical interactions occur over short distances, we also assume that metabolic interactions are close-range. In **chapter 4**, we simulate a cross-feeding consortium in the presence of a cheater species by having particles adjust their growth rate based on the cells in their immediate environment. Using simulations and an experimental consortium, we show how the time it takes for cooperators to meet is the determining factor in whether they outcompete their cheating counterparts.

Finally, in **chapter 5** we explore the patterning that cooperating particles create by mixing. We show that this cooperator mixing is mostly determined by inter-

action strength and is robust against variations in size and interaction symmetry. Additionally, we show that in the presence of cheaters, cooperators intermix but cheaters don't mix with the cooperators and instead remain on the outside. Therefore, we argue that focusing on strong cooperation is a great strategy for cheater exclusion.

Have fun!

SAMENVATTING

Micro-organismen leven vaak in dichte, aan oppervlakken gehechte gemeenschappen die biofilms worden genoemd. Deze biofilms komen voor in diverse omgevingen, van de binnenkant van je darmen en de oppervlakken van je tanden, tot de wortels van je kamerplanten en de binnenkant van je koffiemachine. Deze biofilms, bestaande uit verschillende bacteriën, schimmels en virussen ingekapseld in een zelfgeproduceerde extracellulaire matrix, vertonen complex gedrag. Ze spelen ook een dubbele rol in de menselijke gezondheid en industrie, door bij te dragen aan hardnekkige infecties en antibioticaresistentie, terwijl ze ook cruciaal zijn voor de spijsvertering en industriële toepassingen zoals afvalwaterzuivering. Begrip van biofilmvorming en -functie is essentieel voor het verminderen van hun nadelige effecten en het benutten van al hun potentie in biotechnologische toepassingen.

In dit proefschrift gebruik ik individual-based modellen van sferocilindrische deeltjes om iets te leren over de effecten van ruimtelijke structuur op hun mechanische en sociale interacties.

In **chapter 2** verkennen we de aggregatiedynamiek van op blauwlicht reagerende adhesieve *E. coli* in oplossing. We streven ernaar om experimentele resultaten te begrijpen waarbij bacteriën meer aggregeren en grotere clusters vormen onder pulserend licht. We simuleren een systeem van deeltjes dat Brownse beweging ondergaat, waarbij de cel-cel adhesie periodiek aan en uit kan worden geschakeld, en vergelijken onze simulaties met de experimentele data. We tonen aan dat het afstemmen van de lengte van de periode waarin het licht uit is op de vervaltijd van de adhesie leidt tot toegenomen aggregatie. We concluderen dat gedeeltelijke uiteenvallen van de aggregaten leidt tot effectievere clustering. Daarnaast tonen onze coauteurs aan dat deze toegenomen aggregatie leidt tot toegenomen biofilmvorming in een laboratoriumomgeving. Bovendien kan het worden gebruikt om de productiviteit in een bioreactor te verhogen.

We gebruiken wat we hebben geleerd over cel-cel interacties om groeiende aan oppervlakken gehechte systemen te simuleren in **chapter 3**. We motiveren enkele keuzes over de interacties tussen cellen en de interactie met het oppervlak. We laten vervolgens zien hoe het variëren van de sterkte van deze interacties kan leiden tot verschillende microkolonie-structuren.

Vervolgens gebruiken we dit model van groeiende microkolonies om coöperatieve interacties in een ruimtelijk gestructureerde omgeving te bestuderen. Waar de mechanische interacties over korte afstanden plaatsvinden, gaan we er ook van uit dat metabole interacties op korte afstand zijn. In **chapter 4** simuleren we een cross-feeding consortium in aanwezigheid van een valsspeler door deeltjes hun groeisnelheid te laten aanpassen op basis van de cellen in hun directe omgeving.

Met behulp van simulaties en een experimenteel consortium laten we zien hoe de tijd die nodig is voor coöperators om elkaar te vinden, bepalend is voor de vraag of ze hun valsspelende tegenhangers overtreffen.

Tot slot verkennen we in **chapter 5** de patronen die coöpererende deeltjes creëren door te mengen. We tonen aan dat dit coöperatormenging voornamelijk wordt bepaald door interactiesterkte en dat dit robuust is tegen variaties in grootte en interactiesymmetrie. Daarnaast tonen we aan dat in aanwezigheid van valsspelers, coöperators zich mengen, maar valsspelers niet met de coöperators mengen en in plaats daarvan aan de buitenkant blijven. Daarom stellen we dat het focussen op sterke samenwerking een uitstekende strategie is voor uitsluiting van valsspelers.

Veel plezier!

1

INTRODUCTION

Microorganisms often live together in close-knit communities known as biofilms. These surface-attached structures are found everywhere from natural environments to human-made systems, and they play a crucial role in various ecological and industrial processes [1]. Biofilms generally consist of many different species of bacteria, fungi and viruses, which are encased in an extracellular matrix. They exhibit complex behaviours that influence a wide range of ecological processes, such as nutrient cycling and habitat formation [2], [3]. In medical contexts, biofilms contribute to persistent infections and antibiotic resistance, presenting significant challenges for treatment [4]. In contrast, their ability to convert and break down compounds makes them invaluable in digestion and in industrial applications like wastewater treatment and bioenergy production [5]–[7]. Understanding the formation and function of biofilms is crucial, not only for mitigating their negative impacts but also for harnessing their biotechnological potential.

Biofilms provide resilient and functional habitats for their inhabitants. The multitude of species in a biofilm interact with each other through resource sharing and task specialisation, where individual cells may take on specific roles such as nutrient acquisition or protection [8], [9]. Cells use quorum sensing—communication through chemical and mechanical signalling—to coordinate activities such as biofilm formation, extracellular polymeric substance (EPS) production, and dispersal [10], [11]. The extracellular matrix physically shields the cells from environmental threats, including desiccation, toxins, and antibiotics [12]. These properties enable biofilms to thrive in challenging and changing environments, but they are also what make biofilms difficult to get rid of.

Biofilms arise when planktonic cells attach to a surface and start multiplying there (**fig. 1.1**) [1], [13]. An important part of the biofilm life cycle is the microcolony stage, which is where colonies of up to a few thousand cells form [14]. These microcolonies form the kernel of the eventual biofilm and can determine its

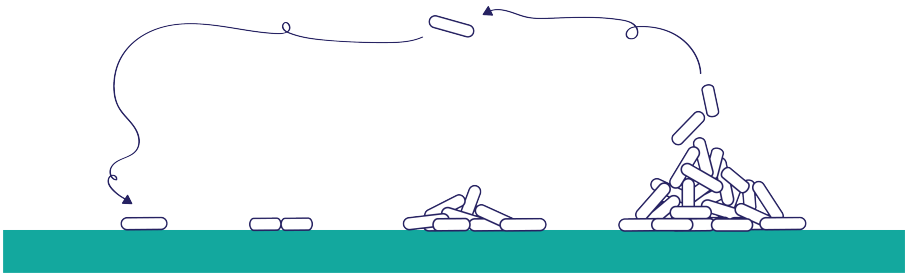

Figure 1.1: Different stages in the biofilm life cycle. A single planktonic bacterium attaches to a surface (far left), where it starts dividing, forming a microcolony (middle). This microcolony can grow flat or into the third dimension. The colony matures into a biofilm, and at some point, dispersal will occur (far right): cells will leave the formed biofilm and become planktonic again.

structure and social make up [15]–[17]. The development of these microcolonies is dependent on the environment as well as the cellular properties of its components [14].

Different species form different microcolonies [18]–[20]. Cell properties like shape, aspect ratio and EPS production will determine the shape and the cell density of a microcolony [21]. Additionally, the interaction with the surface and specific interactions with other cells influence the positioning of cells within a growing microcolony [22]–[24]. The spatiotemporal establishment of microcolonies shows several stages, including initial surface adherence, colony growth, and transitioning from a 2D to a 3D colony [25]–[28]. Processes like core verticalisation and pattern formation can also occur depending on the conditions, creating a myriad of colony shapes and forms [29]–[31].

The spatial structure a colony provides is important in a social context [9]. Bacteria interact over short ranges, because the exchange of metabolites and other molecules is diffusion limited [32], [33]. This means that, in contrast to a mixed system, in a surface attached colony cells are not interacting with all other species present in the system, but only the ones in their immediate vicinity [34]–[36]. Therefore, it is necessary for bacteria that are dependent on each other, to grow within close proximity of each other.

Spatial patterning can help coexistence of species that otherwise would be more easily outcompeted, such as cooperating or selfless species [37], [38]. Cooperation can come in a variety of forms, such as resource sharing, common good production or metabolite exchange. The latter is called cross-feeding, and this appears when two species both produce goods that the other species benefit from [39], [40]. This seemingly altruistic behaviour has been widely studied as it is not clear how such behaviour is stable when it is so easy to exploit [41], [42]. Additionally, cross-feeding consortia are widely used in biotechnological applications, for example in yoghurt production [43]–[45].

Spatial structure has been shown to be essential for both the emergence and the co-existence of cooperating species [46], [47]. Because cells are attached to a surface, they remain close to their next-of-kin, which is called clonal patching [48]. This is useful for intraspecies cooperation, for instance where common goods are produced and shared between cells [49]. On the other hand, strong mutualism has been shown to promote mixing [47], [50]. Together, this can lead to interesting pattern formations in multispecies colonies [51]–[54].

This constant dynamic of being close to kin and encountering other species has a huge effect on the make-up of the population within microcolonies and the resulting biofilms [43], [55]–[57]. Therefore it is important that we understand how exactly bacteria interact with each other in a spatially structured environment [58], [59]. This will increase our understanding of biofilm formation and it can help us build consortia for biotechnological applications.

In this thesis, I make use of individual-based models (IBM) to study bacteria and the microcolonies they form. This means I model bacteria as particles of a certain shape and size, that interact with each other and their environment. This approach allows us to take into account the space bacteria take up, as well as simulate a growing system. Additionally, many model parameters are easy to interpret and sometimes even experimentally measurable [36], [60], [61]. A downside of this type of modelling is that it requires relatively many model choices and parameters, which can make the results difficult to interpret [62]. In this thesis I combine the IBMs with other theoretical approaches as well as experimental work, in order to strengthen our arguments and validate the model choices.

Throughout this thesis, bacteria are modelled as spherocylinders, implemented similarly as in Stork et al. [63], where each particle is composed of two spheres connected by a spring (**fig. 1.2**a). The particles are grown by increasing the rest length of the spring. Once a particle has reached a certain division length, L, it is split into two (**fig. 1.2**b). The aspect ratio of a particle (AR) is defined as L/D, with D being the diameter of the particle. At the point of division, orientational noise is added to the particles to ensure they don't all align. Noise can also be added in the z-direction, to enable particles to escape the 2D plane.

Apart from steric repulsion between the particles and the surface, we also introduce adhesive forces (**fig. 1.2**c-d). We assume these forces act over short distances, as adhesive proteins expressed on membranes are often only a couple nm in size. For each particle pair that is within range of each other, the shortest distance between those two particles is determined. The force is then calculated based on that distance, r in the following way:

$$F(r) = r \cdot \frac{F_{\mathrm{PP}}}{\alpha} \cdot e^{-\frac{r-\alpha}{\alpha}} \quad \text{for } r \geq 0, \tag{1.1}$$

$$F(r) = k_{\mathrm{r}} \cdot r \quad \text{for } r < 0. \tag{1.2}$$

If the distance is smaller than zero, the particles overlap, and a simple elastic repulsion with spring constant k_{r} is applied. If the distance is larger than zero, an

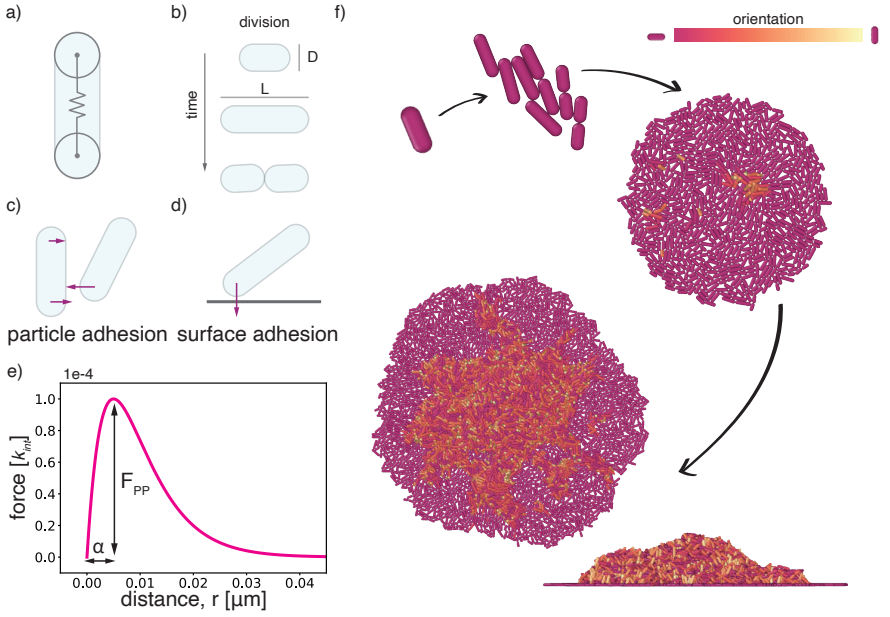

Figure 1.2: **Individual-based model** a) Particles are modelled as two spheres connected by an internal spring. b) Schematic of a particle growing and dividing. c) Schematic representation of adhesion between particles. d) Schematic representation of adhesion to the surface. e) Adhesion force profile as a function of distance between particles. f) Example of the trajectory of a simulation starting with one particle on a surface. Particles are coloured by orientation with respect to the z-axis.

attractive force is applied. Here, F_{PP} determines the magnitude of the particle adhesion force and α determines the range of the force (**fig. 1.2**e). The force is then distributed over the two end points of the particle, inversely proportional to where along the particle the closest point to the other particle is.

The interaction with the surface is applied on each end point of the particle and is of the following form:

$$F(r) = r \cdot \frac{F_{PS}}{\beta} \cdot e^{-\frac{r-\beta}{\beta}} \quad \text{for } r \geq 0, \tag{1.3}$$

$$F(r) = k_r \cdot r \quad \text{for } r < 0, \tag{1.4}$$

Here, similar to the particle adhesion force, F_{PS} determines the magnitude of the surface adhesion force and β determines the range of this force. In this case, r is the distance of an end-point of a particle to the surface.

The particles are grown every so many time steps, which is then followed by a period of relaxation. Every simulation time step, all the forces on all the particles are calculated, and they are moved accordingly. As bacteria live in a low-Reynolds's number environment, we only consider over damped dynamics and ignore the inertial terms. After initialisation of one or more particles, the system is evolved over time, either for a set amount of time, or to a particular amount of particles (**fig. 1.2**f). The resulting structures and dynamics are then analysed to help us understand bacterial interactions and microcolony development.

In this thesis I aim to help understand how species interactions play out in a spatially structured environment. In **chapter 2**, we start with clustering bacteria in solution [64]. Simulating these sticky bacteria and comparing the results so closely with experimental work, taught us a lot about how to think about bacterial adhesion. We then use this knowledge and apply it to surface attached colonies in **chapter 3**. Here we show how the individual-based model can create various colony architectures. In **chapter 4**, we try to understand what determines cooperator success in the presence of cheaters, by looking at a cross-feeding consortium growing on a surface. We then take a deeper dive into the pattern formation of cooperator strains in **chapter 5**, where we look at how cooperators mix and how robust this is against variations in the interactions.

BIBLIOGRAPHY

[1] K. Sauer, P. Stoodley, D. M. Goeres, *et al.*, "The biofilm life cycle: Expanding the conceptual model of biofilm formation", *Nature Reviews Microbiology*, vol. 20, pp. 608–620, Oct. 2022.

[2] K. Z. Coyte, C. Rao, S. Rakoff-Nahoum, and K. R. Foster, "Ecological rules for the assembly of microbiome communities", *PLOS Biology*, vol. 19, I. Gordo, Ed., e3001116, Feb. 19, 2021.

[3] S. Compant, A. Samad, H. Faist, and A. Sessitsch, "A review on the plant microbiome: Ecology, functions, and emerging trends in microbial application", *Journal of Advanced Research*, vol. 19, pp. 29–37, Sep. 2019.

[4] L. Hall-Stoodley, J. W. Costerton, and P. Stoodley, "Bacterial biofilms: From the natural environment to infectious diseases", *Nature Reviews Microbiology*, vol. 2, pp. 95–108, Feb. 2004.

[5] J.-P. Motta, J. L. Wallace, A. G. Buret, C. Deraison, and N. Vergnolle, "Gastrointestinal biofilms in health and disease", *Nature Reviews Gastroenterology & Hepatology*, vol. 18, pp. 314–334, May 2021.

[6] H.-C. Flemming, "Biofouling and me: My stockholm syndrome with biofilms", *Water Research*, vol. 173, p. 115 576, Apr. 2020.

[7] N. Debeni Devi, A. Chaudhuri, and V. V. Goud, "Algae biofilm as a renewable resource for production of biofuel and value-added products: A review", *Sustainable Energy Technologies and Assessments*, vol. 53, p. 102 749, Oct. 2022.

[8] H.-C. Flemming, J. Wingender, U. Szewzyk, P. Steinberg, S. A. Rice, and S. Kjelleberg, "Biofilms: An emergent form of bacterial life", *Nature Reviews Microbiology*, vol. 14, pp. 563–575, Sep. 2016.

[9] C. D. Nadell, K. Drescher, and K. R. Foster, "Spatial structure, cooperation and competition in biofilms", *Nature Reviews Microbiology*, vol. 14, pp. 589–600, Sep. 2016.

[10] X. Zeng, Y. Zou, J. Zheng, S. Qiu, L. Liu, and C. Wei, "Quorum sensing-mediated microbial interactions: Mechanisms, applications, challenges and perspectives", *Microbiological Research*, vol. 273, p. 127 414, Aug. 1, 2023.

[11] S. Mukherjee and B. L. Bassler, "Bacterial quorum sensing in complex and dynamically changing environments", *Nature Reviews Microbiology*, vol. 17, pp. 371–382, Jun. 2019.

[12] S. Banerjee, K. Lo, N. Ojkic, R. Stephens, N. F. Scherer, and A. R. Dinner, "Mechanical feedback promotes bacterial adaptation to antibiotics", *Nature Physics*, vol. 17, pp. 403–409, Mar. 2021.

[13] N. L. Fernandez, B. Y. Hsueh, N. T. Q. Nhu, J. L. Franklin, Y. S. Dufour, and C. M. Waters, "*Vibrio cholerae* adapts to sessile and motile lifestyles by cyclic di-GMP regulation of cell shape", *Proceedings of the National Academy of Sciences*, vol. 117, pp. 29 046–29 054, Nov. 17, 2020.

[14] B. Maier, "How physical interactions shape bacterial biofilms", *Annual Review of Biophysics*, vol. 50, pp. 401–417, May 6, 2021.

[15] G. O'Toole, H. B. Kaplan, and R. Kolter, "Biofilm formation as microbial development", *Annual Review of Microbiology*, vol. 54, pp. 49–79, Volume 54, 2000 Oct. 1, 2000.

[16] G. Mamou, G. B. Malli Mohan, A. Rouvinski, A. Rosenberg, and S. Ben-Yehuda, "Early developmental program shapes colony morphology in bacteria", *Cell Reports*, vol. 14, pp. 1850–1857, Mar. 2016.

[17] T. Ma, J. Rothschild, F. Halabeya, A. Zilman, and J. N. Milstein, "Mechanics limits ecological diversity and promotes heterogeneity in confined bacterial communities", *Proceedings of the National Academy of Sciences*, vol. 121, e2322321121, May 14, 2024.

[18] P. Yadav, S. Verma, R. Bauer, *et al.*, "Deciphering streptococcal biofilms", *Microorganisms*, vol. 8, p. 1835, Nov. 21, 2020.

[19] J. Yan, A. G. Sharo, H. A. Stone, N. S. Wingreen, and B. L. Bassler, "*Vibrio cholerae* biofilm growth program and architecture revealed by single-cell live imaging", *Proceedings of the National Academy of Sciences*, vol. 113, Sep. 6, 2016.

[20] T. Atriwal, K. Azeem, F. M. Husain, *et al.*, "Mechanistic understanding of candida albicans biofilm formation and approaches for its inhibition", *Frontiers in Microbiology*, vol. 12, p. 638 609, Apr. 30, 2021.

[21] H. Jeckel, F. Díaz-Pascual, D. J. Skinner, *et al.*, "Shared biophysical mechanisms determine early biofilm architecture development across different bacterial species", *PLOS Biology*, vol. 20, e3001846, 2022.

[22] M.-C. Duvernoy, T. Mora, M. Ardré, *et al.*, "Asymmetric adhesion of rod-shaped bacteria controls microcolony morphogenesis", *Nature Communications*, vol. 9, p. 1120, Mar. 16, 2018.

[23] R. Hartmann, P. K. Singh, P. Pearce, *et al.*, "Emergence of three-dimensional order and structure in growing biofilms", *Nature Physics*, vol. 15, pp. 251–256, Mar. 2019.

[24] C. Berne, C. K. Ellison, A. Ducret, and Y. V. Brun, "Bacterial adhesion at the single-cell level", *Nature Reviews Microbiology*, vol. 16, pp. 616–627, Oct. 2018.

[25] J. Nijjer, C. Li, Q. Zhang, H. Lu, S. Zhang, and J. Yan, "Mechanical forces drive a reorientation cascade leading to biofilm self-patterning", *Nature Communications*, vol. 12, p. 6632, Nov. 17, 2021.

[26] M. R. Warren, H. Sun, Y. Yan, J. Cremer, B. Li, and T. Hwa, "Spatiotemporal establishment of dense bacterial colonies growing on hard agar", *eLife*, vol. 8, e41093, Mar. 11, 2019.

[27] E. J. Stewart, R. Madden, G. Paul, and F. Taddei, "Aging and death in an organism that reproduces by morphologically symmetric division", *PLoS Biology*, vol. 3, T. Kirkwood, Ed., e45, Feb. 1, 2005.

[28] A. Welker, M. Hennes, N. Bender, T. Cronenberg, G. Schneider, and B. Maier, "Spatiotemporal dynamics of growth and death within spherical bacterial colonies", *Biophysical Journal*, vol. 120, pp. 3418–3428, Aug. 2021.

[29] P. Bravo, S. Lung Ng, K. A. MacGillivray, B. K. Hammer, and P. J. Yunker, "Vertical growth dynamics of biofilms", *Proceedings of the National Academy of Sciences*, vol. 120, e2214211120, Mar. 14, 2023.

[30] F. Beroz, J. Yan, Y. Meir, *et al.*, "Verticalization of bacterial biofilms", *Nature Physics*, vol. 14, pp. 954–960, Sep. 2018.

[31] L. Xiong, Y. Cao, R. Cooper, W.-J. Rappel, J. Hasty, and L. Tsimring, "Flower-like patterns in multi-species bacterial colonies", *eLife*, vol. 9, D. Weigel, A. M. Walczak, and A. Seminara, Eds., e48885, Jan. 14, 2020.

[32] A. Dal Co, S. van Vliet, D. J. Kiviet, S. Schlegel, and M. Ackermann, "Short-range interactions govern the dynamics and functions of microbial communities", *Nature Ecology & Evolution*, vol. 4, pp. 366–375, Mar. 2020.

[33] R. J. van Tatenhove-Pel, T. Rijavec, A. Lapanje, *et al.*, "Microbial competition reduces metabolic interaction distances to the low µm-range", *The ISME Journal*, vol. 15, pp. 688–701, Mar. 2021.

[34] S. Gupta, T. D. Ross, M. M. Gomez, J. L. Grant, P. A. Romero, and O. S. Venturelli, "Investigating the dynamics of microbial consortia in spatially structured environments", *Nature Communications*, vol. 11, p. 2418, May 15, 2020.

[35] A. J. Lopatkin and J. J. Collins, "Predictive biology: Modelling, understanding and harnessing microbial complexity", *Nature Reviews Microbiology*, vol. 18, pp. 507–520, Sep. 2020.

[36] N. I. van den Berg, D. Machado, S. Santos, *et al.*, "Ecological modelling approaches for predicting emergent properties in microbial communities", *Nature Ecology & Evolution*, vol. 6, pp. 855–865, May 16, 2022.

[37] I. Frost, W. P. J. Smith, S. Mitri, *et al.*, "Cooperation, competition and antibiotic resistance in bacterial colonies", *The ISME Journal*, vol. 12, pp. 1582–1593, Jun. 2018.

[38] J. B. Xavier and K. R. Foster, "Cooperation and conflict in microbial biofilms", *Proceedings of the National Academy of Sciences*, vol. 104, pp. 876–881, Jan. 16, 2007.

[39] G. D'Souza, S. Shitut, D. Preussger, G. Yousif, S. Waschina, and C. Kost, "Ecology and evolution of metabolic cross-feeding interactions in bacteria", *Natural Product Reports*, vol. 35, pp. 455–488, 2018.

[40] C. R. Evans, C. P. Kempes, A. Price-Whelan, and L. E. P. Dietrich, "Metabolic heterogeneity and cross-feeding in bacterial multicellular systems", *Trends in Microbiology*, vol. 28, pp. 732–743, Sep. 1, 2020.

[41] E. Pessione, "The less expensive choice: Bacterial strategies to achieve successful and sustainable reciprocal interactions", *Frontiers in Microbiology*, vol. 11, Jan. 20, 2021.

[42] E. Thébault and C. Fontaine, "Stability of ecological communities and the architecture of mutualistic and trophic networks", *Science*, vol. 329, pp. 853–856, Aug. 13, 2010.

[43] R. J. van Tatenhove-Pel, D. H. de Groot, A. S. Bisseswar, B. Teusink, and H. Bachmann, "Population dynamics of microbial cross-feeding are determined by co-localization probabilities and cooperation-independent cheater growth", *The ISME Journal*, vol. 15, pp. 3050–3061, Oct. 2021.

[44] S. Wu, Y. Xue, S. Yang, *et al.*, "Combinational quorum sensing devices for dynamic control in cross-feeding cocultivation", *Metabolic Engineering*, vol. 67, pp. 186–197, Sep. 1, 2021.

[45] R. Kort, N. Westerik, L. Mariela Serrano, *et al.*, "A novel consortium of lactobacillus rhamnosus and streptococcus thermophilus for increased access to functional fermented foods", *Microbial Cell Factories*, vol. 14, p. 195, Dec. 8, 2015.

[46] C. D. Nadell, K. R. Foster, and J. B. Xavier, "Emergence of spatial structure in cell groups and the evolution of cooperation", *PLoS Computational Biology*, vol. 6, T. Pfeiffer, Ed., e1000716, Mar. 19, 2010.

[47] W. Liu, J. Russel, M. Burmølle, S. J. Sørensen, and J. S. Madsen, "Micro-scale intermixing: A requisite for stable and synergistic co-establishment in a four-species biofilm", *The ISME Journal*, vol. 12, p. 1940, Aug. 2018.

[48] F. J. Schwarzendahl and D. A. Beller, "Do active nematic self-mixing dynamics help growing bacterial colonies to maintain local genetic diversity?", *Frontiers in Physics*, vol. 10, p. 940 980, Jul. 12, 2022.

[49] A. Bingham, A. Sur, L. B. Shaw, and H. A. Murphy, "The effect of cooperator recognition on competition among clones in spatially structured microbial communities", *PLOS ONE*, vol. 19, e0299546, 2024.

[50] B. Momeni, K. A. Brileya, M. W. Fields, and W. Shou, "Strong inter-population cooperation leads to partner intermixing in microbial communities", *eLife*, vol. 2, e00230, Jan. 22, 2013.

[51] A. E. Blanchard and T. Lu, "Bacterial social interactions drive the emergence of differential spatial colony structures", *BMC Systems Biology*, vol. 9, p. 59, Sep. 16, 2015.

[52] M. Marchal, F. Goldschmidt, S. N. Derksen-Müller, S. Panke, M. Ackermann, and D. R. Johnson, "A passive mutualistic interaction promotes the evolution of spatial structure within microbial populations", *BMC Evolutionary Biology*, vol. 17, p. 106, Dec. 2017.

[53] J. Kayser, C. F. Schreck, Q. Yu, M. Gralka, and O. Hallatschek, "Emergence of evolutionary driving forces in pattern-forming microbial populations", *Philosophical Transactions of the Royal Society B: Biological Sciences*, vol. 373, p. 20 170 106, May 26, 2018.

[54] D. Ciccarese, A. Zuidema, V. Merlo, and D. R. Johnson, "Interaction-dependent effects of surface structure on microbial spatial self-organization", *Philosophical Transactions of the Royal Society B: Biological Sciences*, vol. 375, p. 20 190 246, Mar. 23, 2020.

[55] S. Xu and J. D. Van Dyken, "Microbial expansion-collision dynamics promote cooperation and coexistence on surfaces", *Evolution*, vol. 72, pp. 153–169, Jan. 2018.

[56] J. D. Van Dyken, M. J. Müller, K. M. Mack, and M. M. Desai, "Spatial population expansion promotes the evolution of cooperation in an experimental prisoner's dilemma", *Current Biology*, vol. 23, pp. 919–923, May 2013.

[57] A. Bridier, J.-C. Piard, C. Pandin, S. Labarthe, F. Dubois-Brissonnet, and R. Briandet, "Spatial organization plasticity as an adaptive driver of surface microbial communities", *Frontiers in Microbiology*, vol. 8, p. 1364, Jul. 20, 2017.

[58] L. Dieltjens, K. Appermans, M. Lissens, *et al.*, "Inhibiting bacterial cooperation is an evolutionarily robust anti-biofilm strategy", *Nature Communications*, vol. 11, p. 107, Jan. 9, 2020.

[59] B. D. Karkaria, A. J. H. Fedorec, and C. P. Barnes, "Automated design of synthetic microbial communities", *Nature Communications*, vol. 12, p. 672, Jan. 28, 2021.

[60] F. L. Hellweger, R. J. Clegg, J. R. Clark, C. M. Plugge, and J.-U. Kreft, "Advancing microbial sciences by individual-based modelling", *Nature Reviews Microbiology*, vol. 14, pp. 461–471, Jul. 2016.

[61] H. Kettle, P. Louis, G. Holtrop, S. H. Duncan, and H. J. Flint, "Modelling the emergent dynamics and major metabolites of the human colonic microbiota: Emergent microbial dynamics in the colon", *Environmental Microbiology*, vol. 17, pp. 1615–1630, May 2015.

[62] L. Eigentler, F. A. Davidson, and N. R. Stanley-Wall, “Mechanisms driving spatial distribution of residents in colony biofilms: An interdisciplinary perspective”, *Open Biology*, vol. 12, p. 220 194, Dec. 2022.

[63] T. Storck, C. Picioreanu, B. Virdis, and D. J. Batstone, “Variable cell morphology approach for individual-based modeling of microbial communities”, *Biophysical Journal*, vol. 106, p. 2037, May 5, 2014.

[64] J. J. Quispe Haro, F. Chen, R. Los, *et al.*, “Optogenetic control of bacterial cell-cell adhesion dynamics: Unraveling the influence on biofilm architecture and functionality”, *Advanced Science*, vol. 11, p. 2 310 079, 2024.

2

Optogenetic Control of Bacterial Cell-Cell Adhesion Dynamics: Unraveling the Influence on Biofilm Architecture and Functionality

Juan José Quispe Haro, Fei Chen, Rachel Los, Shuqi Shi, Wenjun Sun, Yong Chen, Timon Idema, Seraphine V. Wegner

The transition of bacteria from an individualistic to a biofilm lifestyle profoundly alters their biology. During biofilm development, the bacterial cell-cell adhesions are a major determinant of initial microcolonies, which serve as kernels for the subsequent microscopic and mesoscopic structure of the biofilm, and determine the resulting functionality. In this study, the significance of bacterial cell-cell adhesion dynamics on bacterial aggregation and biofilm maturation is elucidated. Using photoswitchable adhesins between bacteria, modifying the dynamics of bacterial cell-cell adhesions with periodic dark-light cycles is systematic. Dynamic cell-cell adhesions with liquid-like behavior improve bacterial aggregation and produce more compact microcolonies than static adhesions with solid-like behavior in both experiments and individual-based simulations. Consequently, dynamic cell-cell adhesions give rise to earlier quorum sensing activation, better intermixing of different bacterial populations, improved biofilm maturation, changes in the growth of cocultures, and higher yields in fermentation. The here presented approach of tuning bacterial cell-cell adhesion dynamics opens the door for regulating the structure and function of biofilms and cocultures with potential biotechnological applications.

This chapter has been has been published in Advanced Science as [1].

2.1. INTRODUCTION

Biofilms bring together different bacteria in communities that allow them to perform tasks, which their planktonic counterparts or a single species cannot accomplish [2], [3]. Within the biofilm, bacteria share communal resources [4], divide tasks among the members and specialize [5]–[8], communicate through quorum sensing [9], [10] and are protected from environmental challenges, all increasing their chances of survival. Despite the well-established relevance of biofilms in both diseases and ecology, as well as their growing relevance for biotechnological applications [8], [11], our ability to engineer them lags behind the advancements in engineering individual bacterial cells. Various biofilm properties, such as total biomass, spatial microstructure, compactness, the relative distribution of different members, and the dynamic evolution of these features over time, significantly impact biofilm performance [12]. However, our current capabilities are primarily limited to analyzing these parameters rather than actively controlling them.

In biofilm maturation, bacteria initially form clusters known as microcolonies, which consist of tens to a few thousand cells [8], [13], [14]. These microcolonies are not merely an intermediate stage in biofilm formation. They serve as the basic kernel for the subsequent microscopic and mesoscopic structure of the biofilm and alter the resulting functionality [15], [16]. A major determinant of the microcolony and biofilm micro- and mesoscale architecture are the bacterial cell-cell adhesions alongside other attractive and repulsive forces [12], [17]. The strength of these cell-cell adhesions and their dynamics (t_{on} and t_{off}) can result in gas-like, liquid-like, and solid-like multicellular organization analogous to different states of matter. Free-floating bacteria in solution have negligible adhesions like molecules in gases. If the adhesions between the cells get stronger but are still dynamic, bacteria are still mobile within the aggregates like molecules in a liquid. On the otherhand, if the interactions between cells are strong and not dynamic, the cells will stay in place like molecules within a solid matrix. This has consequences for bacterial behavior [17]. As shown in *V. cholerae*, lowering the cell-cell adhesions results in larger cellcell distances in biofilms [12]. Moreover, in these rod-shaped bacteria, the cell-cell adhesions also influence nematic order reflected in the roughness of the forming colony [18], [19].In other cases bacterial microcolonies behave like liquids, where they have short-range but no long-range order, form spherical colonies to minimize surface tension, and fuse with each other when they come in contact [20], [21]. The liquid-like dynamics are also important for cell sorting in colonies based on the differential strength of adhesions, as the sorting requires some level of cell mobility [12], [14], [22]. Moreover, whether bacteria exhibit liquid or solid-like properties impacts their ability to colonize capillaries [23] and their antibiotic susceptibility [24]. Regulating the dynamics of bacterial cell-cell adhesions and the transitions of bacteria between the gas, liquid, and solid-like states could provide a viable approach to addressing the challenge of engineering biofilm development, yet this avenue remains largely unexplored. The sensi-

tivity of cell-cell interactions to the dynamics and equilibration of cell-cell adhesions makes them challenging to control experimentally. Current studies predominantly rely on the manipulation of gene expression [25] and genetic modification of adhesin properties [12], [20]. Conversely, various initiatives aim to introduce synthetic adhesins that are either genetically coded (e.g. nanobody/antigen [25], SpyTag/SpyCatcher [26]) or chemically introduced (e.g. click chemistry [27]). Notably, optogenetic tools enabling light-inducible expression of adhesins have enabled the production of micropatterned biofilms [28]–[32]. However, all these adhesions lack reversibility, rely on strong and permanent interactions, and are not dynamic. In contrast, cell-cell adhesions between bacteria are dynamic in many instances. For example, many bacterial species use type 4 pili (T4P) to generate attractive forces between cells, with the pili known to govern liquid-like behavior in microcolonies [17]. Here, T4P binds to pili on neighboring bacteria and continuously retracts, resulting in the observed liquid-like behavior.

In this study, we elucidate how the strength and dynamics of bacterial cell-cell adhesions influence bacterial aggregation, as well as the architecture and function of the resulting biofilms. Using photoswitchable adhesins, we were able to systematically modify the dynamics of bacterial cell-cell adhesions and switch between gas-like, liquid-like, and solid-like multicellular aggregates. Our findings reveal that similar to distinct states of matter, bacterial aggregates, and biofilms possess unique mechanical and biological properties that depend on the cell-cell adhesion dynamics. Consequently, we propose that precise regulation of adhesion dynamics within microcolonies holds significant potential in guiding future strategies for biofilm engineering, as we have exemplified in auxotrophic cocultures and a biofilm reactor.

2.2. Results and Discussion

2.2.1. Pulsed Light Illumination to Control Bacterial Adhesion Dynamics

In this study, we employed blue light switchable bacterial cell-cell adhesions to manipulate adhesion dynamics and consequently control bacterial aggregation into multicellular structures. Specifically, the bacteria could undergo transitions from a gas-like state characterized by weak attractive interactions between cells to a liquid-like state where dynamic cell-cell adhesions enable cell mobility within aggregates, and finally to a solid-like state with strong and static cell-cell adhesions with rigid and unchanging internal configurations (**fig. 2.1**a). The modulation of cell-cell adhesion strength and dynamics was achieved through the expression of photoswitchable proteins, namely nMagHigh or pMagHigh, as adhesins on the outer surface of *E. coli* [33], [34]. nMagHigh and pMagHigh proteins have been derived from the light-dependent homodimerize VVD from *Neurospora crassa* and have been engineered to expose complementary proteins interphases

with negatively (I52D and M55G for nMagHigh) and positively (I52R and M55R for pMagHigh) charged amino acids, respectively, under blue light [35]. This happens due to the blue light-triggered reaction between a key cysteine (C71) reacts with the flavin dinucleotide chromophore, resulting in global conformational changes. The complementary electrostatic interaction between nMagHigh and pMagHigh promotes selective heterodimerization and prevents undesired homodimerization. In our case, these adhesins were displayed on the outer bacterial membrane as fusion proteins with the circularly permutated outer membrane protein OmpX (eCPX). In the dark, nMagHigh and pMagHigh bacteria did not adhere to each other, resembling a gas-like state. On blue light illumination, these two types of bacteria permanently adhered to each other, reminiscent of a solidlike state. Notably, these optogenetic adhesins are reversible in the dark and can be repeatedly switched on and off using pulsed light illumination. The photoactivation of the adhesins occurs within seconds [34], [35], and the rate-limiting step for aggregation is bacteria coming in close proximity in suspension. In our previous work, we observed that the bacterial aggregation plateaus within about 2 h ($t_{1/2} \approx 30$ min) at densities also used in this study. At the molecular level the reversion rate of the nMagHigh-pMagHigh interaction in the dark is significantly slower ($t_{1/2} = 4.7$ h) [35], also resulting in slow reversion rates of the bacterial aggregates in the dark within about 1 h [33], [34].

To investigate the influence of cell-cell adhesion dynamics on bacterial aggregation, we mixed an equal number of *E. coli* MG1655 bacteria expressing nMagHigh (labeled with green fluorescent protein GFP, shown in green) and pMagHigh (labeled with mCherry, shown in red) in PBS and exposed them to various blue light illumination patterns (450 nm blue LED, 270 µW cm^{-2}) for a total duration of 2 h. During this time, there was minimal bacterial growth, excluding the effects of crowing. These mixtures of bacteria aggregated in different manners in terms of aggregation ratio (area occupied by clusters with an area > 35 µm^2 divided by the total area occupied by all bacteria), average cluster size (objects with an area > 35 µm^2), and total number of clusters depending on the illumination as observed with confocal microscopy (**fig. 2.1**b; **fig. S2.3**, Supporting Information). Samples kept in the dark serve as a negative control, showing weak interactions and low levels of background aggregation (gas-like) (Few clusters with > 35 µm^2 were detected in the automated image analysis due to local crowding, i.e., cells statistically being in close proximity due to their overall density). Samples exposed to continuous blue light illumination served as a positive control with strong and static adhesions (solid-like).

Initially, we kept the dark period constant at 20 min, altering the illumination period from 1 to 20 min. With a brief 1-min illumination time, we still observed comparable aggregation to constant blue light illumination. Even more strikingly, there was a significant rise in aggregation ratio and average cluster size at 5 and 20 min illumination periods compared to continuous blue light illumination, despite

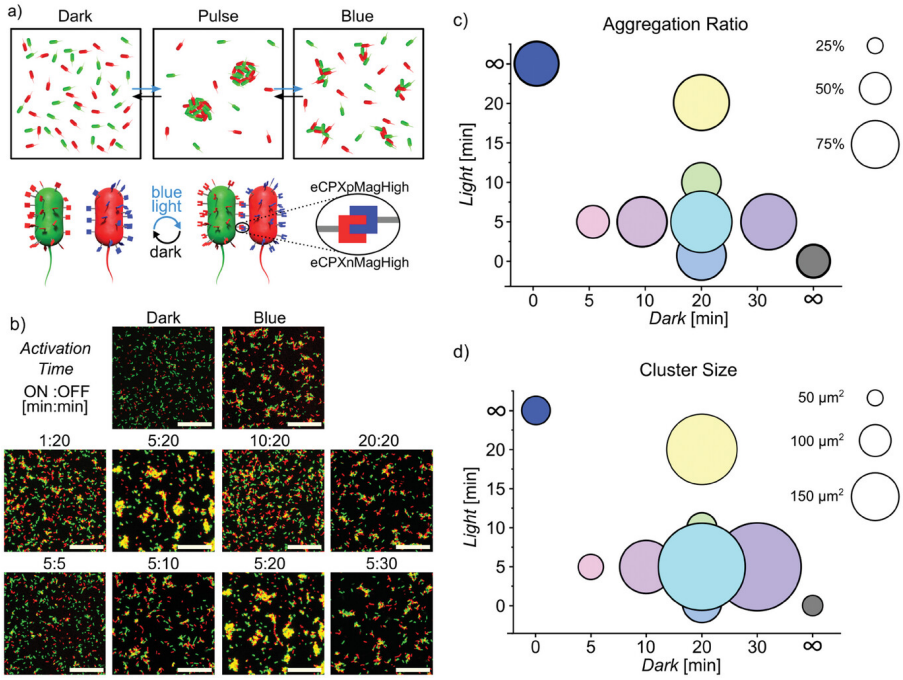

Figure 2.1: Pulsed illumination alters aggregation ratio and cluster size. a) Schematic representation of bacteria expressing nMagHigh-eCPX (labeled green) and pMagHigh-eCPX (red) showing different aggregation levels under different pulse illumination settings. b) Confocal microscopy images of bacteria incubated in the dark, under blue light or different pulsed illumination settings (ON:OFF time in minutes) for a total duration of 2 h, show different amounts of aggregation. Images at 5:20 are shown twice to make trends visible but come from the same experiment. Scale bars are 50µm. Differences in c) aggregation ratio and d) cluster size for different illumination settings. In terms of both aggregation ratio and cluster size, some pulsed light settings outperformed constant blue light illumination. All experiments were performed in 3 biological replicates with 3 technical replicates each.

overall lower light exposure (**fig. 2.1**c;**fig. S2.1**a, Supporting Information). Intriguingly, 10-min photoactivation periods resulted in a reduction in aggregation ratio and average cluster size. In a second set of experiments, we fixed the light period to 5 min, varying the dark period from 5 to 30 min. In this scenario, the aggregation ratio increased compared to continuous blue light illumination whenever the dark period exceeded 10 min. Concurrently, the average cluster size also increased as the dark period was extended from 5 to 20 min (**fig. 2.1**d; **fig. S2.1**c, Supporting Information). In these experiments, a light period of 5 min together with a dark period of 20 min was observed to be optimal for reaching the highest aggregation ratio and the largest cluster size.

2.2.2. LIQUID-LIKE BEHAVIOR IN BACTERIAL AGGREGATES

In addition to the clustering efficiency of the bacteria, the aggregate morphology also changes significantly depending on the illumination protocol. The clusters exhibit a wide range of structures, varying from branched structures to more compact and spherical ones. To assess the morphology, we analyzed the fractal dimensions of the clusters using the FracLac plugin in ImageJ (**fig. 2.2**a). In this analysis, more compact objects have a higher fractal dimension than ones that are less compact with an irregular shape. The median fractal dimension was highest for aggregates under 5 min on and 20 min off light illumination (5:20), measuring 1.477. In comparison, under continuous blue light illumination, the median fractal dimension was only 1.443 (**fig. 2.2**b,c). The initial stages of microcolony formation exhibited striking similarities to the self-assembly of non-living colloidal particles with attractive interactions. This resemblance is particularly expected since the nMagHigh and pMagHigh expressing bacteria in PBS showed low motility. In the self-assembly of colloids, the resulting architectures depend on the dynamics of the interactions. When the interactions are static, diffusion-limited cluster aggregation (DLCA) leads to loosely packed and branched assemblies under kinetic control. Similarly, in our experiments under constant blue light illumination, the rate-limiting step involved different bacteria finding each other, resulting in branched aggregates, i.e., lower fractal dimension. In contrast, dynamic interactions enable reaction-limited cluster aggregation (RLCA) where colloids optimize their position to maximize the interactions with neighbors, leading to compact and spherical structures under thermodynamic control. In our experiments, pulsed light illumination introduced dynamics into the bacterial cell-cell adhesions and increased the fractal dimension, thereby shifting the bacterial assemblies from DLCA under constant light illumination towards RLCA (**fig. S2.2**, Supporting Information). As a benchmark, ideal conditions for 2D aggregation of spherical particles yield fractal dimensions of 1.46 and 1.55 for DLCA and RLCA, respectively [36], [37].

Our comprehensive analysis of aggregation and fractal dimension data leads us to propose a hypothesis regarding the impact of bacterial cell-cell adhesion dynamics. We predict that during the dark periods, the photoswitchable adhesions responsible for holding the clusters together gradually reverse, but not completely if the dark period is lower than the reversion time. Consequently, bacteria residing at the periphery of the clusters that are only weakly attached could escape or reposition themselves, enabling stronger interactions once illumination resumed. These enhanced attachment and detachment dynamics among bacteria—akin to a liquid-like state—result in larger and rounder aggregates. Under constant illumination, this dynamic behavior is absent (i.e. solid-like state), and adhesions occur rapidly among neighboring cells. These cells thus form only small clusters with permanent interactions, absorbing all freefloating bacteria that could contribute to larger clusters. Insufficient reversion, as seen with a short dark period (e.g., 5 min), results in an insignificant improvement in bacterial aggregation, as the bac-

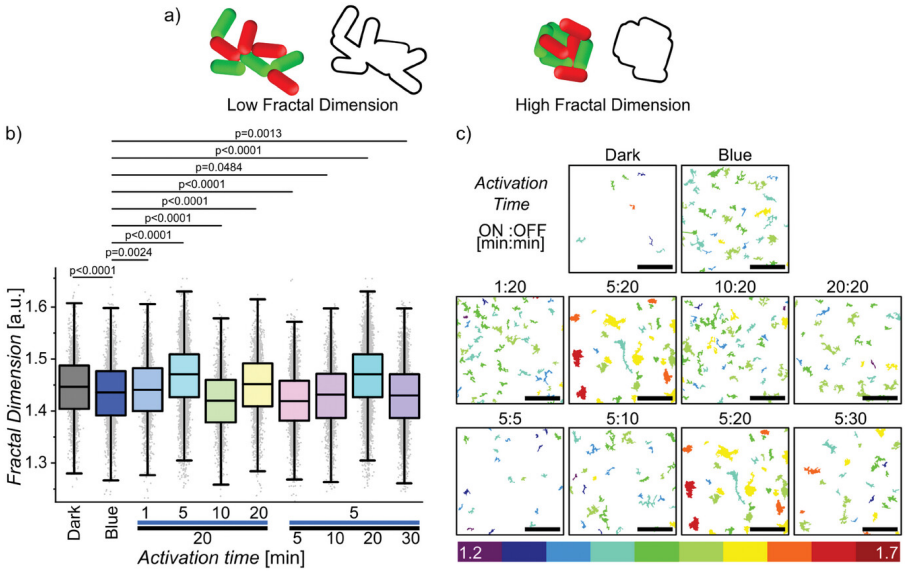

Figure 2.2: Cluster morphology varies under different illumination settings. a) The fractal dimension quantifies the compactness of the clusters, branched and irregular clusters have a low fractal dimension while more regular clusters have a higher score. b) Distribution of bacterial clusters' fractal dimension from different pulse illumination settings (ANOVA with multiple comparisons, $p < 0.0001$). c) Visual categorization of bacterial clusters according to fractal dimension, the key below shows the color code of clusters' respective fractal dimensions from 1.2 to 1.7 with 0.05 increments. ON: OFF time in minutes (total time 2h, scale bars 50µm, all experiments were performed in 3 biological replicates with 3 technical replicates each.). Data and images in (b) and (c) at 5:20 are shown twice to make trends visible but come from the same experiment.

teria lack the motility to reposition. On the other hand, when the dark period extends to 30 min, causing extensive reversion, both the aggregation ratio and the average cluster size decrease, as the cells return to a gas-like state.

2.2.3. Individual-Based Simulations of Bacterial Aggregation

To further investigate the dynamics of bacterial clustering, we used an individual-based model of spherocylindrical particles to simulate the experiments. Besides Brownian forces, each particle is influenced by light-sensitive interactions with other particles and interactions with a hard surface (**fig. 2.3**a). After initialization, the system evolved over time, and particle locations were tracked and analyzed like in the experiments (**fig. 2.3b**). We determined the magnitude of the Brownian forces by estimating the diffusion coefficient for particles of similar size, shape, and environment as the bacteria in the experiments and comparing the expected mean-squared-displacement (MSD) to the MSD of simulated particles with

no adhesive forces (**fig. S2.3**, Supporting Information). With the correct Brownian forces in place, we estimated the magnitudes (P and S) and ranges ($\sigma_p = 5\,\text{nm}$ and $\sigma_s = 10\,\text{nm}$) for the adhesive forces between the particles and the surface, respectively, by comparing aggregation curves from the simulations to those from experiments with constant light illumination (**fig. S2.4**, Supporting Information) [34].

In the model, the part of the force that is affected by the blue light is the magnitude of the particle-particle interaction, P, which is constant under blue light (P_{on}). However, the adhesive force is not immediately set to zero when the light is turned off. Instead, after each period of light exposure, it follows an exponential decay with the decaying adhesive force of the form $P_p = P_{p,on} \cdot e^{(-d \cdot t)}$ where d is the decay rate and t is the time since the light was turned off in minutes. We found the value for d by fitting it to the 5:20 pulse illumination experiments, where the aggregation ratio was the highest (**fig. 2.3**c). For high decay rates ($\lambda = 10\,\text{min}^{-1}$), we observed a complete reversal of the clustering in the periods of darkness, which led to low aggregation ratios like in the dark and no increase in cluster size over multiple cycles of illumination. For low decay rates ($\lambda = 0.1\,\text{min}^{-1}$), there was a persistent rise in aggregation ratio and cluster size over multiple cycles of illumination, which is slightly higher than what we find for constant blue light. The highest aggregation ratio was achieved when the clusters started to disassemble just before the light was turned back on ($\lambda = 0.15\,\text{min}^{-1}$).

When using this value for other illumination conditions we could recreate most of the findings of the experiments, where we clearly observed higher aggregation ratios and bigger cluster sizes for all the pulsed illumination conditions compared to constant blue light (**fig. 2.3d-e**; **Video S1–S3**, Supporting Information). For conditions with an on-time of 5 min, we see that for short off-times up to 10 min, the aggregation and cluster size only slightly increased compared to constant blue light illumination, and the curves remained smooth during the pulsed light illumination (**fig. 2.3**d). However, for an off-time of 20 min there was significant disassembly during dark periods, resulting in a drastic growth of the clusters when the light was turned back on. When the off-time was increased even more, we saw an an extensive reversal of the clustering, which explains the lower aggregation ratios and smaller clusters found in the experiments under these conditions.

The conditions with off-times of 20 min consistently showed higher aggregation levels and bigger clusters compared to constant blue light illuminations, just like in the experiments (**fig. 2.3e**). In contrast, the on-time did not seem to globally affect the aggregation ratio as all curves behaved similarly, but only the cluster size was affected, where longer on-times led to smaller clusters. We also find that for these conditions, the time of measurement can significantly affect the result, which could explain why the 10:20 and 20:20 conditions gave such varying results in the experiments, as both illumination conditions are right at the end of a period of darkness at the time of measurement resulting in a seemingly low aggregation ratio and smaller clusters. Analogous to our experimental results, the fractal di-

mension of the clusters formed under pulse illumination in the simulations was also higher than that of clusters formed under constant blue light and in the dark (**fig. 2.3f**). All in all, these results demonstrate that in our experimental system under pulse illumination, the off-time of 20 min was the critical parameter, which provides just enough time for the clusters to start to disassemble before the light is turned back on. This partial disassembly in turn leads to the particles rearranging significantly and the clusters coming together again in bigger structures leading to higher aggregation ratios and cluster sizes.

To explore how this rearrangement on the particle scale relates to the overall aggregation dynamics, we looked at the neighbor rearrangement of the particles during a 5:20 pulse cycle. For each particle, we tracked which particles were in its close vicinity throughout the simulation. We then compared the neighbors at the beginning and end of one ON: OFF cycle and calculated the rearrangement ϕ as a value between 0 and 1, in the following way,

$$\phi = \frac{1}{N}\sum_i 1 - \frac{|n_{i,beginning} == n_{i,end}|}{|n_{i,end}|}, \tag{2.1}$$

where N is the number of particles and $n_{i,t}$ is the vector of neighbors of particle i at time t.

For the 5:20 pulsing scenario, we looked at the rearrangement for different values of the decay rate. For $\lambda = 0.15\,\mathrm{min}^{-1}$, where we observed the highest aggregation ratio and biggest cluster sizes, we found an average rearrangement of $\approx 35\%$ of neighbors per 25 min cycle (**fig. 2.3g**). In contrast, rearrangement between cycles was almost complete ($\approx 85\%$) for the higher values of λ and in the dark but rearrangement remained below 20% for lower values of λ and under constant blue light illumination. Similarly, when comparing different illumination conditions, we saw that also here, the highest aggregation ratios correspond to a rearrangement of $\approx 35\%$ of neighbors in 25 min. In summary, the highest aggregation is achieved with intermediate dynamics in the neighbor rearrangement, resulting in liquid-like behavior. Here, the timescale of the disassembly process is similar to the off-time in the pulse illumination. Because the disassembly timescale is intrinsic to the system, it is possible to find a pulse condition where the aggregation is optimal by tuning off-time.

2.2.4. Bacterial Cluster Intermixing

Besides the rounding up of the aggregates with increasing bacterial adhesion dynamics, liquid-like behavior is also characterized by the intermixing of similar liquids. To demonstrate that this aspect of liquid-like behavior holds true in the bacterial aggregates, we mixed preformed aggregates of bacterial clusters under different illumination conditions. In particular, we performed two populations of compact bacterial clusters from nMagHigh- and pMagHigh-bacteria either labeled with GFP (shown in green) or mCherry (shown in red) for 2 h under pulsed illumi-

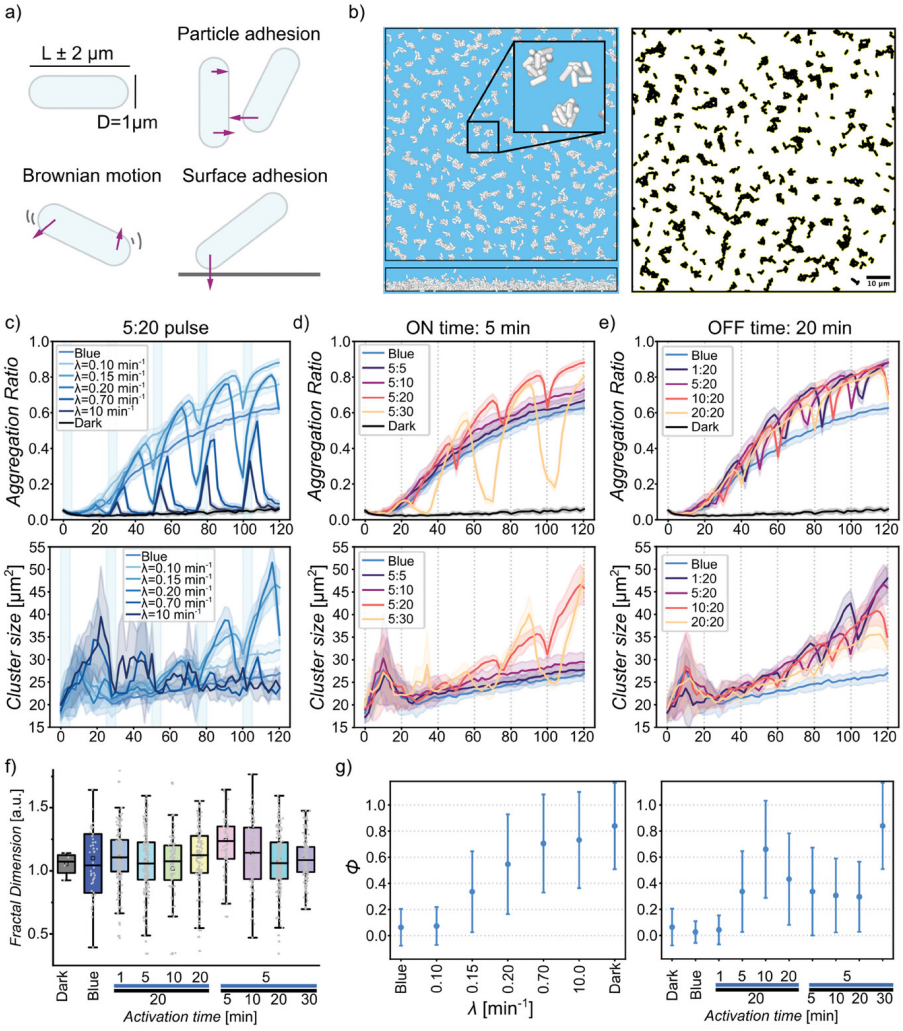

Figure 2.3: Individual-based simulations. a) The bacteria are modeled as spherocylindrical particles. Each timestep, Brownian force, and adhesive forces to the surface and to other particles are exerted for each particle. b) Still of a simulation of 2000 particles after 1 h of constant light (top view and side view) and the resulting 2D image and segmentation used for assessing the aggregation ratio and cluster size. c) Aggregation dynamics and cluster sizes under a pulse illumination of 5:20, with varying decay rates of the adhesive force. Averages and standard deviation of 10 runs per condition are shown. d,e) Aggregation dynamics and cluster sizes under different pulse illumination settings. Averages and standard deviation of ten runs per condition are shown (f) Distribution of the fractal dimension of particle clusters for different pulse illumination settings. (ANOVA with multiple comparisons, $p = 0.0005$.) (g) Neighbor rearrangement of the particles under 5:20 pulse illumination for different values of the decay rate, λ and for different pulse illumination settings with $\lambda = 0.15\,\mathrm{min}^{-1}$.

nation (5:20 ON:OFF, referred to as pulsed light hereafter, if not specified otherwise). Subsequently, we mixed these clusters in equal numbers and kept them for another 2 h in the dark, under continuous or pulsed light illumination, before analyzing the intermixing of the GFP and mCherry labeled populations using confocal microscopy (**fig. 2.4**a). In the dark, the red and green bacteria were predominantly dispersed due to the reversion of the adhesions and only a few clusters of a single color remained. In contrast, in samples kept under blue light, we observed clusters of green and red labeled bacteria with adjacent green and red domains, suggestive of clusters aggregating together. For samples kept under pulsed light, we also observed clusters, which consisted of blended red and green-labeled bacteria, showing substantial intermixing of the two populations. We supported these qualitative observations by calculating the Pearson Correlation Coefficient (PCC) [38] for the green and red channels (**fig. 2.4**b). The PCC was highest for samples under pulsed illumination, indicating a high colocalization of the red and green channels. The PCC was lowest for samples kept in the dark, indicative of only background-level interactions between the green and the red labeled bacteria. Overall, both the rounder and more compact bacterial aggregates (**fig. 2.2**) and the higher degree of intermixing with pulsed light illumination support the higher fluidity of these bacterial aggregates compared to ones formed under constant illumination.

2.2.5. Consequences of Liquid-Like Behavior for Quorum Sensing

Bacteria possess the ability to sense their local population density through quorum sensing [39]. The activation of quorum sensing is highly contingent on the spatial distribution of bacteria, with compact aggregates locally reaching the threshold concentration of the autoinducer earlier than loose structures. To investigate the impact of bacterial aggregation on quorum sensing, we co-transformed bacteria with the photoswitchable adhesins (nMagHigh or pMagHigh, 1:1 ratio) and a quorum sensing reporter plasmid, triggering the production of GFP when quorum sensing is activated. After incubating these co-cultures (OD_{600} = 0.12) for 2 h, we observed comparatively lower quorum sensing reporter activity in samples kept in the dark compared to those under continuous blue light illumination (**fig. 2.4**c; **fig. S2.1**b, Supporting Information). Remarkably, samples subjected to pulsed illumination (5:20 or 5:30) exhibited a two-fold increase in reporter signal compared to samples exposed to constant blue light. Conversely, samples kept under pulsed illumination with shorter periods of darkness (5 min off) or with shorter or longer durations of light showed similar levels of quorum sensing reporter as the constant blue light sample (**fig. 2.4**d). Notably, the more intense reporter signals were localized to larger bacterial aggregates. Overall, the activation of quorum sensing correlated with both cluster size and fractal dimension.

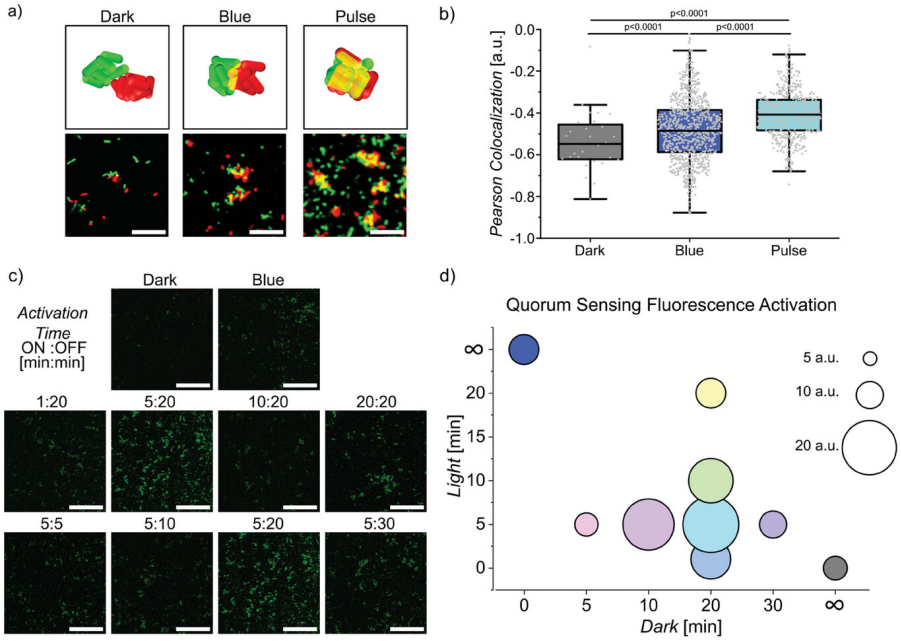

Figure 2.4: Bacterial mixing and quorum sensing. a) Preformed aggregates of *E. coli* expressing nMagHigh and pMagHigh labeled with GFP (shown in green) or mCherry (shown in red) were mixed and allowed to further interact under different illumination settings. Scale bars are 30µm. b) Clusters formed under 5:20 pulse illumination, showed more intermixing of GFP and mCherry expressing bacteria than under blue light or in the dark as confirmed with a higher PCC, p-values from t-tests. c) Confocal microscopy images of *E. coli* with a quorum sensing GFP reporter plasmid and expressing nMagHigh or pMagHigh at their surface under different illumination settings. Scale bars are 50µm. d) Average GFP fluorescence of bacteria in (c). Images in (c) at 5:20 are shown twice to make trends visible but come from the same experiment. All experiments were performed in 3 biological replicates with 3 technical replicates each.

2.2.6. Biofilm Formations is Influenced by Bacterial Cell-Cell Adhesion Dynamics

Bacterial aggregation constitutes an early and pivotal stage in biofilm formation, with these microcolonies serving as structural units that prime the subsequent maturation of the biofilm. To investigate the impact of bacterial cell-cell adhesion dynamics on biofilm mesostructure and maturation, we produced biofilms using 1:1 cocultures of E. coli MG1655 expressing adhesins nMagHigh (co-expressing cyan fluorescent protein, eCFP, depicted in green) and pMagHigh (co-expressing yellow fluorescent protein, eYFP, depicted in red) for 48 h at 37 °C under various illumination conditions. (eCFP and eYFP, being point mutants of each other, are expected to impose an equal metabolic burden.)

We found that biofilms grown under pulsed illumination exhibited the highest overall biomass and denser structures compared to those formed under continuous blue light illumination or in the dark, as evidenced by confocal microscopy (**fig.** 2.5a). In addition, biofilms formed under continuous blue light illumination were thicker than those formed in the dark. Specifically, the average thickness was 16, 30, and 42 µm for biofilms formed in the dark, under continuous blue light and pulsed blue light, respectively. These observations were further supported by crystal violet staining of biofilms in microplates, demonstrating higher total biomass under pulsed light illumination (**fig. S**2.5, Supporting Information).

A detailed analysis of the biofilms, encompassing mesostructure, surface properties, and bacterial distribution, was conducted using the automated image analysis tool for biofilms, Comstat 2, revealing pronounced morphological differences (**fig.** 2.5b; **fig. S**2.6, Supporting Information). Biofilms grown under pulsed light exhibited significantly higher biomass, with a 6.7- and 5.1-fold increase compared to biofilms grown in the dark and under constant blue light illumination, respectively. Furthermore, these biofilms formed under pulsed light displayed smoother surfaces and higher packing density compared to biofilms formed in the dark and under continuous blue light, as indicated by a lower surface-to-volume ratio, a higher average fractal dimension, and a lower roughness coefficient (**fig.** 2.5c). These findings align with our earlier observations of denser bacterial clusters forming under pulsed light. Additionally, biofilms formed under pulsed light exhibited 7- and 5-fold higher average diffusion distances compared to those formed in the dark and under continuous blue light, indicating enhanced connectivity between microdomains.

Drawing an analogy to states of matter, biofilms formed under pulsed illumination—where bacteria exhibit liquid-like behavior—demonstrated enhanced intermixing. Like in bacterial aggregation, liquid-like behavior played a role in bacteria optimizing their positions to maximize contact with neighbors by filling gaps within the biofilm. In contrast, biofilms formed under continuous blue light exhibit solid-like characteristics, resulting in rougher biofilms. It is noteworthy that strong and permanent bacterial cell-cell adhesions do not lead to more mature

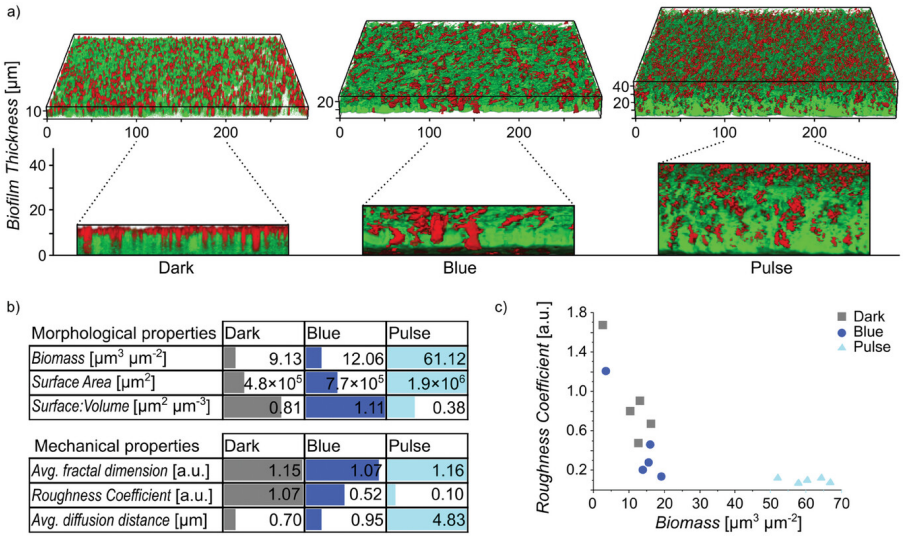

Figure 2.5: Pulse illumination enhances biofilm formation and properties. a) 3D and side view confocal microscopy images of biofilms formed with cocultures of nMagHigh- and pMagHigh- bacteria (shown in green and red, respectively) after 48 h under dark, blue, and pulsed illumination. b) COMSTAT analysis of biofilms. Both mechanical and morphological properties of biofilms were improved under pulsed illumination, resulting in a more massive and compact biofilm. c) Biofilms grown in pulse illumination have a higher biomass and lower surface roughness compared to those grown in the dark or under continuous blue light. ($n = 5$, each independent experiment is shown as one point).

biofilms; rather, the more dynamic and transient adhesions result in enhanced biofilm maturation.

2.2.7. Photoregulation of Bacterial Consortia

In biofilms, diverse bacterial species often come together with various social interactions [40] and such co-cultures bear significant technological importance. Yet, effectively controlling, maintaining, and optimizing these biofilm cocultures is extremely challenging because their success hinges upon numerous factors, including the interplay between different members, the costs and benefits for each participant, the spatial distribution of members, and the availability of nutrients in the medium over time. Consequently, community members within the biofilm adapt their positions based on their needs, relationships (mutualistic, parasitic, commensal, etc.), and environmental factors [41]. We propose that manipulating the illumination conditions can alter the architecture and success of different coculture biofilms, providing a means of optimization.

To investigate this, we introduced the nMagHigh or pMagHigh adhesins onto auxotrophic strains lacking the ability to synthesize threonine (T), proline (P), lysine (K), methionine (M), or tryptophan (W), relying instead on another member

of the community to produce these amino acids for them [42], [43]. The nomenclature of the ten new strains was derived from the amino acid they were unable to produce (T, P, K, M, or W) and the type of adhesin they displayed (n or p). For example, Kn denoted a lysine auxotroph expressing the nMagHigh adhesin. In addition, nMagHigh and pMagHigh expressing strains were labeled with eCFP and eYFP, respectively. Subsequently, we co-cultured the various autotrophic pairs possessing complementary photoswitchable adhesins in minimal M9 medium in the dark, under constant or pulsed blue light illumination. After 48 h of incubation at 37 °C in suspension culture, some pairs demonstrated successful cross-feeding and thrived, showing synergistic growth as monitored by the OD_{600} (optical density at 600 nm) (**fig. 2.6**a). It was intriguing to observe that different co-cultures grew better under specific illumination conditions. The Kn-Mp pair displayed significant growth exclusively in the dark, while the WnKp pair exhibited the highest growth under constant blue light illumination. Contrarily, pulsed light illumination was most favorable for the growth of the three pairs Pn-Kp, Pn-Mp, and KnMp. These initial findings underscore the fact that there is not one procedure that fits all co-cultures and factors beyond bacterial cell-cell adhesion dynamics may be decisive. Nevertheless, in certain cases, cell-cell adhesions prove to be crucial, enabling the adjustmentofproximity between membersand balancing the cost of producing a common good with the benefit derived from receiving metabolites from the other member. Yet, these seem to be extremely sensitive to the precise context, and differences in the metabolic adaptations of the autotrophs seem to of significant. For instance, even switching the places of nMagHigh and pMagHigh, which only differ in two amino acids (D52R and G55R), between the two auxotrophic strains pair altered the outcome.

To examine the differences in biofilm architecture for these auxotrophic pairs, we formed biofilms using pairs that showed significant differences in growth depending on the illumination (**fig. 2.6**b). Different co-cultures formed the thickest biofilms and showed different mesostructures under different illumination conditions, aligning with results from the growth analysis in suspension culture. The Kn-Mp pair formed the thickest biofilms in the dark, almost twice as thick as under continuous or pulsed light. The Wn-Kp pair grew most successfully under continuous blue light, forming a layered biofilm (Wn at the bottom shown in green, Kp at the top shown in red). Finally, the Pn-Kp and Pn-Mp pairs grew the thickest biofilms under pulsed light illumination, with the Pn-Kp strains mixing within the biofilm and the Pn-Mp pair forming a layered biofilm. These differences in biofilm architecture were also visible in the COMSTAD analysis (**fig. S2.7**, Supporting Information), where the thicker biofilms came along with a lower roughness coefficient and higher biomass (**fig. 2.6**c). It is also notable that we were able to regulate the ratio of each constituent strain of bacteria with different illumination settings (**fig. 2.6**d). While we initially mixed the nMagHigh and pMagHigh expressing strains in equal numbers, the biomass fraction of each member changed with

different illumination settings. In some cases, the ratio changed significantly to form the most successful biofilm, as seen in the Kn-Mp culture in the dark where the former outnumbers its neighbor in an 8:2 ratio. In contrast, in the biofilm of Pn-Mp, which grew the best under pulsed light illumination, the ratio remained the same as the initial seeding condition. In the case of blue light and pulse illumination, the higher growth may be linked to a more efficient metabolic exchange between the two strains due to stronger cell-cell adhesions. Yet, in this optimization process, bacterial motility and hence the fluidity within the biofilms at certain stages appear to be important factors. Microbial industrial fermentations usually rely on cocultures of different bacteria strains to carry out the energetically costly synthesis of metabolites [44]. However, minor differences in factors such as growth rate, inoculation density, or preculture age of bacteria used in such processes, lead to the faster member of a coculture outcompeting the others and establishing a monoculture [45]. The described photoswitchable adhesions and different illumination protocols may be used to counteract these challenges.

2.2.8. Pulsed Light Promotes the Production of *L*-Threonine in Immobilized Fermentation

Biofilm bioreactors are of great industrial importance for the production of high-value metabolites. A previous study has already demonstrated that continuous photoactivation of nMagHigh-pMagHigh surface adhesins enhances the production yield of *L*-threonine in immobilized continuous fermentation using *E. coli* W1688 [46]. Here, we hypothesized that pulsed illumination could further improve biofilm formation, fermentation, and bioproduction.

To investigate this, we quantified the biofilm formation process during immobilized fermentation experiments and assessed the yield of *L*-threonine produced by cocultures of nMagHigh and pMagHigh expressing strains (*E. coli* W1688 ΔycgF) under different illumination conditions, including dark, blue light, and pulsed illumination (5:20). The result of crystal violet staining assay revealed that under pulse conditions there was a significant (27.4%) increase in biofilm mass after 24 h compared to the dark treatment (**fig. S2.8**a,b, Supporting Information). Analogously, we produced under different illumination the biofilms on a cotton fiber carrier in a batch biofilm bioreactor, which is suitable for industrial scale-up, and measured *L*-threonine production and glucose consumption (**fig. 2.7**a). Under constant and pulsed illumination, we observed that from batch to batch the *L*-threonine yield increased and the fermentation period stabilized gradually after three cycles, both indicative of a more mature biofilm forming. In the seventh batch of immobilized fermentation in the dark, *L*-threonine yield was $11.47\,\mathrm{g\,L^{-1}}$ with a fermentation period of 34 h marked by low glucose levels. Under blue light conditions in the same batch, the *L*-threonine yield increased by 16.22% to $13.33\,\mathrm{g\,L^{-1}}$ and the fermentation period decreased by 3 to 31 h compared to the dark condition. The highest *L*-threonine yield of $15.61\,\mathrm{g\,L^{-1}}$ was achieved under pulse illumination, resulting in

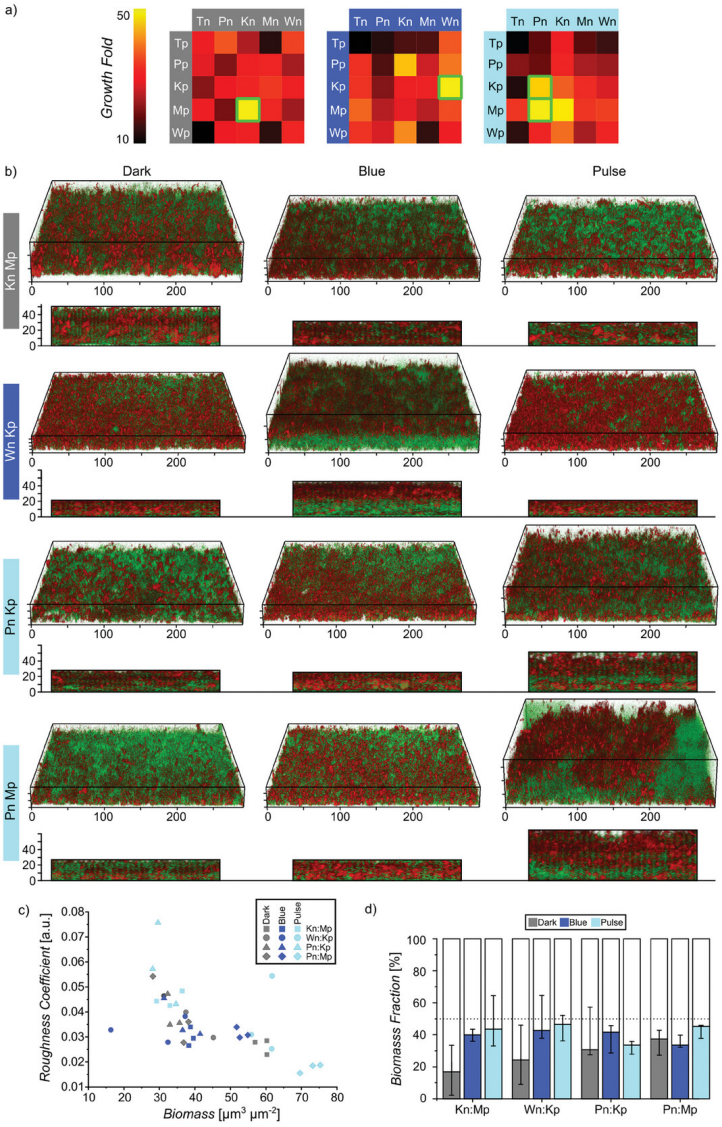

Figure 2.6: Pulsed illumination affects metabolic cooperation pathways in cross-feeding cultures. a) Growth of cocultured auxotrophic strains displaying nMagHigh or pMagHigh after 48 h under different illumination settings in suspension culture. Cocultures thrive in different illumination conditions outlined in green. The experiments were conducted in three biological replicates. b) 3D and side view confocal microscopy images of selected coculture pairs under different illumination settings. nMagHigh and pMagHigh expressing bacteria are shown in green and red, respectively. Scale bars in µm. c) Surface roughness versus biomass for different cocultures under various illumination conditions. (n = 3, each point represents one sample) d) Biomass fraction of nMagHigh (shaded) and pMagHigh (white) for different cocultures that all started at equal numbers. Error bars represent the SD of three biological replicates.

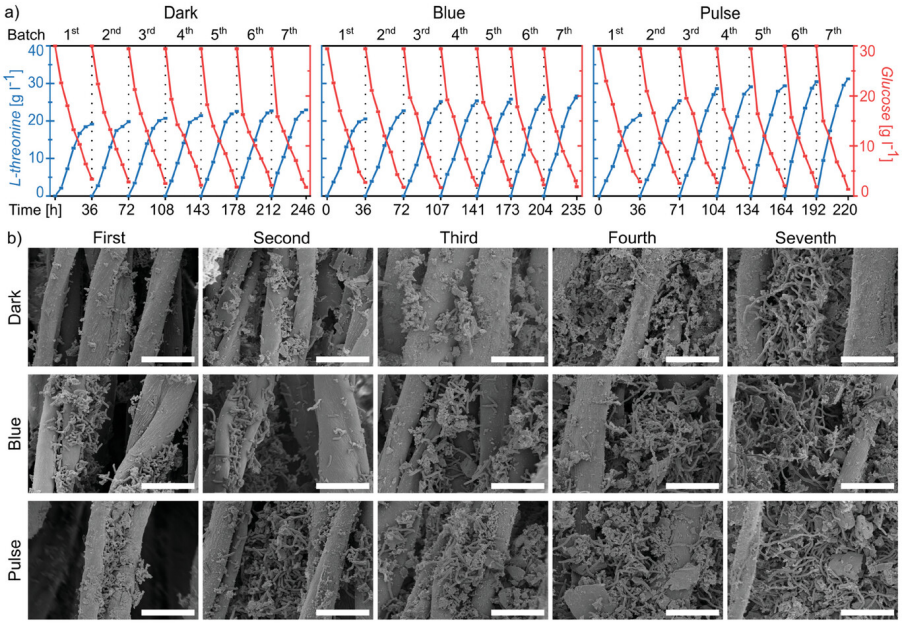

Figure 2.7: Pulse illumination increases biomass and positively affects *L*-threonine production and glucose consumption in immobilized continuous fermentation. a) Along seven fermentation batches, 5:20 pulsed illumination increases the overall yield of *L*-threonine and reduces the batch duration during fermentation in comparison with continuous dark or blue illumination. b) SEM images show that pulse illumination improves the development of surface biofilm on the fermentation carriers. Scale bars are 20µm.

a 36.09% increase compared to dark and a fermentation period reduced by 6 hours, totaling 28 h. To further validate the effectiveness of this strategy, we examined the biofilm structure on the carriers at different time points using scanning electron microscopy (SEM) (**fig. 2.7**b). The SEM images after the first, second, third, fourth, and seventh batches of immobilized fermentation, qualitatively show a gradual increase in the total amount of biofilms from batch to batch, where pulsed illumination produced a greater mass of biofilms which formed within a shorter time. In contrast, there was no effect of light illumination on the *L*-threonine yield nor on the fermentation period in cultures of free-floating bacteria (**fig. S2.8**c, Supporting Information). Overall, in the immobilized fermentation system, both *L*-threonine yield was higher and the fermentation periods were shorter under pulsed light illumination than in the dark or under constant illumination. Therefore, this method holds great potential for enhancing fermentation efficiency and reducing fermentation costs for industrial fermentation processes.

2.3. CONCLUSION

In this study, we tuned bacterial cell-cell adhesion dynamics to alter bacterial aggregation and behavior using photoswitchable adhesions. We showed that pulsed light leads to higher aggregation levels along with bigger and more compact clusters of bacteria compared to continuous light illumination. Using individualbased simulations, we could understand this being the result of different bacteria cell-cell adhesion dynamics, which depend on the interplay of the decay rate of the adhesins with the off-time of the pulsed illumination. Thus, analogous to different states of matter, bacterial aggregates display gas-like, liquid-like, and solid-like behavior in the dark, under pulsed illumination, and under continuous illumination, respectively. We subsequently demonstrate that bacterial aggregates with liquid-like behavior have higher particle intermixing and activate quorum sensing earlier. Moreover, biofilms grew thicker and denser under pulse illumination than under constant blue light or in the dark, highlighting the importance of cell-cell adhesion dynamics in biofilm maturation. We then applied this knowledge to cocultures of different pairs of auxotrophic bacteria, where biofilm growth was significantly affected by light conditions. Here, some pairs indeed did best under pulsed light, whereas others grew best under dark or constant light conditions. Hereby showing that, depending on the system, different light conditions can be employed to optimize cocultures. Finally, we improved *L*-threonine production of biofilms in bulk bioreactors by subjecting the biofilms to pulseillumination, leading to better biofilms, and subsequently higher *L*-threonine yield and shorter fermentation times. Hereby, showing that pulse-illumination can be effectively applied in biotechnological and industrial settings to optimize biofilm formation.

The parallels between phase transitions, colloidal self-assembly, and the assembly of multicellular structures are remarkable. Like for colloidal particles, it is possible for bacterial aggregates to transition from solid-like DLCA under kinetic control to liquid-like RLCA under thermodynamic control by simply increasing the exchange rate between the colloids/bacteria. Moreover, we found similar behavior also during the self-assembly and self-sorting with photoswitchable cell-cell adhesions in mammalian cells [47]. Yet, it should be noted that at later stages of biofilm development, the analogy is distorted by the growth of bacteria, the production of extracellular polymers, and cell differentiation within the biofilm over time. From this perspective, the maturation of a biofilm could be viewed as a transition from gaslike planktonic bacteria to liquid-like microcolonies that become more solid with time. Differently from the light-induced adhesion used here, bacteria alter these cell-cell interaction dynamics through the expression of surface proteins and secreted extracellular polymers [9]. Nonetheless, also within the mature biofilm, the cell-cell adhesion dynamics are clearly of significance, as they determine bacterial mobility and colony fluidity and the dispersion for future colonization.

Optogenetics is increasing in its importance to control bioproduction, cocultures of bacteria, and structuring biofilms, as light is a cheap stimulus that pro-

vides superb spatiotemporal and quantitative control [48], [49]. Illumination with external periodic light stimuli is straightforward to implement in existing reactor designs with no concerns about contamination or offtargeting. Existing tools already allow for optogenetic modulation of bacterial growth to maintain stable co-cultures over long periods [50] and specifically tune the activation of different pathways as desired [45], [51], [52]. Moreover, the light-inducible production of various biofilm-forming molecules also makes it possible to pattern biofilms with high fidelity [28]–[32], [53]. The here presented tuning over cell-cell adhesion dynamics adds another modality to enhance biofilm formation and cocultures that is regulated directly at the level of adhesions and not gene expression. This allows for faster on/off dynamics that are required at the time scale of microcolony formation and biofilm compacting and leaves the possibility to combine with other approaches to modulating biofilms.

In summary, the dynamics of cell-cell adhesion are just as important as the interaction strength in determining the bacterial behavior including quorum sensing and biofilm formation. The photoswitchable bacterial cell-cell adhesions provide a straightforward approach to altering the cell-cell adhesion dynamics and the associated processes systematically. Here, we demonstrate how important cell-cell adhesion dynamics are in engineering bacterial communities at the micro- and mesoscopic scale with potential use in research and industrial applications.

2.4. Experimental Section

Plasmids, Bacteria and Materials: The plasmids pB33-nMagHigh-eCPX or pB33-pMagHigh-eCPX (chloramphenicol resistant, *L*-arabinose inducible) were previously described [34]. Plasmids expressingGFP, mCherry, eCFP, and eYFP in a pTrc99A vector (ampicillin resistant, IPTG inducible) and the quorum sensing plasmid pUA66-P*lsr*-eGFP [9](kanamycin resistant) were a gift from Prof. Victor Sourjik (Max Planck Institute for Terrestrial Microbiology). *E. coli* K-12 MG1655 was purchased from DSMZ and the auxotrophic BL21 (DE3) *E. coli* strains RF2 (Addgene plasmid # 62070, T), RF6 (Addgene plasmid # 62074, P), RF10 (Addgene plasmid # 62076, K), RF11 (Addgene plasmid # 61961, M), and RF12 (Addgene plasmid #62077, W) were a gift from Robert Gennis and Toshio Iwasaki [54].

All chemicals were purchased from Sigma-Aldrich. Eight-well slides (µSlide, 8-well glass bottom) are from ibidi and 96-well microplates are from Greiner Bio-One. The illumination setup used was built with off-the-shelf components including 460 nm LED strips connected to a power regulator, which controlled the intensity, and a programmable timer plug which regulated the pulsing frequency.

Bacterial Strains: *E. coli* K-12 MG1655 was co-transformed with plasmids expressing one of the photoswitchable adhesins (pB33-nMagHigheCPX or pB33-pMagHigh-eCPX) and one of the plasmids expressing a fluorescent protein (pTrc99A- mNeonGreen, mCherry, eYFP or eCFP) or the quorum sensing reporter plasmid (pUA66-P*lsr*-eGFP). All overnight cultures were grown at 37 °C and 250

rpm covering the tubes in aluminum foil to keep samples dark.

Aggregation Assay and Analysis: A single colony of the desired strains (nMagHigh-eCPX/ pTrc99A-mNeonGreen or pMagHigh-eCPX/ pTrc99AmCherry) were picked and cultured in LB medium (10 ml) in the presence of the appropriate antibiotics and inducers (50 µg mL^{-1} ampicillin, 35 µg mL^{-1} chloramphenicol, 0.04% *L*-arabinose, 100 µM IPTG) overnight. Next, the bacteria were diluted in phosphate saline buffer (PBS) to an OD_{600} = 0.12, and cultures expressing complementary photoswitchable adhesins were mixed in a 1:1 ratio. Aliquots of 300 µL were added into 8well slides and incubated at 22 °C under the desired illumination setting (460 nm LED, 300 µW cm^{-2}) for 2 h without shaking. All experiments were performed in 3 biological replicates with 3 technical replicates each.

Microscopy images were acquired on an inverted confocal laser scanning microscope (CLSM, Leica TCS SP8) equipped with a 488 and 552 nm laser for imaging the mNeonGreen and mCherry respectively, and a 40x water-immersion objective. For each sample, 25 images (290 × 290 µm each, total area ca. 2.1 mm^2) were acquired in the mNeonGreen and mCherry channels. All images were processed in FIJI.

To analyze bacterial aggregation, the images in the GFP and mCherry channelswere merged andconverted intoa binaryimage. All bacteria(area ≥ 2 µm^2, area of a single bacteria) and clustered bacteria (area ≥ 35 µm^2, area of at least 15 bacteria) were detected using the Analyze Particles function in FIJI. The aggregation ratio is equal to the total area occupied by clustered divided by the total area occupied by all bacteria. The fractal dimension of the bacterial clusters (area ≥ 35 µm^2) was quantified using the FracLac plugin for FIJI [55], [56].

Individual-Based Simulations: We model our bacteria as spherocylindrical particles as previously implemented [57] with diameter D = 1 µmand a length taken from a uniform distribution between 1 and 2 µm. Because the bacteria in the experiments tend to sediment to the bottom of the wells quite quickly and only the bottom layer is imaged, we initialize the particles in a thin slab right above the surface with periodic boundary conditions on the x and y axis (2000 particles in a 110 × 110 × 5 box). For each time step, the forces on each particle are calculated, and their positions are updated accordingly, using an overdamped dynamics model. The amount of timesteps per experimental minute is set to 25 000.

The particles are subject to Brownian motion which is implemented by giving each end of the particles a kick in a random direction and with a magnitude taken from a normal distribution with mean 0 and standard deviation σ_{bf}. A suitable value for σ_{bf} was chosen by first, estimating the diffusion coefficient for a spherical particle of the same diameter, suspended in PBS buffer. Correcting for the fact that the diffusion takes place near a wall [58], and that the particles are spherocylindrical with an aspect ratio of three [59], gave us a diffusion constant of $D_{\text{particle}} = 0.024\,\mu\text{m}^2\,\text{s}^{-1}$. Measuring the MSD after one hour for 2000 particles we find that $\sigma_{bf} = 1 \cdot 10^{-3}$ gives us an MSD of the expected ≈500 µm^2 (**fig. S2.3**, Sup-

porting Information). For each particle pair that is within reach of each other, the shortest distance between the two particles is determined. The magnitude of the adhesive force they experience depends on this distance r in the following way:

$$F(r) = P \cdot \frac{r}{\alpha} \cdot e^{-\frac{r-\alpha}{\alpha}}, \qquad \text{for } r \geq 0, \tag{2.2}$$

$$F(r) = K_0 \cdot r, \qquad \text{for } r < 0, \tag{2.3}$$

where α determines the interaction range and P determines the amplitude of the attractive forces. If there is overlap between the particles, the force is taken to be in the form of a spring force with spring constant K. The resulting force is then distributed over the two end-points of the particle inversely related to where the closest point is situated along the length of the particle. Because the membrane proteins are not more than a couple of nanometers across, we argue that the range of the interaction should be around twice their size ($\approx 5\,\text{nm}$). The interaction strength should be quite strong, so that once the particles adhere to each other or to the surface, they would not come apart due to Brownian forces. Particles also interact with the surface; this interaction does not depend on the light conditions. The surface adhesion works on both ends of the particles separately because we know that surface interaction is mostly modulated on the ends of *E. coli* [59]. The magnitude of the surface adhesion for each endpoint is calculated as follows:

$$F_{\text{surface}}(r) = S \cdot \frac{r}{\beta} \cdot e^{-\frac{r-\beta}{\beta}}, \qquad \text{for } r \geq 0, \tag{2.4}$$

$$F_{\text{surface}}(r) = K_0 \cdot r, \qquad \text{for } r < 0, \tag{2.5}$$

we chose the magnitude of this adhesion such that it is weaker than the adhesion between particles but stronger than the Brownian forces because we know from the experiments that clusters can pull single particles off the surface. By comparing the aggregation curves under constant blue light over a span of 6 hours between the experiments [34] and simulations we settled on values $P = 5 \cdot 10^{-3}$ and $S = 5 \cdot 10^{-4}$ with ranges $\alpha = 5\,\text{nm}$ and $\beta = 10\,\text{nm}$ (**fig. S2.4**a,b, Supporting Information). Please note that, even though higher adhesive strengths gave a better fit to the data, this resulted in artifacts in the simulations in the form of fast-spinning particles (not shown). Additionally, we show that changing the range α does not affect the results significantly (**fig. S2.4**c, Supporting Information).

Four times every experimental minute, all the particle coordinates and orientations were logged. These were then used to create images of the bottom $1.2\,\mu\text{m}$ slab of the simulation box, which is the z resolution of the microscope used, using Python. The images were then analyzed using ImageJ in the same way that is used for the experimental images (Analyze Particles, etc.). We use this data to track the aggregation ratio and cluster size over the course of the simulation experiments. We also measure the fractal dimension using Fraclac. We also tracked which particles were within each particle's vicinity by logging the neighbors' particle ID's.

Quorum Sensing Activation: Single colonies of the desired strains (nMagHigh-eCPX/pUA66-P*lsr*-eGFP or pMagHigh-eCPX/pUA66-P*lsr*eGFP) were picked and cultured in LB broth (10 mL) with the respective antibiotics (50 µg mL^{-1} ampicillin, 35 µg mL^{-1} chloramphenicol) incubated. The overnight cultures were diluted 1:1000 into 10 mL LB medium supplemented with antibiotics and 0.04% *L*-arabinose. The bacteria were cultured in the dark at 37 °C, at 200 rpm for 3–4 h until OD_{600} = 0.6 was reached. Both cultures were diluted with PBS to OD_{600} = 0.12 and mixed in a 1:1 ratio. Aliquots of 300 µL were added into an 8-well slide and incubated at 22 °C under the respective illumination setting for 2 h. Confocal microscopy images were acquired in the GFP channel and the eGFP reporter signal was quantified with FIJI using the Integrated Density measurement. All experiments were performed in 3 biological replicates with 3 technical replicates each.

Biofilm Formation: Overnight cultures of the desired strains (nMagHigh-eCPX/ pTrc99A-eCFP or pMagHigh-eCPX/ pTrc99A-eYFP) were grown in the presence of antibiotics and inducers (50 µg mL^{-1} ampicillin, 35 µg mL^{-1} Chloramphenicol and inducers 0.04% *L*-arabinose, 100 µM IPTG). The next day, the cultures were diluted into LB medium supplemented with antibiotics and inducers to reach an OD_{600} = 0.01. The two strains were mixed in a 1:1 ratio, and 300 µL aliquots were transferred to 8-well slides. The samples were incubated at 37 °C without shaking under the respective illumination setting for 48 h. The samples were rinsed three times with water, and z-stacks were acquired using the CLSM using the 405 and 488 nm lasers for fluorescence activation of eCFP (475–495 nm) and eYFP (540-560 nm), respectively. The biofilms were 3D reconstructed using the 3D Viewer from the Leica LAS X software. Details of the biofilm morphology were analyzed using the COMSTAT 2 plug-in in FIJI. All experiments were performed in 5 biological replicates.

For crystal violet staining we used a modified version of previously described protocols [60], where the experiment was repeated as described above but the bacteria were only transformed with nMagHigh-eCPX or pMagHigh-eCPX and 200 µL aliquots of the coculture were added into 96well round bottom plates. After 48 h incubation, the samples were gently rinsed three times with water, each well then received 200 µL of a 0.1% solution of crystal violet in water and were incubated for 15 min at room temperature. Then, the wells were rinsed three times with water and the remaining crystal violet was solubilized by adding 200 µL of 30% acetic acid in water. Finally, the solution was diluted 1:5 with water and the absorbance at 550 nm was measured in flat-bottomed transparent 96-well microplates using a plate reader (TECAN Spark). The experiments were conducted in three biological replicates.

Auxotrophic Bacterial Cocultures: Overnight cultures of the desired auxotroph strains (RF2, RF6, RF10, RF11, RF12 were a gift from Robert Gennis and Toshio Iwasaki; Addgene #: 62070, 62074, 62076, 61961, and 62077, respectively) transformed with the photoswitchable adhesins and a fluorescent label (nMagHigh-eCPX/ pTrc99A- eCFP or pMagHigh-eCPX/ pTrc99A- eYFP) were grown in the

presence of antibiotics and inducers (50 µg mL^{-1} ampicillin, 35 µg mL^{-1} Chloramphenicol and inducers 0.04% *L*-arabinose, 100 µM IPTG) were spun and resuspended in minimal M9 media with the same antibiotics and inducers, to reach OD_{600} = 0.01 ($\approx 10^7$ cells mL^{-1}). Combinations of these two strains were mixed in a 1:1 ratio and 500 µL aliquots were transferred to flat-bottomed transparent 48-well microplates and incubated at 37 °C and 200 rpm orbital shaking, under the respective illumination setting for 48 h, when the final OD_{600} was measured and the growth fold was calculated respective to the initial bacterial concentration. All experiments were performed in 3 biological replicates.

Biofilm growth of auxotrophic strains was similar as described above, but 300 µL aliquots of selected cocultures were placed on 8-well slides and incubated at 37 °C without shaking under the respective illumination setting for 48 h. Excess media was pipetted out of the wells without disturbing the delicate biofilms and z-stacks were acquired using the CLSM, which were analyzed as described above.

Free-Cell Fermentation, Immobilized Fermentation, and Carrier SEM Analysis: The study involved testing cocultured *E. coli* strains, specifically the ΔycgF + nMag-High and ΔycgF + pMagHigh, through free-cell fermentation and immobilized continuous fermentation. Cotton fiber carriers previously characterized for industrial fermentation[61], [62], were taken from the fermentation batches and observed through SEM electron microscopy. The methods and instrumentation were employed as previously described [46], illumination conditions set to dark, blue (450 nm; 500 lux), and 5:20 ON:OFF pulses.

Co-cultured *E. coli* ΔycgF + nMagHigh and ΔycgF + pMagHigh were subjected to free-cell fermentation, immobilized continuous fermentation, and their carriers were photographed by SEM electron microscopy. The methods and instrumentation used in the above experiments were also modified from previous literature [46] to include our current illumination settings.

Acknowledgements

This work has been funded by the Deutsche Forschungsgemeinschaft (DFG WE 5745/2-2) and supported by the National Natural Science Foundation of China (Grant No.: 22208157). A research visit of RL was made possible by funding from the Casimir Research School.

Open access funding enabled and organized by Projekt DEAL.

Author Contributions

J.J.Q.H., F.C., and S.V.W. designed the experiments; J.J.Q.H. performed the experiments with support from F.C., analyzed the data, and prepared the figures. R.L. conducted the computational simulations under the guidance of T.I.. S.S., W.S., and Y.C. characterized *L-threonine* production under different conditions. All authors read and reviewed the results and approved the final version of the manuscript.

BIBLIOGRAPHY

[1] J. J. Quispe Haro, F. Chen, R. Los, *et al.*, "Optogenetic control of bacterial cell-cell adhesion dynamics: Unraveling the influence on biofilm architecture and functionality", *Advanced Science*, vol. 11, p. 2 310 079, 2024.

[2] H.-C. Flemming, J. Wingender, U. Szewzyk, P. Steinberg, S. A. Rice, and S. Kjelleberg, "Biofilms: An emergent form of bacterial life", *Nature Reviews Microbiology*, vol. 14, pp. 563–575, Sep. 2016.

[3] P. Stoodley, K. Sauer, D. G. Davies, and J. W. Costerton, "Biofilms as complex differentiated communities", *Annual Review of Microbiology*, vol. 56, pp. 187–209, Volume 56, 2002 Oct. 1, 2002.

[4] N. Kouzel, E. R. Oldewurtel, and B. Maier, "Gene transfer efficiency in gonococcal biofilms: Role of biofilm age, architecture, and pilin antigenic variation", *Journal of Bacteriology*, vol. 197, pp. 2422–2431, Jul. 2015.

[5] J. Lawrence, G. Swerhone, U. Kuhlicke, and T. Neu, "In situ evidence for microdomains in the polymer matrix of bacterial microcolonies", *Canadian Journal of Microbiology*, vol. 53, pp. 450–458, Mar. 2007.

[6] G. O'Toole, H. B. Kaplan, and R. Kolter, "Biofilm formation as microbial development", *Annual Review of Microbiology*, vol. 54, pp. 49–79, Volume 54, 2000 Oct. 1, 2000.

[7] L. Vidakovic, P. K. Singh, R. Hartmann, C. D. Nadell, and K. Drescher, "Dynamic biofilm architecture confers individual and collective mechanisms of viral protection", *Nature Microbiology*, vol. 3, pp. 26–31, Jan. 2018.

[8] L. Hall-Stoodley, J. W. Costerton, and P. Stoodley, "Bacterial biofilms: From the natural environment to infectious diseases", *Nature Reviews Microbiology*, vol. 2, pp. 95–108, Feb. 2004.

[9] L. Laganenka, R. Colin, and V. Sourjik, "Chemotaxis towards autoinducer 2 mediates autoaggregation in escherichia coli", *Nature Communications*, vol. 7, p. 12 984, Sep. 30, 2016.

[10] K. Sauer, A. K. Camper, G. D. Ehrlich, J. W. Costerton, and D. G. Davies, "Pseudomonas aeruginosa displays multiple phenotypes during development as a biofilm", *Journal of Bacteriology*, vol. 184, pp. 1140–1154, Feb. 2002.

[11] M. Cavaliere, S. Feng, O. S. Soyer, and J. I. Jiménez, "Cooperation in microbial communities and their biotechnological applications", *Environmental Microbiology*, vol. 19, pp. 2949–2963, 2017.

[12] R. Hartmann, P. K. Singh, P. Pearce, *et al.*, "Emergence of three-dimensional order and structure in growing biofilms", *Nature Physics*, vol. 15, pp. 251–256, Mar. 2019.

[13] A. J. Paula, G. Hwang, and H. Koo, "Dynamics of bacterial population growth in biofilms resemble spatial and structural aspects of urbanization", *Nature Communications*, vol. 11, p. 1354, Mar. 13, 2020.

[14] W. Pönisch, K. B. Eckenrode, K. Alzurqa, *et al.*, "Pili mediated intercellular forces shape heterogeneous bacterial microcolonies prior to multicellular differentiation", *Scientific Reports*, vol. 8, p. 16 567, Nov. 8, 2018.

[15] W. Liu, J. Russel, M. Burmølle, S. J. Sørensen, and J. S. Madsen, "Micro-scale intermixing: A requisite for stable and synergistic co-establishment in a four-species biofilm", *The ISME Journal*, vol. 12, p. 1940, Aug. 2018.

[16] Z. You, D. J. G. Pearce, A. Sengupta, and L. Giomi, "Geometry and mechanics of microdomains in growing bacterial colonies", *Physical Review X*, vol. 8, p. 031 065, Sep. 12, 2018.

[17] B. Maier, "How physical interactions shape bacterial biofilms", *Annual Review of Biophysics*, vol. 50, pp. 401–417, May 6, 2021.

[18] N. Rana, P. Ghosh, and P. Perlekar, "Spreading of nonmotile bacteria on a hard agar plate: Comparison between agent-based and stochastic simulations", *Physical Review E*, vol. 96, p. 052 403, Nov. 7, 2017.

[19] M. Basaran, Y. I. Yaman, T. C. Yüce, R. Vetter, and A. Kocabas, "Large-scale orientational order in bacterial colonies during inward growth", *eLife*, vol. 11, P. Sens, A. M. Walczak, and S. Shankar, Eds., e72187, Mar. 7, 2022.

[20] A. Welker, T. Cronenberg, R. Zöllner, *et al.*, "Molecular motors govern liquidlike ordering and fusion dynamics of bacterial colonies", *Physical Review Letters*, vol. 121, p. 118 102, Sep. 11, 2018.

[21] Z. You, D. J. G. Pearce, and L. Giomi, "Confinement-induced self-organization in growing bacterial colonies", *Science Advances*, vol. 7, eabc8685, Jan. 22, 2021.

[22] E. R. Oldewurtel, N. Kouzel, L. Dewenter, K. Henseler, and B. Maier, "Differential interaction forces govern bacterial sorting in early biofilms", *eLife*, vol. 4, R. Kolter, Ed., e10811, Sep. 24, 2015.

[23] D. Bonazzi, V. Lo Schiavo, S. Machata, *et al.*, "Intermittent pili-mediated forces fluidize *Neisseria meningitidis* aggregates promoting vascular colonization", *Cell*, vol. 174, 143–155.e16, Jun. 28, 2018.

[24] T. Cronenberg, M. Hennes, I. Wielert, and B. Maier, "Antibiotics modulate attractive interactions in bacterial colonies affecting survivability under combined treatment", *PLOS Pathogens*, vol. 17, e1009251, Feb. 1, 2021.

[25] D. S. Glass and I. H. Riedel-Kruse, "A synthetic bacterial cell-cell adhesion toolbox for programming multicellular morphologies and patterns", *Cell*, vol. 174, 649–658.e16, Jul. 2018.

[26] M. T. Kozlowski, B. R. Silverman, C. P. Johnstone, and D. A. Tirrell, "Genetically programmable microbial assembly", *ACS Synthetic Biology*, vol. 10, pp. 1351–1359, Jun. 18, 2021.

[27] W.-F. Song, W.-Q. Yao, Q.-W. Chen, D. Zheng, Z.-Y. Han, and X.-Z. Zhang, "In situ bioorthogonal conjugation of delivered bacteria with gut inhabitants for enhancing probiotics colonization", *ACS Central Science*, vol. 8, pp. 1306–1317, Sep. 28, 2022.

[28] X. Jin and I. H. Riedel-Kruse, "Biofilm lithography enables high-resolution cell patterning via optogenetic adhesin expression", *Proceedings of the National Academy of Sciences*, vol. 115, pp. 3698–3703, Apr. 3, 2018.

[29] L. Pu, S. Yang, A. Xia, and F. Jin, "Optogenetics manipulation enables prevention of biofilm formation of engineered pseudomonas aeruginosa on surfaces", *ACS Synthetic Biology*, vol. 7, pp. 200–208, Jan. 19, 2018.

[30] F. Zhao, M. S. Chavez, K. L. Naughton, *et al.*, "Light-induced patterning of electroactive bacterial biofilms", *ACS Synthetic Biology*, vol. 11, pp. 2327–2338, Jul. 15, 2022.

[31] Y. Huang, A. Xia, G. Yang, and F. Jin, "Bioprinting living biofilms through optogenetic manipulation", *ACS Synthetic Biology*, vol. 7, pp. 1195–1200, May 18, 2018.

[32] Y. Wang, X. Wang, D. Ren, Y. Ma, and C. Wang, "Effect of asymmetry on cooperation in spatial evolution", *Physical Review E*, vol. 103, p. 032 414, Mar. 29, 2021.

[33] F. Chen and S. V. Wegner, "Blue light switchable bacterial adhesion as a key step toward the design of biofilms", *ACS Synthetic Biology*, vol. 6, pp. 2170–2174, Dec. 15, 2017.

[34] F. Chen and S. V. Wegner, "Blue-light-switchable bacterial cell–cell adhesions enable the control of multicellular bacterial communities", *ACS Synthetic Biology*, vol. 9, pp. 1169–1180, May 15, 2020.

[35] F. Kawano, H. Suzuki, A. Furuya, and M. Sato, "Engineered pairs of distinct photoswitches for optogenetic control of cellular proteins", *Nature Communications*, vol. 6, p. 6256, Feb. 24, 2015.

[36] P. Meakin, "Diffusion-controlled aggregation on two-dimensional square lattices: Results from a new cluster-cluster aggregation model", *Physical Review B*, vol. 29, pp. 2930–2942, Mar. 15, 1984.

[37] S. Lazzari, L. Nicoud, B. Jaquet, M. Lattuada, and M. Morbidelli, "Fractal-like structures in colloid science", *Advances in Colloid and Interface Science*, vol. 235, pp. 1–13, Sep. 2016.

[38] K. W. Dunn, M. M. Kamocka, and J. H. McDonald, "A practical guide to evaluating colocalization in biological microscopy", *American Journal of Physiology-Cell Physiology*, vol. 300, pp. C723–C742, Apr. 2011.

[39] S. Mukherjee and B. L. Bassler, "Bacterial quorum sensing in complex and dynamically changing environments", *Nature Reviews Microbiology*, vol. 17, pp. 371–382, Jun. 2019.

[40] L. Goers, P. Freemont, and K. M. Polizzi, "Co-culture systems and technologies: Taking synthetic biology to the next level", *Journal of The Royal Society Interface*, vol. 11, p. 20 140 065, Jul. 6, 2014.

[41] S. Elias and E. Banin, "Multi-species biofilms: Living with friendly neighbors", *FEMS Microbiology Reviews*, vol. 36, pp. 990–1004, 2012.

[42] M. T. Lin, R. Fukazawa, Y. Miyajima-Nakano, *et al.*, "Escherichia coli auxotroph host strains for amino acid-selective isotope labeling of recombinant proteins", *Methods in Enzymology*, vol. 565, pp. 45–66, 2015.

[43] K. Szydlo, Z. Ignatova, and T. E. Gorochowski, "Improving the robustness of engineered bacteria to nutrient stress using programmed proteolysis", *ACS Synthetic Biology*, vol. 11, pp. 1049–1059, Mar. 18, 2022.

[44] C. Aditya, F. Bertaux, G. Batt, and J. Ruess, "A light tunable differentiation system for the creation and control of consortia in yeast", *Nature Communications*, vol. 12, p. 5829, Oct. 5, 2021.

[45] M. A. Lalwani, H. Kawabe, R. L. Mays, S. M. Hoffman, and J. L. Avalos, "Optogenetic control of microbial consortia populations for chemical production", *ACS Synthetic Biology*, vol. 10, pp. 2015–2029, Aug. 20, 2021.

[46] W. Sun, S. Shi, J. Chen, *et al.*, "Blue light signaling regulates escherichia coli w1688 biofilm formation and l-threonine production", *Microbiology Spectrum*, vol. 10, e0246022, Oct. 26, 2022.

[47] M. Mueller, S. Rasoulinejad, S. Garg, and S. V. Wegner, "The importance of cell–cell interaction dynamics in bottom-up tissue engineering: Concepts of colloidal self-assembly in the fabrication of multicellular architectures", *Nano Letters*, vol. 20, pp. 2257–2263, Apr. 8, 2020.

[48] A. Levskaya, A. A. Chevalier, J. J. Tabor, *et al.*, "Engineering escherichia coli to see light", *Nature*, vol. 438, pp. 441–442, Nov. 2005.

[49] S. A. Wegner, R. M. Barocio-Galindo, and J. L. Avalos, "The bright frontiers of microbial metabolic optogenetics", *Current Opinion in Chemical Biology*, vol. 71, p. 102 207, Dec. 2022.

[50] J. Gutiérrez Mena, S. Kumar, and M. Khammash, "Dynamic cybergenetic control of bacterial co-culture composition via optogenetic feedback", *Nature Communications*, vol. 13, p. 4808, Aug. 16, 2022.

[51] L. A. Hartsough, M. Park, M. V. Kotlajich, *et al.*, "Optogenetic control of gut bacterial metabolism to promote longevity", *eLife*, vol. 9, J. Gruber, J. K. Tyler, and W. Mair, Eds., e56849, Dec. 16, 2020.

[52] S. Sankaran, S. Zhao, C. Muth, J. Paez, and A. del Campo, "Toward light-regulated living biomaterials", *Advanced Science*, vol. 5, p. 1 800 383, 2018.

[53] F. Moser, E. Tham, L. M. González, T. K. Lu, and C. A. Voigt, "Light-controlled, high-resolution patterning of living engineered bacteria onto textiles, ceramics, and plastic", *Advanced Functional Materials*, vol. 29, p. 1 901 788, 2019.

[54] T. Iwasaki, R. Fukazawa, Y. Miyajima-Nakano, *et al.*, "Dissection of hydrogen bond interaction network around an iron–sulfur cluster by site-specific isotope labeling of hyperthermophilic archaeal rieske-type ferredoxin", *Journal of the American Chemical Society*, vol. 134, pp. 19 731–19 738, Dec. 5, 2012.

[55] C. A. Schneider, W. S. Rasband, and K. W. Eliceiri, "NIH image to ImageJ: 25 years of image analysis", *Nature Methods*, vol. 9, pp. 671–675, Jul. 2012.

[56] Karperien, A, *Fraclac for imagej*, 2013.

[57] T. Storck, C. Picioreanu, B. Virdis, and D. J. Batstone, "Variable cell morphology approach for individual-based modeling of microbial communities", *Biophysical Journal*, vol. 106, p. 2037, May 5, 2014.

[58] M. Bevan and D. Prieve, "Hindered diffusion of colloidal particles very near to a wall: Revisited", *The Journal of Chemical Physics*, vol. 113, pp. 1228–1236, Jul. 15, 2000.

[59] M.-C. Duvernoy, T. Mora, M. Ardré, *et al.*, "Asymmetric adhesion of rod-shaped bacteria controls microcolony morphogenesis", *Nature Communications*, vol. 9, p. 1120, Mar. 16, 2018.

[60] G. A. O'Toole, "Microtiter dish biofilm formation assay", *Journal of Visualized Experiments: JoVE*, p. 2437, Jan. 30, 2011.

[61] C. Liang, S. Ding, W. Sun, *et al.*, "Biofilm-based fermentation: A novel immobilisation strategy for saccharomyces cerevisiae cell cycle progression during ethanol production", *Applied Microbiology and Biotechnology*, vol. 104, pp. 7495–7505, Sep. 2020.

[62] D. Zhang, F. Wang, Y. Yu, *et al.*, "Effect of quorum-sensing molecule 2-phenylethanol and ARO genes on saccharomyces cerevisiae biofilm", *Applied Microbiology and Biotechnology*, vol. 105, pp. 3635–3648, May 2021.

2.5. SUPPLEMENTARY INFORMATION

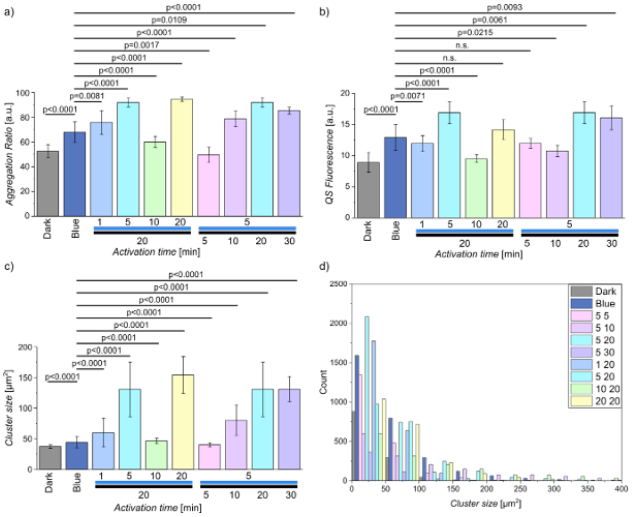

Supplementary Figure 2.1: (a) Average aggregation ratio. (b) Average GFP fluorescence of QS reporter bacteria. (c-d) Cluster size distribution and mean. p-Values correspond to individual t-tests.

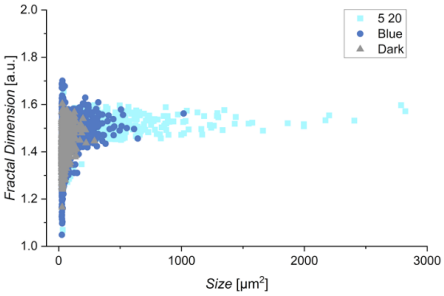

Supplementary Figure 2.2: Correlation of cluster size with fractal dimension.

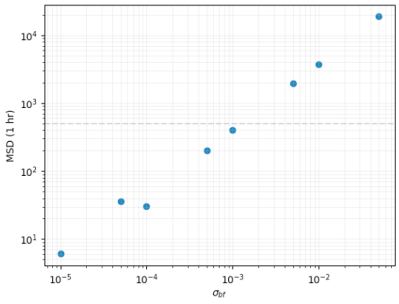

Supplementary Figure 2.3: Mean-squared displacement (MSD) of particles after 1 hour of darkness for different values of σ_{bf}. Dashed line represents the expected MSD for the bacteria at 500 μm^2.

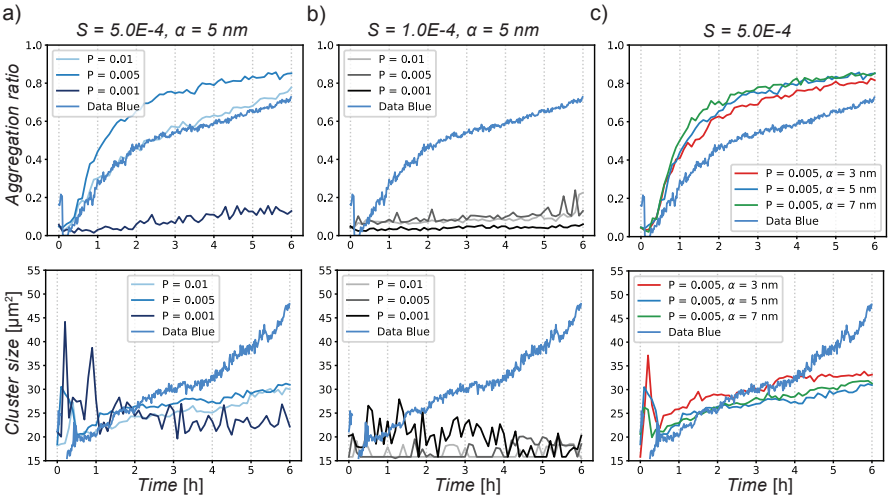

Supplementary Figure 2.4: Determining the parameters of the interaction parameters. Aggregation ratio and cluster size curves for different values of P, S and α.

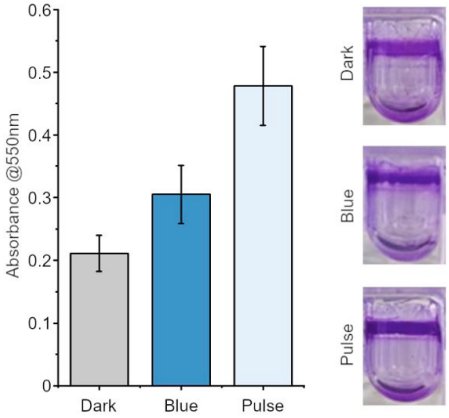

Supplementary Figure 2.5: Pulse illumination enhances biofilm formation of *MG1655 E. coli K-12* expressing nMagHigh and pMagHigh adhesins. Biofilm grown in 96-well plates were stained with crystal violet to quantify the total biofilm biomass by light absorption spectroscopy at 550 nm. Experiments were performed in biological triplicates.

	Dark	Blue	Pulse
Biomass ($\mu m^3\ \mu m^{-2}$)	12.459	15.802	60.448
Maximum diffusion distance (μm):	13.769	13.918	27.431
Average diffusion distance (μm):	0.608	0.768	5.244
Average fractal dimension:	1.145	1.067	1.168
Average thickness (μm):	16.000	31.000	43.000
Roughness Coefficient (Ra*):	0.928	0.465	0.096
Surface Area (μm^2):	5.9×10^5	1.1×10^6	1.7×10^6
Surface to biovolume ratio ($\mu m^2\ \mu m^{-3}$):	0.831	1.305	0.344

Supplementary Figure 2.6: Biofilm analysis from *MG1655 E. coli* K-12 expressing nMagHigh or pMagHigh. Pulse illumination enhances biofilm formation and has a significant effect on all the properties analyzed using COMSTAT.

Kn-Mp Coculture	Dark	Blue	Pulse
Biomass ($\mu m^3/\mu m^2$)	54.227	38.852	32.851
Maximum diffusion distance (μm):	18.997	13.234	12.978
Average diffusion distance (μm):	1.755	1.607	1.125
Average fractal dimension:	1.127	1.150	1.157
Maximum thickness (μm):	103.500	68.000	66.667
Surface Area (μm^2):	1.2E+07	9.1E+06	7.3E+06
Surface to biovolume ratio ($\mu m^2/\mu m^3$):	2.589	2.773	3.454
Average volume of colonies at substratum (μm^3):	4.1E+06	3.3E+06	2.7E+06

Wn-Kp Coculture	Dark	Blue	Pulse
Biomass ($\mu m^3/\mu m^2$)	33.663	36.437	30.799
Maximum diffusion distance (μm):	13.940	13.594	12.996
Average diffusion distance (μm):	1.412	1.266	1.261
Average fractal dimension:	1.163	1.160	1.179
Maximum thickness (μm):	61.667	69.000	60.333
Surface Area (μm^2):	7.4E+06	8.9E+06	6.6E+06
Surface to biovolume ratio ($\mu m^2/\mu m^3$):	2.593	2.906	2.537
Average volume of colonies at substratum (μm^3):	2.7E+06	3.0E+06	2.5E+06

Pn-Kp Coculture	Dark	Blue	Pulse
Biomass ($\mu m^3/\mu m^2$)	37.980	28.673	57.085
Maximum diffusion distance (μm):	15.329	14.428	14.931
Average diffusion distance (μm):	2.016	1.893	1.391
Average fractal dimension:	1.184	1.173	1.199
Maximum thickness (μm):	63.000	59.333	118.000
Surface Area (μm^2):	7.1E+06	7.2E+06	1.5E+07
Surface to biovolume ratio ($\mu m^2/\mu m^3$):	2.233	2.379	3.009
Average volume of colonies at substratum (μm^3):	2.8E+06	2.9E+06	4.6E+06

Pn-Mp Coculture	Dark	Blue	Pulse
Biomass ($\mu m^3/\mu m^2$)	34.390	53.082	72.680
Maximum diffusion distance (μm):	11.793	14.484	17.742
Average diffusion distance (μm):	1.287	1.311	1.964
Average fractal dimension:	1.149	1.163	1.157
Maximum thickness (μm):	68.333	107.667	128.000
Surface Area (μm^2):	8.4E+06	1.3E+07	1.8E+07
Surface to biovolume ratio ($\mu m^2/\mu m^3$):	2.895	2.813	2.865
Average volume of colonies at substratum (μm^3):	2.8E+06	4.4E+06	6.1E+06

Supplementary Figure 2.7: Biofilm analysis from E. coli auxotroph strains expressing nMagHigh or pMagHigh. Pulse illumination allows for tunable responses in biofilm growth and properties of consortia cocultures.

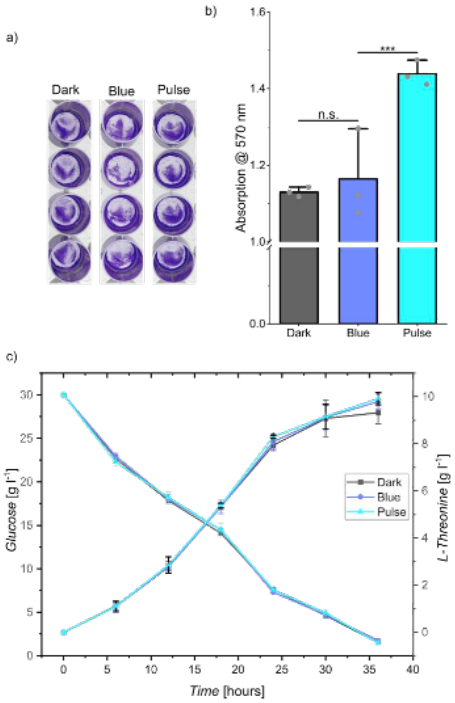

Supplementary Figure 2.8: Effects of various light frequencies on biofilm formation in *E. coli*. (a) *E. coli* ΔycgF + nMagHigh or pMagHigh strains were co-inoculated into a 24-well plate, incubated at 37°C in dark, blue and 5: 20 pulse conditions for 30 h and then imaged after crystal violet staining before washing, and the corresponding absorbance at 570 nm (b) (Student's t-test, n.s.: not significant; ***: $p < 0.001$). Experiments were performed in biological triplicates. (c) Effect of three light frequencies on L-threonine production and glucose consumption in freecell fermentation of *E. coli* ΔycgF expressing the surface adhesins.

3

3D ARCHITECTURE OF GROWING MICROCOLONIES

Rachel LOS, Timon IDEMA

Bacterial biofilms form through initial surface adherence and microcolony development. These processes are influenced by cellular shape, motility, and environmental context. Using an individual-based model, we examine how varying surface and cell-cell adhesion affects biofilm architecture. Our results show that strong surface adhesion leads to flat colonies, while stronger cell-cell adhesion promotes dome-shaped structures. The model can provide various global architectures, but cannot provide variation in internal structure. Despite these limitations, the model effectively simulates diverse and realistic microcolony architectures, providing insights into the mechanical forces.

3.1. INTRODUCTION

Bacteria make up an enormous diversity of the species present on earth. The vast majority of them live in surface-attached communities. A key step in the colonisation of a surface is the initial adherence of one or more cells to a surface, and the subsequent formation of microcolonies [1], [2]. These microcolonies serve as the foundation for biofilm development, significantly influencing the overall architecture and make up of the biofilm [3], [4]. However, the mechanical development of microcolonies is highly complex, varying across different species and environmental conditions.

One critical factor at the cellular level that affects the three-dimensional structure of a colony is cell shape [5], [6]. While primarily species-dependent, cell shape can also be modulated through quorum sensing mechanisms [7]–[9]. Cell motility, including crawling, swimming, or gliding, introduces spatial patterns such as depletion zones and droplet formation [10]–[13]. Biofilms, being surface-attached colonies, require cells to interact with surfaces through mechanisms such as pili formation, general affinity, or anchoring [14], [15]. Additionally, cells can actively modulate their surface attachment which makes them adaptable to different environments and surfaces [16]. These surface interactions can strongly affect colony architecture [14], [17], [18].

The environmental context in which a biofilm establishes itself significantly impacts colony shape as more viscous environments will lead to denser colonies [19]. Bacteria can modulate the viscosity of their environment themselves by excreting polymeric substances [20]. Additionally, bacteria engage in specific cell-cell interactions via adhesive proteins on their membranes [21]–[23]. Taken together, these effects influence the development of the colony's structure through modulation of the cell-density [6], [10], [24].

Experimental and simulation studies have demonstrated that competing forces within a growing colony can drive the transition from a two-dimensional to a three-dimensional structure [25], [26]. This transition could emerge from something as simple as balancing cellular growth and division with friction with the surface [27], but could also include any or all of the other competing effects mentioned above. As a counter force to growth and division, dying cells also influence the structure significantly by inducing heterogeneity in the developing colony [28], [29].

Understanding the establishment and development of bacterial colonies is crucial for addressing challenges in biofouling, bacterial infections, and the biotechnological application of biofilms [29]–[33]. However, due to all these competing processes, individual mechanisms are difficult to isolate. Computational modelling offers valuable insights into these processes, as it allows simplification and isolation of mechanisms and it enables the exploration of parameters that are difficult to probe experimentally. These models help elucidate complex aspects of colony development and architecture [34]–[37].

3.2. METHODS

The model is set up as described in **chapter 1**. In short, we model bacteria as spherocylindrical particles that grow and divide on a surface. The particles have short-range mechanical interactions with each other and with the surface. Each simulation starts with a single particle on a surface. Every five simulation time steps, the particle is grown. The system is then allowed to relax for the other simulation time steps. Each time step, all forces on all the particles are calculated and the particles are moved accordingly, assuming overdamped dynamics. The system is evolved until a colony size of 10 000 particles is reached. Values for the simulation parameters used in this chapter, can be found in **table 3.1**.

Parameter	**Explanation**	**Value**
k_{int}	spring constant of the internal spring	0.1
D	particle diameter	1 µm
L	length of the spring at division	varied
k_{r}	spring constant of the overlap potential	$2 \cdot k_{\text{int}}$
F_{PP}	particle-particle adhesion force magnitude	varied
α	particle-particle adhesion range	5 nm
F_{PS}	particle-surface adhesion force magnitude	varied
β	particle-surface adhesion range	5 nm
R_{int}	interaction range for which mechanical interactions are calculated	$2 \cdot L$
μ	growth rate	2×10^{-4} µm$(5 \cdot \text{ts})^{-1}$
σ_μ	standard deviation for the growth rate noise	$0.1 \cdot \mu$
σ_θ	standard deviation for the orientational noise	0.1
σ_ϕ	standard deviation for the orientational noise in the z-direction	0.01

Table 3.1: Explanation and values used for the simulation parameters.

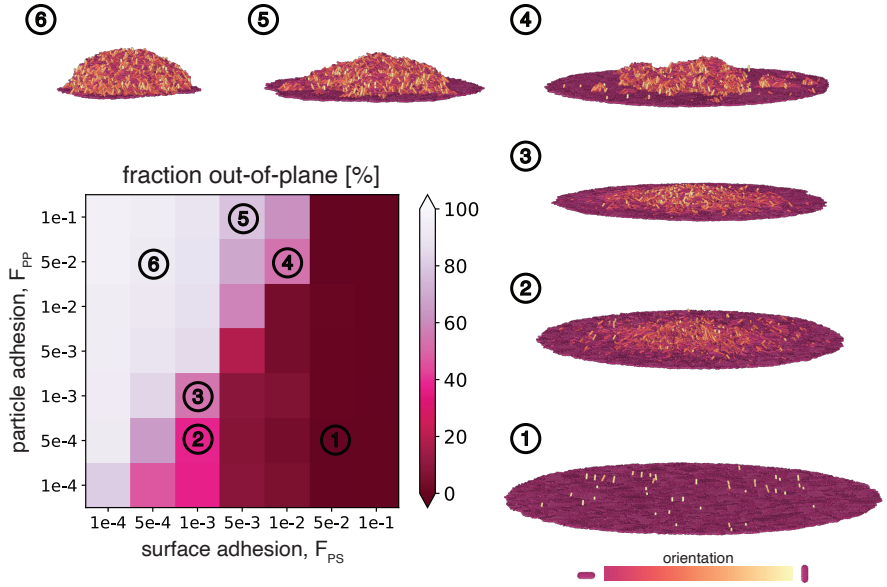

Figure 3.1: Fraction of the particles (AR = 4) that have moved out of the 2D plane for different magnitudes of the surface adhesion and particle adhesion. Shown here with snapshots of example colonies of 10000 particles. Particles are coloured by orientation with respect to the z-axis.

3.3. RESULTS

Varying the magnitudes of the two adhesive forces - particle adhesion and surface adhesion - results in colonies of a variety of shapes. Architectures range from fully flat colonies for high surface adhesion, to dome shaped colonies for high particle adhesion and low surface adhesion. One way of characterising the global structures is by measuring the fraction of cells that have (partially) moved out of the 2D plane and have moved away from the surface (**fig. 3.1**).

Focusing in on the part of the colonies that have escaped to the third dimension, we see that this process can occur in different ways for similar out-of-plane fractions (**fig. 3.2**a). For lower magnitudes of the particle adhesion, particles escape the plane somewhat homogeneously throughout the colony, forming a dome in the center, while the edge of the colony remains flat. For higher particle adhesion, we see highly localised spots where particles grow out of the plane. In these structures, crisp ridges are formed that sometimes even grow all the way to the edge of the colony. The rest of the colony remains perfectly flat.

The pressure the particles experience, shows that particles experiencing stronger particle adhesion, also experience more pressure for the in-plane particles (**fig. 3.2**b). Pressure for the particles that moved out of the plane is higher than

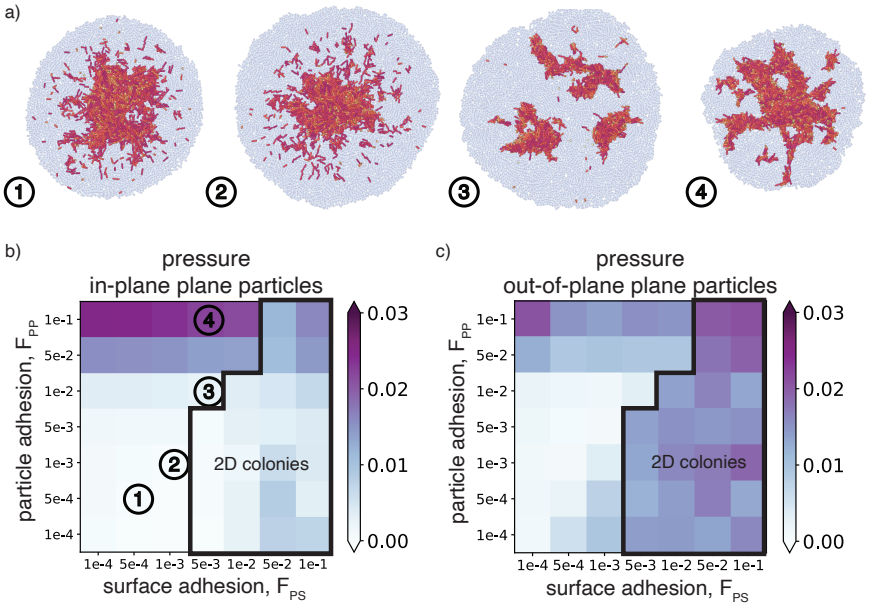

Figure 3.2: a) Snapshots of example colonies of 5000 particles (AR = 4). Particles are coloured by orientation with respect to the z-axis as in **fig. 3.1**, particles that have not moved out of the plane are blurred out. b) Pressure experienced by particles in the 2D plane. The black cutout denotes the part of the phase space where colonies are mostly flat. c) Pressure experienced by particles out of the 2D plane.

the ones in the plane for colonies with high surface adhesion. For colonies with higher particle adhesion than surface adhesion, this is reversed, and the in-plane particles experience more pressure.

When we look at the internal structure of these colonies, we can look at the orientation of the particles with respect to the z-axis (**fig. 3.3**a). This tells us something about how vertical or horizontal the colony is. Colonies that are fully flat, appear as pink. The more vertical the colony, the more yellow the average orientation. We see that for colonies with a similar out-of-plane fraction, the average verticalisation is also similar.

We can also compare each particle's orientation to the orientation of its direct neighbours. Averaged over all the particles in the colony, this gives us a value for the orientational order of the system (**fig. 3.3**b). Here a value of 0 would mean a fully disordered system, and a value of 1 would mean a fully aligned colony. Flat colonies have roughly the same orientational order, which is slightly higher than the order for 3D colonies.

We show 4 µm slices of some of the colonies in **fig. 3.3**c. This shows how vertical cells are equally dispersed. Cells somewhat align with their neighbours, however,

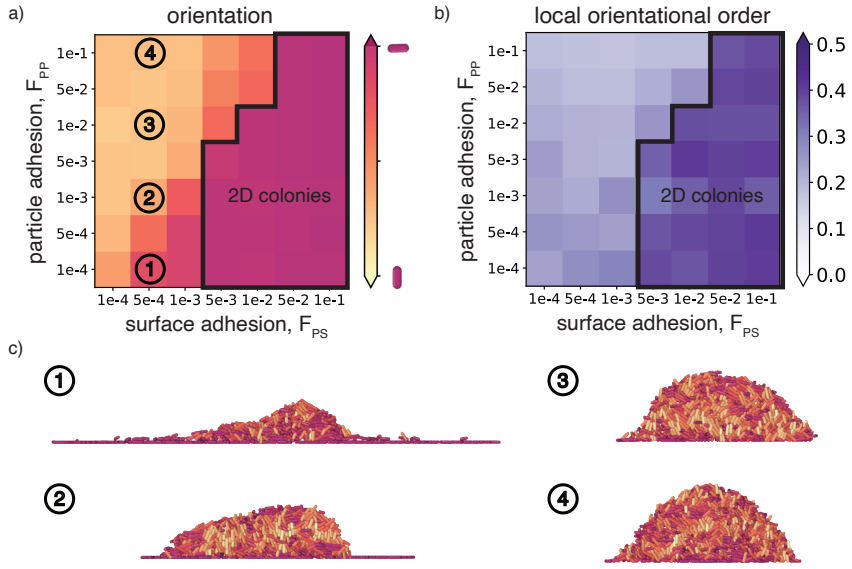

Figure 3.3: a) Average orientation of particles (AR = 4) with respect to the z-axis. The black cutout denotes the part of the phase space where colonies are mostly flat. b) Average local orientational order. c) Slices of 4µm of example colonies of 10000 particles (AR = 4). Particles are coloured by individual orientation with respect to the z-axis as in a).

there is no clear pattern in orientation throughout the 3D colony.

3.4. Discussion

Varying the strength of surface adhesion and particle adhesion gives rise to a varied set of colony architectures (**fig. 3.1**). For low particle and surface adhesion, we get relatively flat colonies with a raised center similar to *E. coli* colonies reported in literature [25]. When particle adhesion becomes stronger than surface adhesion we see more dome-shaped colonies as earlier observed in for example *V. cholerae* biofilms [38].

In the part of the phase space where the magnitudes for the surface adhesion and particle adhesion are very similar, we see high variation in global architecture. For example, for $F_{PP} = F_{PS} = 10^{-3} \cdot k_{int}$, the resulting colony is a mostly flat colony with a raised center. Varying either magnitude less than an order of magnitude up or down leads to colonies that are either entirely flat or fully dome-shaped. This suggests that a bacterium could regulate its shape by slightly up- or down-regulating its adhesion properties [15].

The onset of the transition into a 3D colony is, in this case, due to the force

balancing between the in-plane attraction forces and the pressure build-up. Looking at the pressure the particles in the plane experience, we see that for weaker adhesive forces, particles escape from the plane throughout the colony (**fig. 3.2**b). It appears that for stronger particle adhesion, particles actually keep each other in the plane, increasing the pressure. Once one particle escapes the plane, it can trigger other particles around it to do the same, resulting in ridge like structures (**fig. 3.2**b). These structures are somewhat reminiscent of the wrinkling observed in more developed colonies, although it should be noted that those appear at a much larger scale [39]. It should be noted here, that the pressure that cells experience is dependent on the interplay between growth and relaxation. Altering the growth rate and/or the amount of relaxation time steps will influence at which point in the development of the colony the pressure reaches its critical value [8].

Dimensional transition has been studied computationally, where often the first particle starts completely flush with a perfectly flat surface [27]. This scenario becomes less and less relevant once cells inoculate a surface in small bacterial clusters or the surface is not smooth [2]. A different initialisation condition could be chosen to immediately give particles the opportunity to extrude from the surface.

Looking at the internal structure of the colonies, we only see an obvious difference between fully flat colonies and 3D colonies (**fig. 3.3**). Within 3D colonies, varying surface or particle adhesion has very little effect on the alignment or ordering within the colony. This means that, with this model, we cannot capture the verticalisation of the colony core that has been observed in experiments [26], [38]. It is very likely that this is due to the fact that we do not implement any anchoring to the surface and the friction particles experience is isotropic [6], [14]. Our adhesion to the surface is more like a general affinity to the surface and not an adherence to a specific spot on the surface.

Additionally, in our simulations, there is no active alignment between the particles. This is in contrast to earlier work where particles where simulated as interacting ellipses [20]. Because we distribute our forces over the end points of the cells, we do not need an explicit torque. Besides, there is little evidence that bacteria make an active effort to be aligned.

This individual-based model can produce a wide variety of 3D structures by just changing 2 parameters, the magnitude for the surface adhesion and the magnitude for the particle adhesion. There are many more parameters to choose from and change, which would undoubtedly significantly alter the results. This is analogous to real microcolonies, where there are numerous cellular and environmental factors influencing the 3D architecture. That means that one should be careful in drawing conclusions from the model alone, as different sets of parameters and choices, might lead to very similar colony architectures. Nonetheless, it is a useful tool, and it allows us to grow virtual bacterial colonies of a reasonable shape and size.

BIBLIOGRAPHY

[1] L. Hall-Stoodley, J. W. Costerton, and P. Stoodley, "Bacterial biofilms: From the natural environment to infectious diseases", *Nature Reviews Microbiology*, vol. 2, pp. 95–108, Feb. 2004.

[2] K. Sauer, P. Stoodley, D. M. Goeres, *et al.*, "The biofilm life cycle: Expanding the conceptual model of biofilm formation", *Nature Reviews Microbiology*, vol. 20, pp. 608–620, Oct. 2022.

[3] W. Liu, J. Russel, M. Burmølle, S. J. Sørensen, and J. S. Madsen, "Micro-scale intermixing: A requisite for stable and synergistic co-establishment in a four-species biofilm", *The ISME Journal*, vol. 12, p. 1940, Aug. 2018.

[4] Z. You, D. J. G. Pearce, A. Sengupta, and L. Giomi, "Geometry and mechanics of microdomains in growing bacterial colonies", *Physical Review X*, vol. 8, p. 031 065, Sep. 12, 2018.

[5] W. P. J. Smith, Y. Davit, J. M. Osborne, W. Kim, K. R. Foster, and J. M. Pitt-Francis, "Cell morphology drives spatial patterning in microbial communities", *Proceedings of the National Academy of Sciences*, vol. 114, Jan. 17, 2017.

[6] H. Jeckel, F. Díaz-Pascual, D. J. Skinner, *et al.*, "Shared biophysical mechanisms determine early biofilm architecture development across different bacterial species", *PLOS Biology*, vol. 20, e3001846, 2022.

[7] N. L. Fernandez, B. Y. Hsueh, N. T. Q. Nhu, J. L. Franklin, Y. S. Dufour, and C. M. Waters, "*Vibrio cholerae* adapts to sessile and motile lifestyles by cyclic di-GMP regulation of cell shape", *Proceedings of the National Academy of Sciences*, vol. 117, pp. 29 046–29 054, Nov. 17, 2020.

[8] B. Maier, "How physical interactions shape bacterial biofilms", *Annual Review of Biophysics*, vol. 50, pp. 401–417, May 6, 2021.

[9] X. Zeng, Y. Zou, J. Zheng, S. Qiu, L. Liu, and C. Wei, "Quorum sensing-mediated microbial interactions: Mechanisms, applications, challenges and perspectives", *Microbiological Research*, vol. 273, p. 127 414, Aug. 1, 2023.

[10] P. Bera, A. Wasim, and P. Ghosh, "Interplay of cell motility and self-secreted extracellular polymeric substance induced depletion effects on spatial patterning in a growing microbial colony", *Soft Matter*, vol. 19, pp. 8136–8149, Nov. 1, 2023.

[11] A. Welker, T. Cronenberg, R. Zöllner, *et al.*, "Molecular motors govern liquidlike ordering and fusion dynamics of bacterial colonies", *Physical Review Letters*, vol. 121, p. 118 102, Sep. 11, 2018.

[12] A. I. Curatolo, N. Zhou, Y. Zhao, *et al.*, "Cooperative pattern formation in multi-component bacterial systems through reciprocal motility regulation", *Nature Physics*, vol. 16, pp. 1152–1157, Nov. 2020.

[13] C. Li, A. Hurley, W. Hu, *et al.*, "Social motility of biofilm-like microcolonies in a gliding bacterium", *Nature Communications*, vol. 12, p. 5700, Sep. 29, 2021.

[14] M.-C. Duvernoy, T. Mora, M. Ardré, *et al.*, "Asymmetric adhesion of rod-shaped bacteria controls microcolony morphogenesis", *Nature Communications*, vol. 9, p. 1120, Mar. 16, 2018.

[15] A. Bridier, J.-C. Piard, C. Pandin, S. Labarthe, F. Dubois-Brissonnet, and R. Briandet, "Spatial organization plasticity as an adaptive driver of surface microbial communities", *Frontiers in Microbiology*, vol. 8, p. 1364, Jul. 20, 2017.

[16] Z. Jiang, T. Nero, S. Mukherjee, R. Olson, and J. Yan, "Searching for the secret of stickiness: How biofilms adhere to surfaces", *Frontiers in Microbiology*, vol. 12, Jul. 8, 2021.

[17] S. Shyam, S. Misra, S. Mitra, and S. K. Mitra, "Bacteria–surface interactions: Role of impacting bacteria-laden droplets", *Soft Matter*, vol. 20, pp. 3425–3435, Apr. 24, 2024.

[18] K. Thijssen, M. R. Nejad, and J. M. Yeomans, "Role of friction in multidefect ordering", *Physical Review Letters*, vol. 125, p. 218 004, Nov. 20, 2020.

[19] J. Nijjer, C. Li, M. Kothari, *et al.*, "Biofilms as self-shaping growing nematics", *Nature Physics*, vol. 19, pp. 1936–1944, Dec. 2023.

[20] R. Hartmann, P. K. Singh, P. Pearce, *et al.*, "Emergence of three-dimensional order and structure in growing biofilms", *Nature Physics*, vol. 15, pp. 251–256, Mar. 2019.

[21] C. Berne, C. K. Ellison, A. Ducret, and Y. V. Brun, "Bacterial adhesion at the single-cell level", *Nature Reviews Microbiology*, vol. 16, pp. 616–627, Oct. 2018.

[22] R. Zöllner, T. Cronenberg, N. Kouzel, A. Welker, M. Koomey, and B. Maier, "Type IV pilin post-translational modifications modulate material properties of bacterial colonies", *Biophysical Journal*, vol. 116, pp. 938–947, Mar. 2019.

[23] D. S. Glass and I. H. Riedel-Kruse, "A synthetic bacterial cell-cell adhesion toolbox for programming multicellular morphologies and patterns", *Cell*, vol. 174, 649–658.e16, Jul. 2018.

[24] F. J. Lobo-Cabrera, A. Patti, F. Govantes, and A. Cuetos, "Polymer-induced microcolony compaction in early biofilms: A computer simulation study", *Physical Review E*, vol. 103, p. 052 407, May 12, 2021.

[25] P.-T. Su, C.-T. Liao, J.-R. Roan, S.-H. Wang, A. Chiou, and W.-J. Syu, "Bacterial colony from two-dimensional division to three-dimensional development", *PLOS ONE*, vol. 7, e48098, Nov. 14, 2012.

[26] F. Beroz, J. Yan, Y. Meir, *et al.*, "Verticalization of bacterial biofilms", *Nature Physics*, vol. 14, pp. 954–960, Sep. 2018.

[27] Z. You, D. J. G. Pearce, A. Sengupta, and L. Giomi, "Mono- to multilayer transition in growing bacterial colonies", *Physical Review Letters*, vol. 123, p. 178 001, Oct. 21, 2019.

[28] C. I. Abreu, J. Friedman, V. L. Andersen Woltz, and J. Gore, "Mortality causes universal changes in microbial community composition", *Nature Communications*, vol. 10, p. 2120, May 9, 2019.

[29] A. Welker, M. Hennes, N. Bender, T. Cronenberg, G. Schneider, and B. Maier, "Spatiotemporal dynamics of growth and death within spherical bacterial colonies", *Biophysical Journal*, vol. 120, pp. 3418–3428, Aug. 2021.

[30] G. Mamou, G. B. Malli Mohan, A. Rouvinski, A. Rosenberg, and S. Ben-Yehuda, "Early developmental program shapes colony morphology in bacteria", *Cell Reports*, vol. 14, pp. 1850–1857, Mar. 2016.

[31] M. R. Warren, H. Sun, Y. Yan, J. Cremer, B. Li, and T. Hwa, "Spatiotemporal establishment of dense bacterial colonies growing on hard agar", *eLife*, vol. 8, e41093, Mar. 11, 2019.

[32] J. Nijjer, C. Li, Q. Zhang, H. Lu, S. Zhang, and J. Yan, "Mechanical forces drive a reorientation cascade leading to biofilm self-patterning", *Nature Communications*, vol. 12, p. 6632, Nov. 17, 2021.

[33] G. O'Toole, H. B. Kaplan, and R. Kolter, "Biofilm formation as microbial development", *Annual Review of Microbiology*, vol. 54, pp. 49–79, Volume 54, 2000 Oct. 1, 2000.

[34] F. L. Hellweger, R. J. Clegg, J. R. Clark, C. M. Plugge, and J.-U. Kreft, "Advancing microbial sciences by individual-based modelling", *Nature Reviews Microbiology*, vol. 14, pp. 461–471, Jul. 2016.

[35] M. R. Frederick, C. Kuttler, B. A. Hense, and H. J. Eberl, "A mathematical model of quorum sensing regulated EPS production in biofilm communities", *Theoretical Biology and Medical Modelling*, vol. 8, p. 8, Dec. 2011.

[36] M. Zaccaria, S. Dedrick, and B. Momeni, "Modeling microbial communities: A call for collaboration between experimentalists and theorists", *Processes*, vol. 5, p. 53, Sep. 25, 2017.

[37] B. Li, D. Taniguchi, J. P. Gedara, *et al.*, "NUFEB: A massively parallel simulator for individual-based modelling of microbial communities", *PLOS Computational Biology*, vol. 15, A. E. Darling, Ed., e1007125, Dec. 12, 2019.

[38] J. Yan, A. G. Sharo, H. A. Stone, N. S. Wingreen, and B. L. Bassler, "*Vibrio cholerae* biofilm growth program and architecture revealed by single-cell live imaging", *Proceedings of the National Academy of Sciences*, vol. 113, Sep. 6, 2016.

[39] J. Kayser, C. F. Schreck, Q. Yu, M. Gralka, and O. Hallatschek, "Emergence of evolutionary driving forces in pattern-forming microbial populations", *Philosophical Transactions of the Royal Society B: Biological Sciences*, vol. 373, p. 20 170 106, May 26, 2018.

4

TIME OF FIRST CONTACT DETERMINES COOPERATOR SUCCESS IN A THREE-MEMBER MICROBIAL CONSORTIUM

Rachel LOS, Tobias FECKER, P.A.M. VAN TOUW, Rinke J. VAN TATENHOVE-PEL, Timon IDEMA

Microbial communities are characterised by complex interaction, including cooperation and cheating, which have significant ecological and applied implications. However, the factors determining the success of cooperators in the presence of cheaters remain poorly understood. Here, we investigate the dynamics of cooperative interactions in a consortium consisting of a cross-feeding pair and a cheater strain using individual-based simulations and an engineered L. cremoris toy consortium. Our simulations reveal first contact time between cooperators as a critical predictor for cooperator success. By manipulating the relative distances between cooperators and cheaters or the background growth rates, influenced by the cost of cooperation, we can modulate this first contact time and influence cooperator success. Our study underscores the importance of cooperators coming into contact with each other on time, which provides a simple and generalizable framework for understanding and designing cooperative interactions in microbial communities. These findings contribute to our understanding of cross-feeding dynamics and offer practical insights for synthetic and biotechnological applications.

This chapter has been accepted for publication in ISME Communitations.

4.1. INTRODUCTION

Microorganisms often live together in surface-attached communities of many strains and species, called biofilms. An early stage of the planktonic cell to biofilm life cycle are microcolonies, which make up the initial kernels that later grow into larger biofilms [1]. Studying the formation of these microcolonies provides valuable insight into biofilm development [2]. The organisms living in biofilms can form complicated networks of antagonistic, mutualistic, competing or cooperating interactions [3]–[5]. One of the ways species can cooperate is by cross-feeding, where both species produce metabolites or other essential compounds, that benefits the other [6]. The production of these compounds often comes at a cost for the producer in the form of extra expended energy, e.g. in the form of ATP. This creates opportunities for cheater species to exploit cooperators, by reaping the same benefits from the cross-fed compounds without contributing to the cooperation themselves [7]. Studying the interactions in bacterial systems can have implications for applications concerning biofilms in medical, biotechnological and industrial contexts [8]–[10]. Moreover, because mutualism and cooperative interactions can be observed in all branches of the phylogenetic tree, there is general interest in what makes this type of social behaviour evolutionary stable [7]. Due to their relative simplicity, microbial systems can be used as model systems for studying broader social behaviours in biology [11]. The interactions between microorganisms are in general complex, with many inter-dependent variables which are difficult to isolate [12]. An important factor on the dynamics of any collection of interacting species is spatial organisation [13]–[18]. This spatial structure plays a role in both the emergence and the maintenance of cooperator co-existence [19]. For example, spatially structured environments can promote clonal patching which is useful for intraspecies cooperation [20], [21] as well as pattern formation in multi-species colonies [16], [22].

In this paper we employ Individual-Based Modelling (IBM) to simulate a consortium of two cooperating species and a selfish cheater growing on a surface. By incorporating spatial structure and proximity in metabolic interactions we attempt to uncover the factors that govern cooperative success in the face of cheating [23]. This will contribute to our understanding of population dynamics in cooperative biological systems.

4.2. RESULTS + DISCUSSION

4.2.1. COOPERATOR SUCCESS IS HIGHLY DEPENDENT ON INITIAL PLACEMENT OF PARTICLES

To explore the impact of local cross-feeding interactions on the development of a multi-species microcolony, we modelled interacting particles growing on a surface (**fig. 4.1**a). We defined three different species, two cooperators A and B, and a cheater C (**fig. 4.1**b). We made use of the fact that metabolic interactions have

been shown to take place at very short distances and have the particles adjust their growth rate based on the number of their beneficial nearest neighbours [24], [25]. The strength of the cross-feeding interaction between cooperators A and B is characterised by two main factors: the metabolic cost the cooperators pay to contribute to the cooperation, and the added growth benefit they experience from this interaction. The cheaters don't pay the cost but experience the same benefit (**fig. 4.1**c). For now, the interaction with the cooperators is symmetric, in the sense that the cheater responds similarly to cooperator A as to cooperator B and it needs both to grow. Further on in this manuscript we also explore asymmetric cheater interactions. The particles, are spherocylindrical particles that grow and divide. We start each run with 10 of each species randomly distributed on a surface. We then let them grow till the colonies reach a size of 10^4 particles.

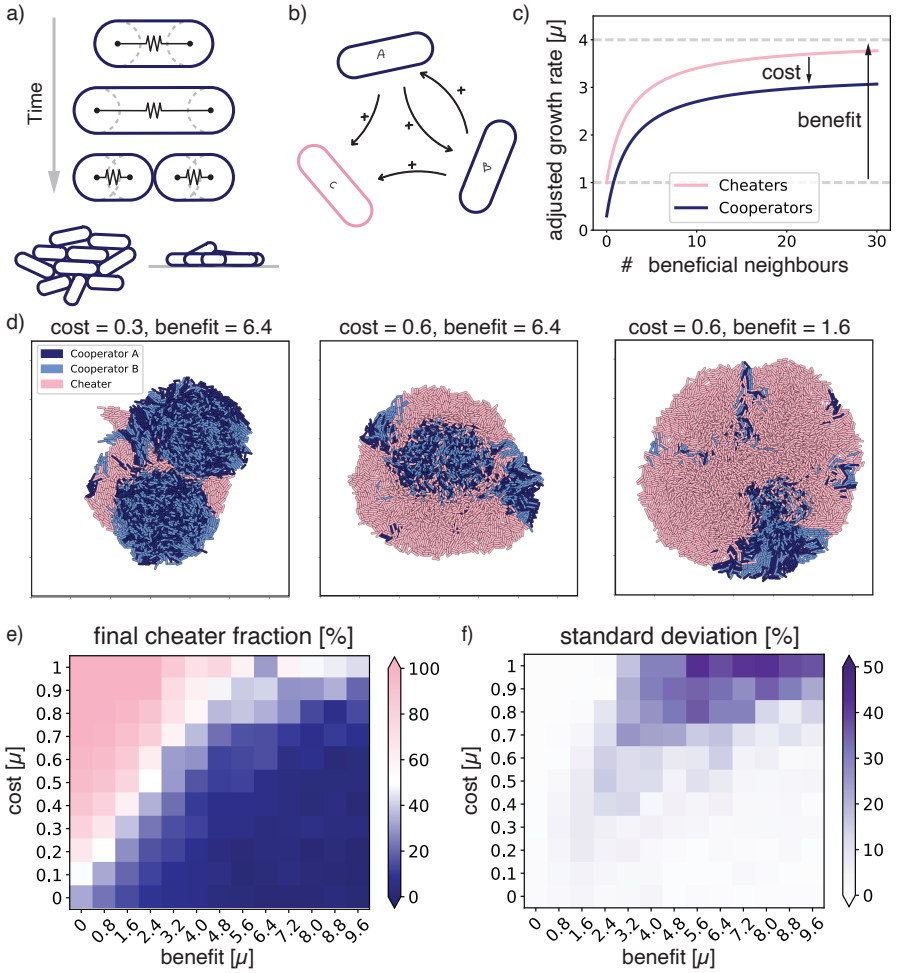

Figure 4.1: **Effect of cost and benefit of cooperation on cooperator success in individual-based simulations** a) schematic representation of the individual-based-model. Spherocylindrical particles grow and divide, forming a 3D colony. b) The simulated consortium of two cooperators (A & B) which benefit each other and a cheater (C) which benefits from both cooperators A and B but does not reciprocate. c) Growth rate of both the cooperators and the cheaters, dependent on the number of beneficial neighbours (i.e., neighbours that provide a useful compound). The growth rate is affected by the cost and benefit of cooperation. d) Snapshots of the final 3D colonies for different combinations of cost and benefit. Area shown is always $130 \times 130\,\mu m^2$. e) Final cheater fractions for varying cost and benefit. Averages taken over 15 runs and in f) the standard deviation of those runs.

In order to understand how the strength of the local interactions shaped the development of the microcolony, we simulated growing colonies for varying costs and benefits and recorded the cheater fraction. Typical simulation snapshots of

the final colonies are shown in **fig. 4.1**d. The final cheater fractions averaged over 15 runs are shown in **fig. 4.1**e, the bottom left data point represents a situation with no cost and no benefit, which means that the particles are not interacting at all and their growth rate remains the same. As the cost of cooperation increases while the benefit stays zero, the final cheater fraction increases. In turn, increasing the benefit decreases the cheater fraction and favours the cooperators. Interestingly, there are not many intermediate values for the final cheater fraction, showing more switch-like behaviour than would be expected from a well-mixed system (Supplemental methods, **fig. S4.2**).

Surprisingly, the simulations gave a large variation between runs with the same interaction parameters, particularly for higher costs and benefits (**fig. 4.1**f). Here, we found standard deviations of up to 50% which indicates that the final cheater fraction can be anywhere between 0% and 100% for simulations with the same interaction input parameters. Since, the only difference between these runs was the initialisation of the 30 particles at the start of the run, the large variance had to be a result of the initial placement of the particles, which we explored next.

4.2.2. First contact time determines cooperator success

In order to investigate how the initial placement of the particles leads to different final cheater fractions, we visually inspected the resulting colonies of the simulations. In general, we observed that colonies were fairly segregated, akin to clonal patches observed in 2D colonies [9]. The cooperator patches are often well mixed, with equal amounts of A and B, which we expect is due to a combination of nematic mixing and the mutualism between these species [20], [26], [27]. In different simulations with the same input parameters, we observed a varying number of these patches of mixed cooperators (**fig. S4.1**). Because the cooperators depend on each other's proximity to cross-feed, we speculated that the final cheater fractions might be determined by how likely it is for cooperators to meet.

In order to investigate this relation between the likelihood of meeting and final cheater fraction, we took all the runs and we recorded the first time point where a cooperator A particle comes into contact with a cooperator B particle. Plotting the final cheater fraction as a function of these first contact times for each value of the benefit, yielded clearly defined curve with comparatively little variance (**fig. 4.2**a). Therefore, for a given benefit, the time of first contact was a more informative predictor for cooperator success than the cost of cooperation.

This dependence on cooperators encountering each other is in line with earlier findings on the importance of co-localisation probabilities in a similar consortium growing in microdroplets [28]. Other work on two-species cooperator-defector consortia growing plates showed the importance of founder cell configuration [29]. Additionally, expansion-collision dynamics and initial distance between microorganisms have been shown to be important factors for cooperator-defector co-existence [30]. Although all these systems are not identical, they do

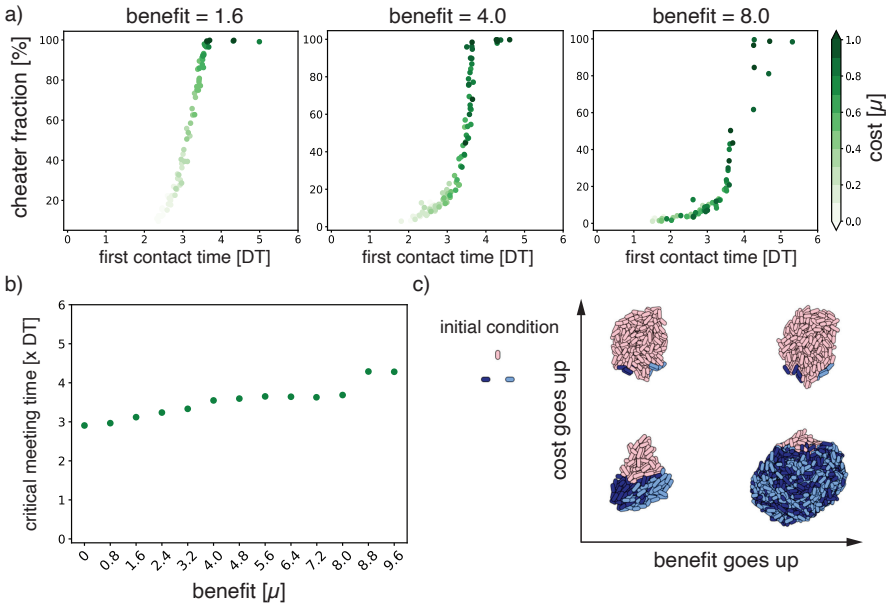

Figure 4.2: **First contact time determines cooperator success.** a) Final cheater fraction of single runs plotted as a function of first encounter time (measured in DT = 10^5 simulation time steps) for three different benefits. Cost is denoted in green. b) Critical meeting time as a function of benefit. c) Toy system for a well defined initial condition of three particles positioned in a triangle and the resulting colonies, for the combinations of two values for the cost (0.2 and 0.7) and two values for the benefit (5.6 and 8.8).

point to a general principle in cooperative dynamics.

To explore this further, for each value of the benefit, we determined a critical meeting time before which A and B need to make contact in order to outcompete the cheaters and make up > 50% of the final population (**fig.** 4.2b). If the first contact time happened after this point, cheaters dominated the final colony of 10^4 particles. The critical meeting time depended on the cooperator benefit, where a higher benefit allowed for a later critical meeting time. In this case, once first contact had been made, cooperators were able to make up for lost time by growing faster once they were together. Conversely, if the cooperator benefit was lower, the cooperators needed to meet earlier to outcompete the cheaters.

It is important to note that first contact time is determined not only by the cost and benefit, but also the relative distance between the cooperators in the initial placement. To illustrate this, we visualised the outcome of simulations with a well-defined initial placement of the three particles (**fig.** 4.2c). Here, the initial distance between the particles is always the same, and out of range from each other. The cost then affects the time it takes for the particles to traverse that distance since

the cost affects the growth rate of the particles when they are on their own, i.e. their background growth. A higher cost causes the cooperators A and B to have a lower background growth rate, so they are slower to reach each other. If they are too slow, as shown in the top-left, cheater particles grow in between them before they get the chance to make contact. In this case, having a higher benefit (top-right) will not help the cooperators as they never get to reap the rewards of their cooperation. If the cost is lower and A and B find each other before the critical meeting time (bottom-left), they can compete effectively with the cheaters. When the benefit becomes larger (bottom-right), they can significantly out-compete the cheaters once they meet. In our system of random initial distances between particles, this interplay between distance and background growth is what leads to the high variation in competitive outcome. From these simulation results, we propose that it is not just the initial distances between cooperators nor just the details of the cooperative interaction, but it is the first contact time that determines cooperator success in surface attached colonies.

4.2.3. EXPERIMENTAL CONSORTIUM OF ENGINEERED *L. cremoris*

To test if the first contact time between cooperator species is also critical in a biological system, we attempted to translate our simulated consortium to a laboratory setting. We constructed a consortium of three *L. cremoris* strains (**fig. 4.3**a, Table 4.1) growing on agar plates containing lactose as a carbon source and casein as an amino acid source. Cooperator A, NZ9000 Lac^+ Glc^-, can metabolize the galactose moiety of lactose, but exports the glucose moiety from the cell. The glucose can then be used by cooperator B, MG610, which cannot metabolise lactose. In return, MG610 expresses an extracellular enzyme to break down the casein into amino acids, which benefits A, which cannot metabolize the casein. Lastly, we engineered a cheater C, MG1363_GFP Lac^+, by transforming a plasmid containing the genes necessary to metabolise lactose into MG1363_GFP. This constructed cheater can metabolise lactose and both resulting moieties, but, similar to A, lacks the enzyme to degrade casein. C also expresses GFP, which we use to determine the cheater fraction. We grew A, B and C individually on agar plates, and measured the total growth by comparing the final cell count to the initial cell count and calculating the amount of times the cells had doubled. On the single strain plates there was very little growth, which is what we expected from the designed cross-feeding interaction (**fig. 4.3**b). When growing all the pairwise combinations, we observed that A+B massively outgrew the other combinations. From this we concluded that, as expected, these two strains experience a strong mutual benefit from growing together. Similarly, we concluded that on plates with C+A and B+C, there is no such mutualism, as the total cell abundance, measured in amount of doublings, stalled. Furthermore, when we measured cheater fractions for these combined plates, we saw that C outgrows both A and B in a pairwise combination, pointing to a general advantage in growth rate that C has over both A and B (**fig. 4.3**c). All in all, we

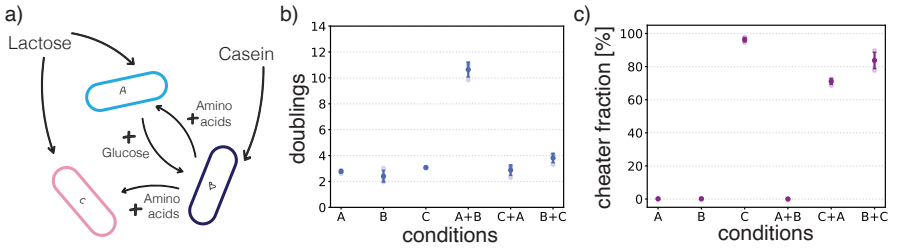

Figure 4.3: **Engineered consortium on agar plates** a) *L. cremoris* consortium, consisting of cooperators A and B and cheater C. b) Control experiments showing the amount of doublings for single strain plates and pairwise combinations after three days incubation. c) Control experiments showing cheater fractions for all single strain plates and pairwise combinations. All conditions are measured in triplicate.

concluded that our experimental consortium accurately represents a cross-feeding pair together with a cheater.

4.2.4. Relative average distance between cooperators determines cooperator success in plate experiments

To investigate how the first contact time would affect our experimental system, we needed a way to modulate the distance between cooperators on the plates. Unfortunately, it is not so simple to closely control the initial placement or the respective growth rates of the microorganisms on plates. Therefore, we needed a different way to adjust the chance of cooperators meeting each other. Unlike our simulated cheater, the cheater in our experimental consortium is not symmetric in the sense that it does not benefit as much from cooperator A as it does from cooperator B. Since both cooperator A and the cheater, C, need cooperator B for their amino acid production, we argue that the relative difference between the distance between B and A (r_{AB}) and the distance between B and C (r_{CB}) sets the chance of cooperators meeting. In essence it's a race between A and C, to reach B first.

To modulate the relative distances between A and B, and C and B, we adjusted the ratio of [C]/[A]. When [C]/[A] is small (< 1), there is more A on the plate than C. In this case, the chance of B finding itself close to an A is larger than B finding itself close to a C. If [C]/[A] is large (> 1), the reverse is true, so on average it is more likely for a B to be surrounded by cheaters (**fig. 4.4**a). The relationship between [C]/[A] and the expectation value of the relative distance can be derived analytically (see SI, **fig. 4.4**b).

From our simulation results, we expected the final cheater fraction to rise with a higher relative distance between cooperators, as it would take longer for them to find each other. To test if this would also occur in our experimental consortium, we inoculated cells on plates in different A:B:C ratios, and after 3 days of incubation we washed the plates and measured the total cell count and the final cheater

fraction (**fig.** 4.5a & c). Consistent with our expectations, a small [C]/[A] resulted in final cheater fractions of as low as 20%,where when the ratio was high, the final cheater fraction increased to almost 70%. Note that the total amount of cells after incubation was similar for all starting ratios (**fig.** 4.5c & d).

We show 2 sets of experiments, one where the initial cheater fraction is always 10% and one where it is 25%. Apart from the leftmost points of the respective curves (discussed below), they fall onto the same curve. From this we concluded that, regardless of initial cheater fraction, the relative abundance of A and C and therefore the relative average distance between cooperators determines cooperator success or failure in our experimental consortium.

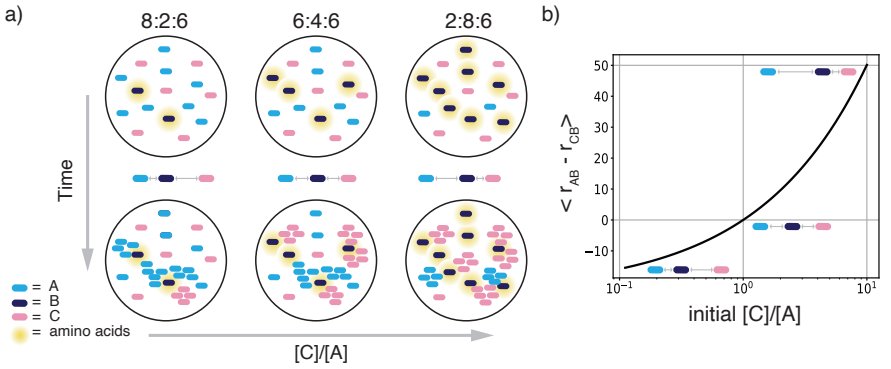

Figure 4.4: **[C]/[A] ratio as a proxy for relative cooperator-cheater distances** a) Schematic of how changing the A:B:C ratios is expected to affect the first contact time between cooperators A and B. b) Relation between the expected average difference between the distance from B to A (r_{AB}) and from B to C (r_{CB}) to the [C]/[A] ratio. For the derivation, see Supplemental methods.

4.2.5. TOO FEW NUCLEATION SITES RESULT IN HIGHER CHEATER FRACTIONS

As shown in **fig.** 4.5a, most data points fall onto the same curve. However, for the smallest [C]/[A] for both the 10% and the 25% curve, the final cheater fractions were higher than expected. These points correspond to A:B:C ratios of 89:1:10 and 74:1:25, respectively, so in both cases there is a minimal amount of cooperator B present. Because there is so much more cooperator A than cheater C, present, we had expected that B coming into contact with A would be inevitable, and therefore the final cheater fraction would be low. Instead, we measured the final cheater fraction at low B to be around 50%.

In order to generate a hypothesis of what happens for low amounts of B, we went back to our simulations. To better reflect the asymmetric interaction the cheater has with cooperators A and B in our experimental consortium, we adapted the model so that the cheater would only benefit from cooperator B, while keeping

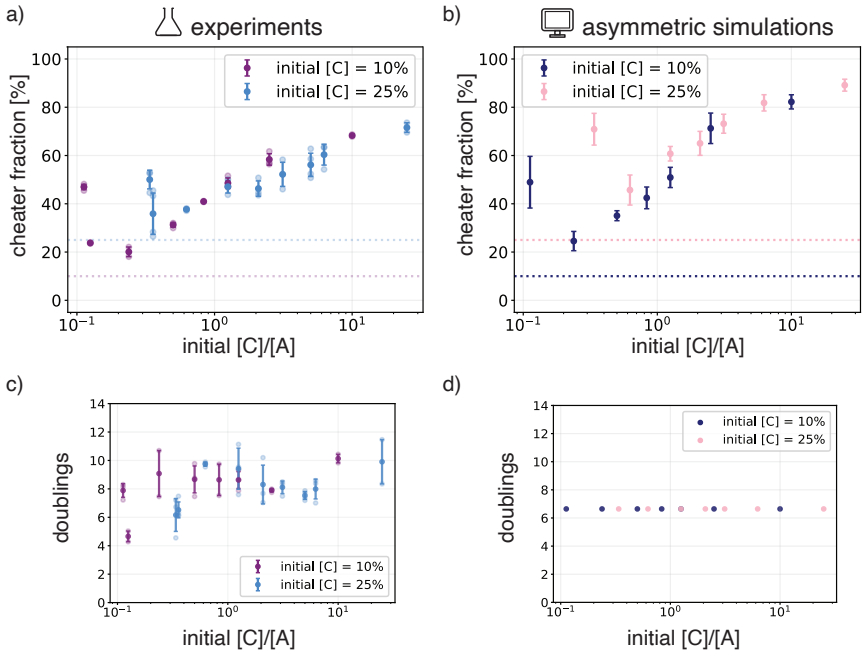

Figure 4.5: **Final cheater fractions depend on initial A:B:C ratios in experiments and simulations** a) Final cheater fraction of plate experiments with different initial starting ratios of A:B:C, with a constant starting fraction of 10% C in purple and 25% C in blue. Error bars are standard deviation for 3 replicates. b) Final cheater fraction for simulations with the same starting ratios of A:B:C. Simulations are of an asymmetric interaction where A and B interact as before, but C only benefits from B. The cost and benefit for these runs are 0.5 and 2.4. c) Amount of times the cells doubled between the time of initialisation and measurement on the plates and d) in the simulations.

the interaction between cooperators A and B the same. When we performed these asymmetric simulations for all the ratios we tested in the experiments, the simulations results were similar to the experimental data (**fig.** 4.5a & b). Additionally, we got the same sudden increase in cheater fraction for very low B. Following the trajectories of the composition of these colonies over time, we see that indeed, B always finds A (**fig. S**4.3). However, there is only one nucleation site, defined as a site where an A and a B are initialised close enough to interact and start a cooperator patch. Because there is only one nucleation site, the development of the colony takes longer, and by the time cooperators A and B have grown to a significant size cooperator patch, the cheaters have already taken up a large part of the colony. This suggests that, next to meeting on time, there is also a minimal amount of nucleation sites necessary for cooperator success.

4.2.6. LOWERING THE BACKGROUND GROWTH OF COOPERATORS RESULTS IN HIGHER CHEATER FRACTIONS

The symmetric simulations demonstrated that not only the initial distance between cooperators determined cooperator success, but also how fast this distance could be traversed (**fig. 4.2**c). This speed is set by the background growth of the particles. In the simulation, we can set the background growth of the cooperator particles by changing the cost of cooperation (**fig. 4.2**c). A higher cost for cooperators means a lower background growth, which we expected to result in a shift of the curve to the left, where more of cooperator A, i.e. a smaller [C]/[A] ratio, would be needed to achieve the same final cheater fraction. Indeed, increasing the cost in the asymmetric simulations slightly, results in a shift to the left, shown as the blue data points in **fig. 4.6**b.

Again, we attempted to test these results from the simulations experimentally. While the cost and benefit of cooperation could not be directly altered, we hypothesised that by selectively inhibiting cooperator A we could achieve a similar effect. To that end, we used erythromycin which is an antibiotic that only affects the growth of A as both B and C are resistant. We tested for a concentration of erythromycin that would only slightly inhibit the growth of A, which we found to be $0.04\,\mu g\,mL^{-1}$ (**fig. S4.4**). We then performed the same experiment for the 10% initial cheater fraction on both normal (untreated) plates and on plates containing the antibiotic (**fig. 4.6**a). For the final cheater fraction on the antibiotic plates, we observed a shift to the left compared to the normal plates, where the same final cheater fraction on standard plates could be achieved on antibiotic plates with a lower ratio of [C]/[A].

Note that in the simulations, we increased the cost for both A and B, where in the experiments, the antibiotic only affects cooperator A. Regardless, we achieved good agreement between the experimental and simulated data. This demonstrates that increasing the cost of cooperation or decreasing the background growth of the cooperators results in higher cheater fractions. Together with our previous results, we propose that this is because the background growth sets the first contact time for the cooperators, which is the main determinant for cooperator success.

The general concept of first contact times being instrumental in cooperator success, suggests several strategies for cooperators to increase their survival rate. For instance, cooperators could increase their affinity for each other in solution, forming mixed aggregates. These would then function as the kernels that establish colonies elsewhere, which would greatly improve their chance of survival [1]. Interestingly, the spontaneous developing of cell-cell affinity has been previously shown in mutualistic strains of *E. coli* [16]. Alternatively, chemotactic motility would be a way for cooperators that are already on a surface to establish contact early on, thereby ensuring a beneficial cooperative environment.

Another strategy would be for cooperators to economise on the production of the cross-fed compound when growing on their own and using quorum sensing to

only start production when encountering other cells [31], [32]. Both these strategies could also be explored in synthetic systems making use of specific adhesins and quorum sensing pathways [33], [34].

Not only can the first contact time be exploited by cooperators, it can also provide tactics in a biotechnological application. An example of a widely applied cross-feeding interaction is the yoghurt consortium. Here protease negative strains can form, which act as a cheater, being able to take over the protease positive strain. Our framework explains why this is less of a problem in a surface-attached or otherwise spatially structured environment [35]. In kombucha production, aggregation between interacting species has a positive effect on the yield [36], [37]. We can now hypothesize that this is due to the metabolically interacting species being in contact early on in the process, outcompeting other strains present and increasing overall yield. Although this should be further tested and verified, the framework proposed in this work should be applicable to similar consortia of different species.

Finally, what this work also shows, is that approximating metabolic interactions by only considering the next neighbours, is a valid way of modelling cross-feeding. Even though our model is quite simple, it is able to capture and predict behaviour of a real system that is much more complex and has many more interdependent variables than we include in the model. For example, the species in our simulations only differ from each other in how they respond to their neighbours, whereas the strains in our experiment also show variability in overall growth rate. Moreover, in our experiments the nutrient density probably changes over time as the plates grow more dense. Regardless, our simple model of metabolic interactions on a surface is capable of capturing important features of the real system, providing insight into cross-feeding in the presence of cheating.

4.3. SUMMARY

Microbial collaboration is an abundant phenomenon with ecological and applied relevance, yet the factors contributing to cooperator success in the presence of cheaters are poorly understood. We set out to investigate the factors contributing to cooperator success in the presence of an exploiting cheater growing together on a surface. Individual-based simulations of a consortium consisting of three species, a cross-feeding pair and a cheater, indicated a strong influence of the initial placement of the microorganisms on the final outcome. Focusing in on the mechanisms, we demonstrated that first contact time was a better predictor for cooperator success than the value of the interaction parameters alone. We then showed how a combination of cost and initial placement together affect this first contact time.

We translated our simulations to an engineered *L. cremoris* toy consortium, consisting of two mutualistic strains and a cheater strain growing on agar plates. We show that by changing the relative distance between cooperators and cheaters

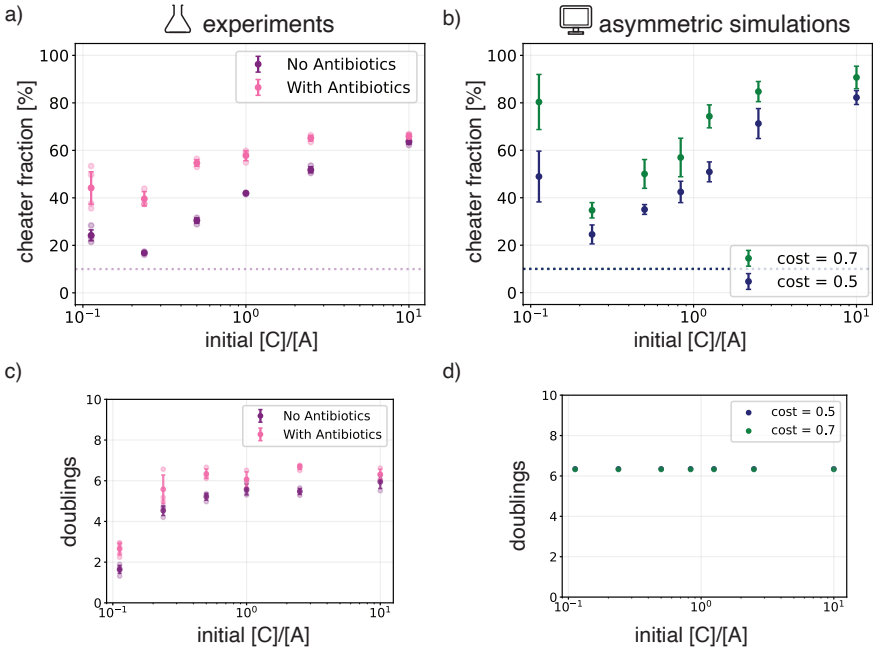

Figure 4.6: **Higher cost of cooperation leads to higher cheater fractions** a) Final cheater fraction for experiments with different [C]/[A] initial ratios on plates containing $0.04\,\mu g\,mL^{-1}$ erythromycin (in pink) and plates without erythromycin (in purple). b) Final cheater fraction for asymmetric simulations of different [C]/[A] initial ratios for two values of the cost. The benefit is 2.4 and all data points are averages and standard deviations of 5 runs. c) Amount of times the cells doubled between the time of initialisation and measurement on the plates and d) in the simulations.

by altering the starting ratios of A, B and C, we could directly influence cooperator success. We recreated our experimental findings by a simple adjustment to the model, making the cheater an asymmetric cheater, further showing how the average distance between cooperators is responsible for cooperator success.

Finally, we showed that, next to the relative distance between cooperators, the time it takes to traverse that distance affects the final cheater fraction as well. This time is set by the background growth, which is dependent on the cost of cooperation in the simulations. In the experiments we used antibiotics to selectively inhibit the background growth of cooperator A, giving good agreement with the simulations.

We conclude that in a cross-feeding cooperative interaction between strain A and strain B, the ability to find each other on time is the determining factor in cooperator success in the presence of a cheater strain.
Additionally, we have shown that metabolic cross-feeding can be modelled by ad-

justing the growth rate of particles depending on their nearest-neighbours. Our findings provide better understanding of cross-feeding dynamics in surface attached communities, as well as an intuitive framework for designing and altering cross-feeding consortia in synthetic and biotechnological applications.

4.4. Materials and Methods

4.4.1. Individual based model

In our simulations we initialise spherocylindrical particles on a surface and let them grow, divide and interact with each other [38]. The mechanical interactions of the particles are the same for all species: in addition to steric repulsion between the particles, they have an attractive potential which makes them stick together and to the surface (see SI). The cross-feeding interaction between the different species is implemented by adjusting their growth rates based on their immediate environment (**fig. 4.1**c) [24], [25]. In particular, for every growth step, we count for each particle how many beneficial neighbours they have in their immediate vicinity and use this number as input for a scaled Monod equation:

$$\mu'_A = \mu'_B = \mu \cdot (1 + \frac{n}{K_s + n} \cdot b - c), \tag{4.1}$$

$$\mu'_C = \mu \cdot (1 + \frac{n}{K_s + n} \cdot b), \tag{4.2}$$

which determines the growth rate of the particle, μ'. Here, n is the number of beneficial neighbours, K_s is the Hill coefficient, which we set to 2.5 as this is the average number of beneficial direct neighbours in a well-mixed colony of 10^4 particles, μ is the background growth of the cheaters, i.e., the growth rate of an isolated cheater particle. Both benefit, b, and cost, c, are given as fractions of μ, where b sets the maximal growth rate a particle can achieve and c gives a downward shift which can have any value between 0 and 1.

4.4.2. Cross-feeding simulations

We implement a symmetric cross-feeding interaction by having species A and B increase their growth rate depending how many of their neighbours are B and A, respectively. C increases its growth rate based on the minimum number of A and B in its vicinity. At the beginning of the simulation, 10 particles of each species are randomly initialised on a 50×50 μm^2 patch of surface. We grow the system to a final size of 10^4 particles.

4.4.3. Asymmetric simulations

For the asymmetric case that resembles our experimental consortium, the interactions remain the same except that for the growth rate of C, n is taken to be the

number of B particles in the neighbourhood. Additionally, 100 particles are initialised in different A:B:C ratios, and the system is grown to a final size of $7 \cdot 10^3$ particles.

4.4.4. Microbial strains and growth conditions

Strains and plasmids used in this study are listed in **table 4.1**. All strains were grown on CDMpc, described by Price *et al.* [39] at 30 °C in a stationary incubator. We used glucose and lactose as carbon sources, in the concentrations as indicated. Where indicated, the strains were grown on $CDMpc_{cas}$, containing 0.2 wt% casein sodium salt (from bovine milk, #C8654, Sigma Aldrich, Saint Louis, MO, USA) instead of amino acids. To prepare agar plates, liquid medium was supplemented with 2 wt% BD Difco™ Bacto™ Agar (BD, NJ, USA).

L. cremoris NZ9000 Glc^- Lac^+ [40], *L. cremoris* MG5267 and MG1363_GFP Lac^+ (this study) were precultured in 25 mL CDMpc + 0.09 wt% lactose, *L. cremoris* MG610 [41] and MG1363_GFP [42] were precultured in 25 mL CDMpc + 0.09 wt% glucose. Freezer stocks were prepared by growing the strains in CDMpc with the appropriate carbon source and storing the stationary culture at -80°C with 20 vol% glycerol. Where indicated, erythromycin (Sigma-Aldrich, 856193, Saint Louis, MO, USA) was added at the indicated concentration. For the isolation of pMG820 and transformation into MG1363_GFP, M17 medium was used (from powder, Thermo Fisher Scientific, MA, USA).

4.4.5. Isolation of pMG820 and transformation into MG1363_GFP

To construct MG1363_GFP Lac^+, pMG820 was isolated from 5 mL of a stationary NZ9000 Glc^- Lac^+ culture, cultivated in M17 + 0.5 wt% lactose, as follows. The culture was centrifuged using a Sorvall ST40 centrifuge (Thermo Fisher Scientific, MA, USA) (10 min, 5000g), and resuspended in 30 mM Tris-Hcl pH 8, 3 mM $MgCl_2$, 25 wt% sucrose and 2 mg/mL lysozyme (from egg white, 10837059001 Roche, Basel, Switzerland) and incubated for 30 min at 37 °C. Afterwards, the plasmid was isolated using the GeneJET Plasmid Miniprep Kit (Thermo Fisher Scientific, MA, USA). Once obtained, the plasmid was transformed into MG1363_GFP as described by Wells et al. [43] with the following adaptations. The MG1363_ GFP cells were precultured in 50 mL M17 broth with 17 wt% (0.5 M) sucrose, 2.5 wt% glycine and 0.5 wt% glucose at 30 °C. After overnight incubation, they were centrifuged (6000 g, 20 min) and washed with 400 mL 17 wt% (0.5 M) sucrose, 10 wt% glycerol (4°C), spun down and resuspended in 200 mL 17 wt% (0.5 M) sucrose, 10 wt% glycerol + 50 mM EDTA (4°C). After incubating on ice for 15 min and spinning down (6000g, 10 min) the cells were washed again as described above and resuspended in 4 mL 17 wt% (0.5 M) sucrose, 10 wt % glycerol (4°C). 40 µL of the cell solution with 1 µL DNA (100 ng/µL in Tris-Buffer) was added to a chilled cuvette and pulsed using a Bio-rad Genepulser (Bio-Rad, CA, USA) for 5.7 ms (2000

V, 25 µF, 200 Ω), after which 1 mL M17 broth with 17 wt% (0.5 M) sucrose, 2.5 wt% glycine, 0.5 wt% glucose, 20 mM $MgCl_2$ and 2 mM $CaCl_2$ was added. The solution was added to M17 agar plates containing 0.5 wt% lactose. After incubation for 48 h, colonies were picked and restreaked.

4.4.6. GROWTH RATE DETERMINATION

To check the phenotype of *L. cremoris* MG1363_GFP Lac^+, we tested whether the strain was fluorescent, and whether the growth rate was similar to the growth rate on lactose of *L. cremoris* MG5267, a lactose-positive *L. cremoris* strain, and similar on glucose to its ancestor strain MG1363. Fluorescence of the strain was confirmed using flow cytometry (Accuri C6, BD, NJ, USA). To prepare the cells for inoculation for the growth rate determination, MG1363_GFP Lac^+ was precultured in CDMpc on both glucose and lactose, and MG5267 and MG1363 were precultured as described above. After 16 h, the OD_{660} was determined using a Jenway 7200 Spectrophotometer (Cole-Palmer, Stone, United Kingdom) and the cells were inoculated in duplicates in 30 mL of the same medium as in the preculture at an OD_{660} of 0.01. To determine the growth rate, the OD_{660} was measured every hour (**??**).

4.4.7. CO-CULTIVATION ON PLATES

L. cremoris MG1363_GFP Lac^+, NZ9000 Glc^- Lac^+ and MG610 were precultured as described above, spun down (8000g, 15 min), washed in sterile PBS and resuspended in PBS to a final concentration of $3x10^7$ cells / mL, as determined by flow cytometry (Accuri C6, BD, NJ, USA). To make the cell mixtures, cells were added together to the indicated cell concentration and strain ratio. Of the cell mixtures, 100 µL was added to plates containing $CDMpc_{cas}$.The plates were incubated for 90 h at 30 °C. Afterwards, the cells were removed from the plate by adding 2 mL sterile PBS and spreading it using a sterile spreader, as described in [44]. The cell suspension was removed from the plate, and the cell concentration and cheater abundance was determined using flow cytometry (Accuri C6, BD, NJ, USA). The final cell concentration was then used to calculate a total final cell count. Together with the known initial cell count this was used to calculate the amount of times the cells had doubled using the following formula:

$$d = \log_2\left(\frac{N_f}{N_i}\right) \tag{4.3}$$

Here, d is the amount of doublings and N_f and N_i are the final and initial cell counts, respectively. To selectively lower the growth rate of cooperator A, erythromycin was added to the agar plates at the indicated concentrations.

	Description	Reference
Strains		
NZ9000 Glc$^-$ Lac$^+$	*L. cremoris* NZ9000Δ*glk*Δ*ptnABCD*, carrying pMG820.	Pool et al., 2006 [40]
MG610	*L. cremoris* MG1363 with two *prtMP* copies integrated into the genome. Erythromycin resistant.	(Leenhouts et al., 1991) [41]
MG1363_GFP	*L. cremoris* MG1363 with Dasher-GFP gene integrated into the genome. Erythromycin resistant.	(Van Tatenhove-Pel et al., 2019) [42]
MG1363_GFP Lac$^+$	MG1363_GFP carrying pMG820. Erythromycin resistant.	This study
MG5267	*L. cremoris* MG1363 with lactose operon integrated into the genome.	(Tarazanova et al., 2017) [45]
Plasmids		
pMG820	23.7 kb lactose miniplasmid containing *lacFEGABCD*.	(Maeda & Gasson, 1986) [46]

Table 4.1: Strains and plasmids used in this study.

Author contributions statement

R.L. designed the research. R.L and T.I. designed the simulations. R.L. and P.v.T. performed simulations and analysed the data. R.L. and T.F. performed experiments and analysed the data. T.F. and R.v.T. designed the experiments. R.v.T. and T.I. supervised the research. R.L. wrote the manuscript with input from all authors.

Acknowledgments

We thank Sagarika Bangalore Govindaraju for her support with the experiments. We thank Felix Frey for reviewing the manuscript.

BIBLIOGRAPHY

[1] K. Sauer, P. Stoodley, D. M. Goeres, *et al.*, "The biofilm life cycle: Expanding the conceptual model of biofilm formation", *Nature Reviews Microbiology*, vol. 20, pp. 608–620, Oct. 2022.

[2] L. Hall-Stoodley, J. W. Costerton, and P. Stoodley, "Bacterial biofilms: From the natural environment to infectious diseases", *Nature Reviews Microbiology*, vol. 2, pp. 95–108, Feb. 2004.

[3] C. D. Nadell, J. B. Xavier, and K. R. Foster, "The sociobiology of biofilms", *FEMS Microbiology Reviews*, vol. 33, pp. 206–224, Jan. 2009.

[4] S. Mitri, J. B. Xavier, and K. R. Foster, "Social evolution in multispecies biofilms", *Proceedings of the National Academy of Sciences*, vol. 108, pp. 10 839–10 846, supplement_2 Jun. 28, 2011.

[5] I. M. Deutschmann, G. Lima-Mendez, A. K. Krabberød, *et al.*, "Disentangling environmental effects in microbial association networks", *Microbiome*, vol. 9, p. 232, Dec. 2021.

[6] G. D'Souza, S. Shitut, D. Preussger, G. Yousif, S. Waschina, and C. Kost, "Ecology and evolution of metabolic cross-feeding interactions in bacteria", *Natural Product Reports*, vol. 35, pp. 455–488, 2018.

[7] S. A. West, G. A. Cooper, M. B. Ghoul, and A. S. Griffin, "Ten recent insights for our understanding of cooperation", *Nature Ecology & Evolution*, vol. 5, pp. 419–430, Apr. 2021.

[8] P. L. Conlin, J. R. Chandler, and B. Kerr, "Games of life and death: Antibiotic resistance and production through the lens of evolutionary game theory", *Current Opinion in Microbiology*, vol. 21, pp. 35–44, Oct. 2014.

[9] I. Frost, W. P. J. Smith, S. Mitri, *et al.*, "Cooperation, competition and antibiotic resistance in bacterial colonies", *The ISME Journal*, vol. 12, pp. 1582–1593, Jun. 2018.

[10] L. Dieltjens, K. Appermans, M. Lissens, *et al.*, "Inhibiting bacterial cooperation is an evolutionarily robust anti-biofilm strategy", *Nature Communications*, vol. 11, p. 107, Jan. 9, 2020.

[11] E. Pessione, "The less expensive choice: Bacterial strategies to achieve successful and sustainable reciprocal interactions", *Frontiers in Microbiology*, vol. 11, Jan. 20, 2021.

[12] A. R. Pacheco and D. Segrè, "A multidimensional perspective on microbial interactions", *FEMS Microbiology Letters*, vol. 366, fnz125, Jun. 1, 2019.

[13] E. Thébault and C. Fontaine, "Stability of ecological communities and the architecture of mutualistic and trophic networks", *Science*, vol. 329, pp. 853–856, Aug. 13, 2010.

[14] J. D. Van Dyken, M. J. Müller, K. M. Mack, and M. M. Desai, "Spatial population expansion promotes the evolution of cooperation in an experimental prisoner's dilemma", *Current Biology*, vol. 23, pp. 919–923, May 2013.

[15] C. D. Nadell, K. Drescher, and K. R. Foster, "Spatial structure, cooperation and competition in biofilms", *Nature Reviews Microbiology*, vol. 14, pp. 589–600, Sep. 2016.

[16] M. Marchal, F. Goldschmidt, S. N. Derksen-Müller, S. Panke, M. Ackermann, and D. R. Johnson, "A passive mutualistic interaction promotes the evolution of spatial structure within microbial populations", *BMC Evolutionary Biology*, vol. 17, p. 106, Dec. 2017.

[17] S. Gupta, T. D. Ross, M. M. Gomez, J. L. Grant, P. A. Romero, and O. S. Venturelli, "Investigating the dynamics of microbial consortia in spatially structured environments", *Nature Communications*, vol. 11, p. 2418, May 15, 2020.

[18] S. Gude, E. Pinçe, K. M. Taute, A.-B. Seinen, T. S. Shimizu, and S. J. Tans, "Bacterial coexistence driven by motility and spatial competition", *Nature*, vol. 578, pp. 588–592, Feb. 27, 2020.

[19] C. D. Nadell, K. R. Foster, and J. B. Xavier, "Emergence of spatial structure in cell groups and the evolution of cooperation", *PLoS Computational Biology*, vol. 6, T. Pfeiffer, Ed., e1000716, Mar. 19, 2010.

[20] F. J. Schwarzendahl and D. A. Beller, "Do active nematic self-mixing dynamics help growing bacterial colonies to maintain local genetic diversity?", *Frontiers in Physics*, vol. 10, p. 940 980, Jul. 12, 2022.

[21] A. Bingham, A. Sur, L. B. Shaw, and H. A. Murphy, "The effect of cooperator recognition on competition among clones in spatially structured microbial communities", *PLOS ONE*, vol. 19, e0299546, 2024.

[22] J. Kayser, C. F. Schreck, Q. Yu, M. Gralka, and O. Hallatschek, "Emergence of evolutionary driving forces in pattern-forming microbial populations", *Philosophical Transactions of the Royal Society B: Biological Sciences*, vol. 373, p. 20 170 106, May 26, 2018.

[23] N. I. van den Berg, D. Machado, S. Santos, *et al.*, "Ecological modelling approaches for predicting emergent properties in microbial communities", *Nature Ecology & Evolution*, vol. 6, pp. 855–865, May 16, 2022.

[24] A. Dal Co, S. van Vliet, D. J. Kiviet, S. Schlegel, and M. Ackermann, "Short-range interactions govern the dynamics and functions of microbial communities", *Nature Ecology & Evolution*, vol. 4, pp. 366–375, Mar. 2020.

[25] R. J. van Tatenhove-Pel, T. Rijavec, A. Lapanje, *et al.*, "Microbial competition reduces metabolic interaction distances to the low µm-range", *The ISME Journal*, vol. 15, pp. 688–701, Mar. 2021.

[26] B. Momeni, K. A. Brileya, M. W. Fields, and W. Shou, "Strong inter-population cooperation leads to partner intermixing in microbial communities", *eLife*, vol. 2, e00230, Jan. 22, 2013.

[27] W. Liu, J. Russel, M. Burmølle, S. J. Sørensen, and J. S. Madsen, "Micro-scale intermixing: A requisite for stable and synergistic co-establishment in a four-species biofilm", *The ISME Journal*, vol. 12, p. 1940, Aug. 2018.

[28] R. J. van Tatenhove-Pel, D. H. de Groot, A. S. Bisseswar, B. Teusink, and H. Bachmann, "Population dynamics of microbial cross-feeding are determined by co-localization probabilities and cooperation-independent cheater growth", *The ISME Journal*, vol. 15, pp. 3050–3061, Oct. 2021.

[29] L. Eigentler, M. Kalamara, G. Ball, C. E. MacPhee, N. R. Stanley-Wall, and F. A. Davidson, "Founder cell configuration drives competitive outcome within colony biofilms", *The ISME Journal*, vol. 16, pp. 1512–1522, Jun. 2022.

[30] S. Xu and J. D. Van Dyken, "Microbial expansion-collision dynamics promote cooperation and coexistence on surfaces", *Evolution*, vol. 72, pp. 153–169, Jan. 2018.

[31] E. L. Bruger, D. J. Snyder, V. S. Cooper, and C. M. Waters, "Quorum sensing provides a molecular mechanism for evolution to tune and maintain investment in cooperation", *The ISME Journal*, vol. 15, pp. 1236–1247, Apr. 1, 2021.

[32] X. Zeng, Y. Zou, J. Zheng, S. Qiu, L. Liu, and C. Wei, "Quorum sensing-mediated microbial interactions: Mechanisms, applications, challenges and perspectives", *Microbiological Research*, vol. 273, p. 127 414, Aug. 1, 2023.

[33] S. Wu, Y. Xue, S. Yang, *et al.*, "Combinational quorum sensing devices for dynamic control in cross-feeding cocultivation", *Metabolic Engineering*, vol. 67, pp. 186–197, Sep. 1, 2021.

[34] J. J. Quispe Haro, F. Chen, R. Los, *et al.*, "Optogenetic control of bacterial cell-cell adhesion dynamics: Unraveling the influence on biofilm architecture and functionality", *Advanced Science*, vol. 11, p. 2 310 079, 2024.

[35] H. Bachmann, D. Molenaar, M. Kleerebezem, and J. E. T. van Hylckama Vlieg, "High local substrate availability stabilizes a cooperative trait", *The ISME Journal*, vol. 5, pp. 929–932, May 1, 2011.

[36] D. Laureys, F. Leroy, T. Hauffman, *et al.*, "The type and concentration of inoculum and substrate as well as the presence of oxygen impact the water kefir fermentation process", *Frontiers in Microbiology*, vol. 12, Feb. 11, 2021.

[37] S. Michielsen, G. T. Vercelli, O. X. Cordero, and H. Bachmann, "Spatially structured microbial consortia and their role in food fermentations", *Current Opinion in Biotechnology*, vol. 87, p. 103 102, Jun. 1, 2024.

[38] T. Storck, C. Picioreanu, B. Virdis, and D. J. Batstone, "Variable cell morphology approach for individual-based modeling of microbial communities", *Biophysical Journal*, vol. 106, p. 2037, May 5, 2014.

[39] C. E. Price, F. Branco dos Santos, A. Hesseling, *et al.*, "Adaption to glucose limitation is modulated by the pleotropic regulator CcpA, independent of selection pressure strength", *BMC Evolutionary Biology*, vol. 19, p. 15, Jan. 10, 2019.

[40] W. A. Pool, A. R. Neves, J. Kok, H. Santos, and O. P. Kuipers, "Natural sweetening of food products by engineering *Lactococcus lactis* for glucose production", *Metabolic Engineering*, vol. 8, pp. 456–464, Sep. 1, 2006.

[41] K. J. Leenhouts, J. Gietema, J. Kok, and G. Venema, "Chromosomal stabilization of the proteinase genes in lactococcus lactis", *Applied and Environmental Microbiology*, vol. 57, pp. 2568–2575, Sep. 1991.

[42] R. J. van Tatenhove-Pel, E. Zwering, A. Solopova, O. P. Kuipers, and H. Bachmann, "Ampicillin-treated lactococcus lactis MG1363 populations contain persisters as well as viable but non-culturable cells", *Scientific Reports*, vol. 9, p. 9867, Jul. 8, 2019.

[43] J. M. Wells, P. W. Wilson, and R. W. Le Page, "Improved cloning vectors and transformation procedure for lactococcus lactis", *The Journal of Applied Bacteriology*, vol. 74, pp. 629–636, Jun. 1993.

[44] E. N. Junkins and B. S. Stevenson, "Using plate-wash PCR and high-throughput sequencing to measure cultivated diversity for natural product discovery efforts", *Frontiers in Microbiology*, vol. 12, Jul. 20, 2021.

[45] M. Tarazanova, T. Huppertz, M. Beerthuyzen, *et al.*, "Cell surface properties of lactococcus lactis reveal milk protein binding specifically evolved in dairy isolates", *Frontiers in Microbiology*, vol. 8, Sep. 7, 2017.

[46] S. Maeda and M. J. Gasson, "Cloning, expression and location of the streptococcus lactis gene for phospho-beta-d-galactosidase", *Journal of General Microbiology*, vol. 132, pp. 331–340, Feb. 1986.

4.5. SUPPLEMENTAL METHODS

INDIVIDUAL-BASED SIMULATION DETAILS

Each particle is modelled as a spherocylinder that consists of two spheres of diameter, D, connected by a spring with a rest length L (**fig. 4.1**a). This rest length is incrementally increased with growth rate μ until it reaches the division length L_d. The particle then splits up into two daughter particles. Here, a tiny bit of noise is added in the orientation to make sure that the particles don't grow in a perfect line. For each particle pair that is within interaction range, R_{int}, of each other, the repulsive or attractive force is determined. First, the shortest distance between the particles is determined. If it is negative, i.e. there is overlap between the particles or the surface, the repulsive force is calculated as a spring force with spring constant k_r, scaling with the amount of overlap d,

$$F(d) = -k_r \cdot d. \tag{4.4}$$

This force is then distributed along the backbone inversely proportional to where along the backbone the overlap occurred.

Particles also experience an attractive force between each other and with the surface. The magnitude of the particle adhesion force depends on the distance r between the centres of the particles and their relative orientations in the following way:

$$F(r,\theta,\phi) = F_{PP} \cdot \left(4\left(\frac{0.95D}{r}\right)^5 - 4\left(\frac{0.95D}{r}\right)^9\right) \cdot \cos\theta \cdot \cos\phi, \qquad \text{for } r > D, \tag{4.5}$$

where D is the diameter of the particles, F_{PP} determines the amplitude of the attractive forces, and θ and ϕ are the angles between the backbones of the two particles. The resulting force is then distributed over the two end-points of the particle inversely related to where the closest point between the particles is situated along the length of the particle.

The attractive force to the surface is implemented similarly, but r is now the distance from the center of the particle to the surface.

$$F(r,\theta) = F_{PS} \cdot \left(4\left(\frac{0.95R}{r}\right)^5 - 4\left(\frac{0.95R}{r}\right)^9\right) \cdot \cos\theta, \qquad \text{for } r > R, \tag{4.6}$$

where R is the radius of the particles or half the diameter, and θ is the angle the particle makes with the surface. Again the force is distributed over the two spheres that make up the particle, inversely proportional to the distance of each end point to the surface. Consequently, the particles experience both a force and a torque due to the attractive and repulsive interactions.

Every time step all the forces that the particles undergo are calculated and they are moved accordingly. We grow all the particles once every 5 time steps. We grow the system to a set amount of particles and then count how many of those particles are cheaters. Values for all the parameters used can be found in **table S4.1**.

Parameter	Explanation	Value
k_{int}	spring constant of the internal spring	$0.1\,\mathrm{N\,m^{-1}}$
D	particle diameter	1 µm
L_d	length of the spring at division	4 µm
k_r	spring constant of the overlap potential	$0.2\,\mathrm{N\,m^{-1}}$
F_{PS}	particle-surface adhesion prefactor	10^{-5} N
F_{PP}	particle-particle adhesion prefactor	10^{-5} N
DT	division time for a particle growing with growth rate μ	10^5 ts
R_{int}	interaction range for which mechanical interactions are calculated	$2 \cdot L_d$
μ	background growth rate for a cheater particle	$0.0002 \cdot$ µm$(5 \cdot \mathrm{ts})^{-1}$
K_s	Hill coefficient for the growth rate adjustment	2.5

Supplementary Table 4.1: Explanation and values used for the simulation parameters.

WELL-MIXED MODEL OF COSTLY COOPERATION

In order to show the effect of spatial structure on our simulated consortium, we compare it to a well-mixed system. For this we solve the following system of equations for the evolution of populations of interacting species A, B and C:

$$\frac{dA}{dt} = (1 - c + H(B, N, b))\, A, \tag{4.7}$$

$$\frac{dB}{dt} = (1 - c + H(A, N, b))\, B, \tag{4.8}$$

$$\frac{dC}{dt} = (1 + H(\min(A, B), N, b))\, C. \tag{4.9}$$

$$\tag{4.10}$$

Here A, B, and C are the size of the population of the corresponding strain. N is the total size of the population. The growth of the populations depends on c, which is the cost of cooperation, and H, which calculates the benefit depending on the ratio of the cooperative species as follows:

$$H(n, N, b) = \frac{\frac{n}{N} \cdot \bar{n}}{K_s + \frac{n}{N} \cdot \bar{n}} \cdot b, \tag{4.11}$$

$$\tag{4.12}$$

where n is the amount of beneficial particles in the total population and N is the size of the total population. Additionally, b is the benefit of cooperation, K_s is the Hill coefficient which is set to 2.5, and $\bar{n}$ is the average number of neighbours a particle has, which is set to 7.5.

The initial conditions are the same as for the simulations, so 10 of each strain, the cheater fraction is measured when a population size of 10^4 particles is reached. The results are summarised in **fig. S4.2**.

A:B:C RATIOS AND HOW THEY RELATE TO EFFECTIVE DISTANCE BETWEEN COOPERATORS

If we look from the perspective of a B particle on a plate, the amount of particles that we find within radius, r, away from that particle follows a Poisson distribution,

$$P(k) = \frac{\lambda^k \cdot e^{-\lambda}}{k!}, \text{ with } \lambda = \pi r^2 \sigma. \tag{4.13}$$

Here, k is the amount of particles and λ is the expectation value of the amount of particles in a circle of radius r, based on the density of the particles σ. Because we are interested in what the first encounter will be, we want to compare the radii for the first encounter with an A particle and the one with a C particle. The probability of having at least one A particle within a radius, r, is given by,

$$\begin{aligned} P(A) &= 1 - P(0), \\ &= 1 - e^{-\pi r^2 \sigma_A}. \end{aligned} \tag{4.14}$$

From this we can get a probability density function,

$$\begin{aligned} f(r) &= \frac{\mathrm{d}}{\mathrm{d}r} P(A), \\ &= 2\pi r \sigma_A \cdot e^{\pi r^2 \sigma_A}, \end{aligned} \tag{4.15}$$

which we can then use to find an expectation value of what the distance is that a B will encounter its first neighbour of type A.

$$\begin{aligned} \langle r_{AB} \rangle &= \int_0^\infty r \cdot 2\pi r \sigma_A \cdot e^{\pi r^2 \sigma_A} \, \mathrm{d}r \\ &= \frac{1}{2\sqrt{\sigma_A}}. \end{aligned} \tag{4.16}$$

Similarly, the first neighbour of type C is expected to be found at,

$$\langle r_{CB} \rangle = \frac{1}{2\sqrt{\sigma_C}}. \tag{4.17}$$

When we subtract the two we get the expected relative distance which denotes who is expected to be further away from B, A or C:

$$\langle r_{AB} - r_{CB} \rangle = \frac{1}{2\sqrt{\sigma_A}} - \frac{1}{2\sqrt{\sigma_C}}. \tag{4.18}$$

Strain	Carbon source	R^2 rep. 1	R^2 rep. 2	μ_{max} (1/h) ± SD
MG1363-GFP (Lac$^+$)	0.09 wt% glc	0.997	0.998	0.67 ± 0.00
MG1363-GFP	0.09 wt% glc	0.997	0.998	0.57 ± 0.01
MG1363-GFP (Lac$^+$)	0.09 wt% lac	0.996	0.999	0.66 ± 0.00
MG5267	0.09 wt% lac	0.998	0.996	0.64 ± 0.00

Supplementary Table 4.2: Goodness-of-fit of all extracted growth curves as determined by the R^2 of the $\ln(OD_{660})$ over time and resulting μ_{max} ± SD (n=2)

The particle density at inoculation, σ, can be easily calculated, as it is always the same, namely $3 \cdot 10^6$ cells on a petri dish with a diameter of 9 cm. This gives us an overall initial particle density of

$$\sigma = \frac{3 \cdot 10^6}{\pi (4.5 \cdot 10^4)^2}, \tag{4.19}$$

$$= 0.00465 \ \mu m^{-2} \tag{4.20}$$

The densities of A and C are then simply the fractions of those particles times this overall density. $\langle r_{AB} - r_{CB} \rangle$ is plotted for all [C]/[A] ratios used in the 10% cheater fraction experiments in **fig. 4.4**b.

Growth study

fig. S4.5 shows a representative example of how we calculated the growth rate μ_{max}. As example, we describe the growth study of MG1363-GFP Lac$^+$ on 0.09 wt% glucose. We measured the OD_{660} from duplicate shake-flasks hourly (**fig. S4.5**a). We extracted the exponential phase by plotting the log-linear of OD_{660} versus time and fitting a linear curve to the segment where the $\log(OD_{660})$ increased linearly, as determined by the least-squares method (**fig. S4.5**b). We determined the goodness-of-fit for all replicate curves by R^2 (**table S4.2**).

Gating strategy

fig. S4.6 shows the flow cytometry gating strategy for a representative example.

Step 1: Exclude noise We determined the location of the background noise by the buffer by plotting the forward and side scatter of a sample consisting of only the buffer. This yielded gate 1. From a sample with cells, gate 2 containing everything except the noise was drawn.

Step 2: Determining the fraction of the fluorescent cheater cells Gate 2, containing the cells, was the reference for plotting fluorescence against forward scatter. In this plot, the fluorescent cheater cells were marked as Gate 3. To calculate the cheater fraction, we divided the number of these fluorescent cells by the total cell count, excluding the noise.

4.6. SUPPLEMENTAL FIGURES

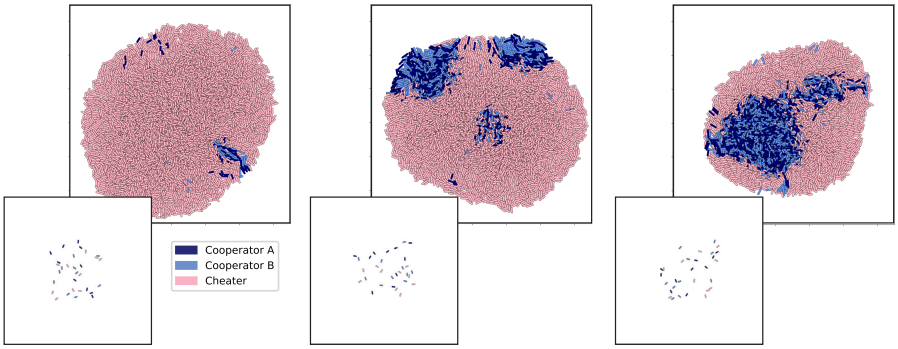

Supplementary Figure 4.1: Examples of three different final colonies for the same input parameters for the cross-feeding interaction; value for cost = 0.8 and benefit = 4.0. In the bottom-left corner of each final colony, the initial configuration of that run is shown. Area shown is always $130 \times 130\ \mu m^2$.

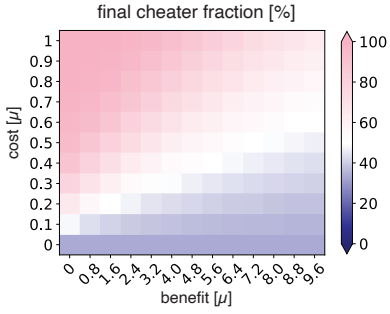

Supplementary Figure 4.2: Final cheater fraction for a well-mixed system of A, B and C growing to a population size of 10^4. Interactions are implemented similarly to the IBM, see SI.

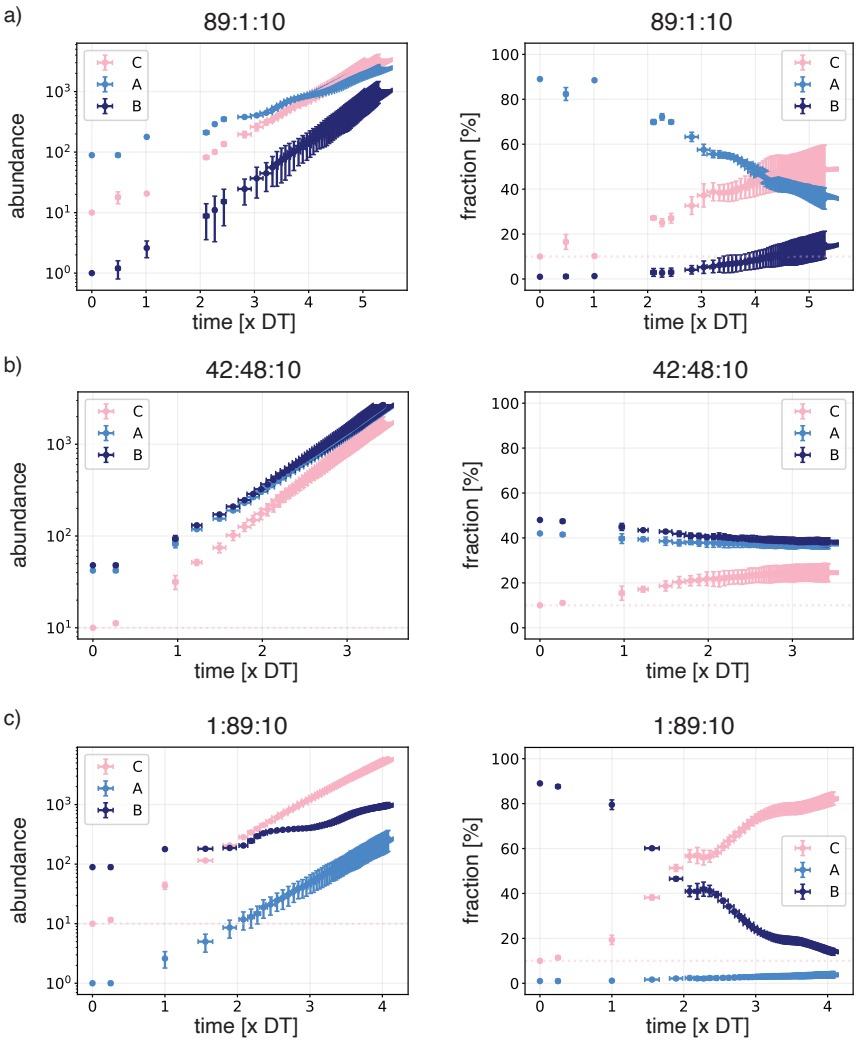

Supplementary Figure 4.3: Abundance and fraction of the different particle types over simulation time for the simulation data points of **fig.** 4.5b A:B:C ratios a) 89:1:10, b) 42:48:10, and c) 1:89:10. All points are averages and standard deviations of 5 runs.

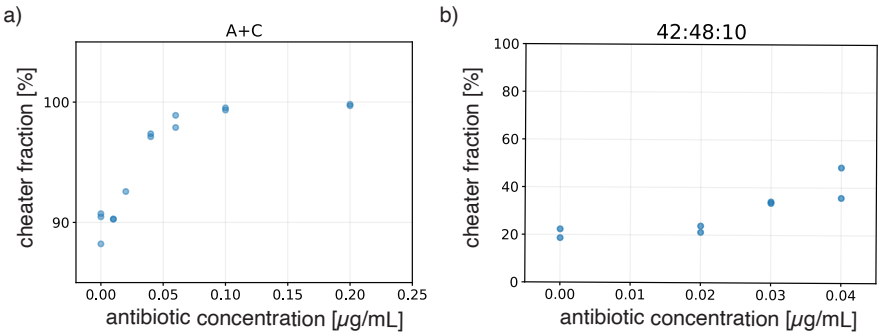

Supplementary Figure 4.4: Final cheater fraction for different concentrations of erythromycin a) in plates containing casein and amino acids inoculated with A & C together, and b) in plates containing casein inoculated with A, B & C in a 42:48:10 ratio.

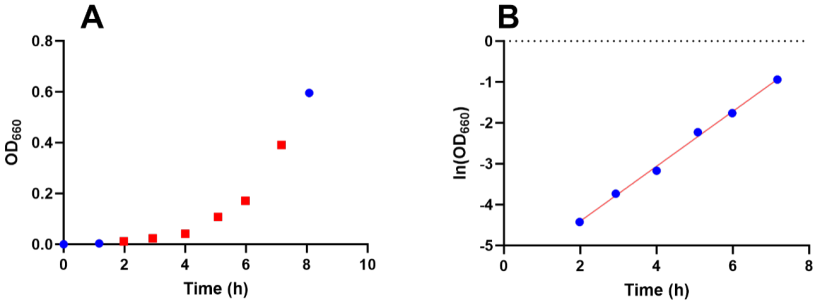

Supplementary Figure 4.5: Growth curve of MG1363-GFP Lac$^+$ (cheater). a) OD_{660} over time. The exponential phase is marked with red squares. b) $\ln(OD_{660})$ of the exponential phase measurements over time. A linear curve was fit to the measurements by least-squares fit.

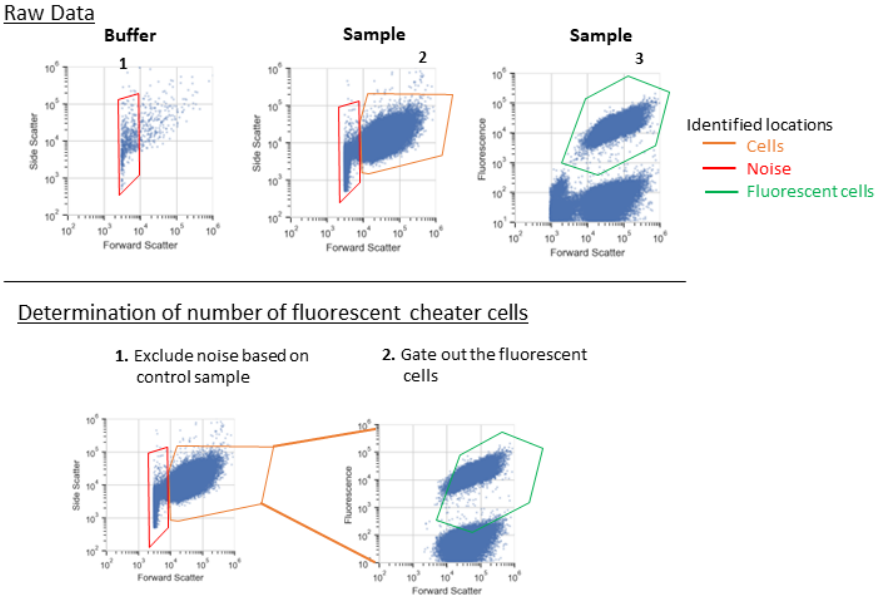

Supplementary Figure 4.6: Flow cytometry gating strategy. Areas within the forward scatter – side scatter and fluorescence – forward scatter were identified using control samples. The gating excluded noise and was able to clearly distinguish between fluorescent and non-fluorescent cells to calculate the %cheater fraction.

5

COOPERATOR INTERMIXING IS AN EFFECTIVE COMPETITIVE STRATEGY AGAINST CHEATERS

Bacteria live closely together with many other species in surface-attached communities. They interact with neighbouring cells through metabolite exchange and resource sharing. This chapter investigates the spatial structuring of these bacterial colonies through individual-based modelling. We focus on mutualistic interactions which have been shown to induce mixing. Here we demonstrate that such cooperative mixing within colonies is robust against variations in bacterial shape and asymmetries in cooperative contributions. We additionally show that mixing is effective in excluding non-reciprocal cheaters. The strength of cooperation is the most influential factor for successful intermixing and competitive stability.

5.1. INTRODUCTION

Bacteria live with many different species which all interact and co-exist together in surface-attached communities. They exhibit cooperative, competitive and antagonistic behaviour, forming complicated population networks [1], [2]. Studying these interaction networks is important for our understanding of biofilms, but it is also a good simple framework to study population dynamics in general [3]–[5].

An important feature of surface-attached colonies is that they are spatially structured. This means that individual bacteria are not interacting with all of the other bacteria in the biofilm at all times, but only the ones surrounding them. Multi-species spatial patterning has been shown to emerge in many different experimental and computational systems [6], [7]. Pattern formation can occur through passive processes such as clonal patching or genetic drift [8], [9]. It can also occur through active competition or quorum sensing induced processes [10], [11]. Additionally, variations in shape and other types of heterogeneity can cause phase separation in active systems, causing patches [11], [12]. Strong mutualistic interactions, on the other hand, have been shown to promote mixing in lattice-based simulations and experiments [6], [13].

Physical delineation between species is essential for the stabilisation of cooperative interactions and the co-existence of competing strains [11], [14]–[16]. Moreover, structural complexity has been shown to disrupt competitive dynamics and stabilise otherwise unstable interactions [17], [18]. Additionally, spatial patterning is important in evolutionary phenomena such as gene-surfing and the emergence of cooperation [7], [8], [19]–[21].

Species interactions play out differently on a surface than they do in solution. Here we use an individual-based approach to study spatially structured growing colonies of cooperating bacteria. We are particularly interested in the spatial patterning that results from mutualistic cooperation and how robust it is against perturbations of the system.

5.2. MATERIALS AND METHODS

INDIVIDUAL BASED MODEL

We simulate a cross-feeding pair of bacterial strains (**fig. 5.1**a). We simulate the cells as spherocylindrical particles on a surface and let them grow, divide and mechanically interact with each other as described in **chapter 1**. Here, we keep the particles in 2D and do not let them grow into the third dimension (**fig. 5.1**b).

The cross-feeding interaction between the different cooperators is implemented by adjusting their growth rates based on their immediate environment (**fig. 5.1**c) [22], [23]. In particular, for every growth step, we count for each particle how many of their neighbours are cooperators of them. For cooperator A this means, how many of its neighbours are cooperator B, and vice versa. We use this

number as input for a scaled Monod equation:

$$\mu_i' = \mu \cdot \left(1 + \frac{n}{K_s + n} \cdot b_i\right). \tag{5.1}$$

This determines the growth rate, μ', of particle i, where, n is the number of beneficial neighbours. K_s is the Hill coefficient, which we set to 1.5 as this is the half-way point of the curve at the average number of beneficial direct neighbours in a well-mixed colony, μ is the background growth of the cooperators, i.e., the growth rate of an isolated cooperator particle. Benefit, b, is given as multiples of μ, where b sets the maximal growth rate a particle can achieve. We start with 2 cooperators next to each other, and evolve the system until the colony reaches a size of 3×10^3 particles.

We also introduce a cheater species, C. These grow similarly to A and B, except that they have a growth advantage of μ, as such:

$$\mu_C' = \mu \cdot \left(2 + \frac{n}{K_s + n} \cdot b_C\right). \tag{5.2}$$

In simulations with cheaters we start with 2 cooperators next to each other and 6 cheater particles surrounding them, pointing radially outward. Again, we evolve the system to a size of 3×10^3 particles.

5.2.1. Well-mixed model of cooperative interactions

In order to show the effect of spatial structure on our simulated consortium, we compare it to a well-mixed system. For this we solve the following system of equations for the evolution of populations of interacting species A and B:

$$\frac{\mathrm{d}A}{\mathrm{d}t} = \left(1 + H\left(\frac{B}{N}, b_A\right)\right) A, \tag{5.3}$$

$$\frac{\mathrm{d}B}{\mathrm{d}t} = \left(1 + H\left(\frac{A}{N}, b_B\right)\right) B. \tag{5.4}$$

Here A, and B represent the size of the population of the corresponding strain. N is the total size of the population. The growth of the populations depends on H, which calculates the benefit depending on the ratio of the cooperative species in the population as follows:

$$H(X, b) = \frac{X \cdot \bar{n}}{K_s + X \cdot \bar{n}} \cdot b, \tag{5.5}$$

where X is the fraction of beneficial particles in the total population and b is the benefit of cooperation that the strain experiences. Moreover, K_s is the Hill coefficient which is set to 1.5, and $\bar{n}$ is the average number of neighbours a particle has, which is set to 6 as that is what the measured amount of neighbours is for 2D colonies (**fig. S5.1**).

Parameter	**Explanation**	**Value**
k_{int}	spring constant of the internal spring	0.1
D	particle diameter	1 µm
L	length of the spring at division	varied
AR	aspect ratio	L/D
k_{r}	spring constant of the overlap potential	$2\cdot\ k_{\text{int}}$
F_{PP}	particle-particle adhesion force magnitude	$1\times10^{-4}\,k_{\text{int}}$
α	particle-particle adhesion range	5 nm
F_{PS}	particle-surface adhesion force magnitude	$1\times10^{-4}\,k_{\text{int}}$
β	particle-surface adhesion range	5 nm
R_{int}	interaction range for which mechanical interactions are calculated	$2\cdot L$
μ	growth rate	1×10^{-4} µm$(5\cdot$ ts$)^{-1}$
σ_μ	standard deviation for the growth rate noise	$0.1\cdot\mu$
σ_θ	standard deviation for the orientational noise	0.1
K_s	Hill coefficient for the cooperative interaction	1.5
$\bar{n}$	average number of neighbours for the continuum model	6

Table 5.1: Explanation and values used for the simulation parameters.

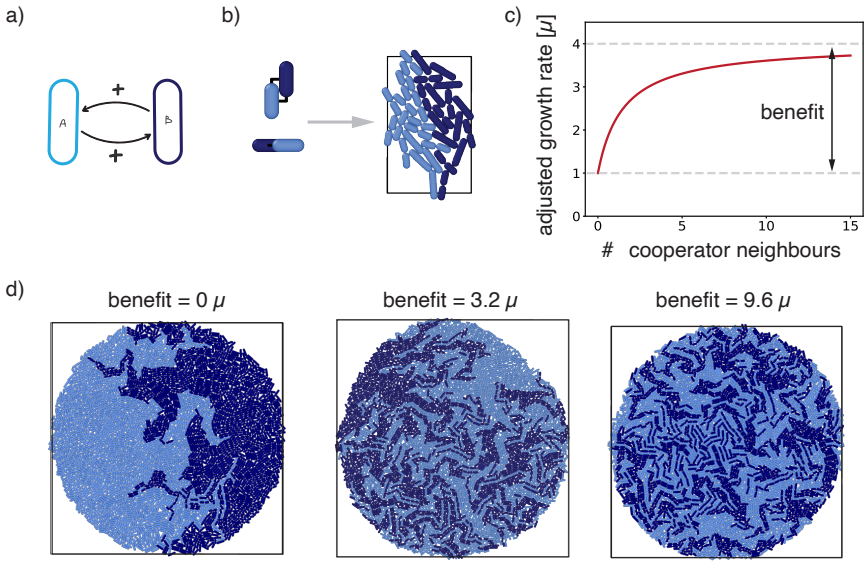

Figure 5.1: **Reciprocal cooperation leads to mixing** a) Schematic representation of a cross-feeding interaction between strain A and strain B. b) Stills from our individual-based model of spherocylindrical particles, growing and dividing. c) Example of how the growth rate of a particle depends on the amount of neighbours of the other strain it has in its immediate vicinity. Note that the average number of neighbours of a particle in these simulations is around 6. d) Snapshots of colonies of 3×10^3 particles for different values for the benefit.

The initial conditions are the same as for the simulations, so 1 of each strain, population fractions are measured when a population size of 3×10^3 particles is reached. The results are summarised in **fig. S5.3**.

We also introduce a cheater species C, as follows:

$$\frac{\mathrm{d}C}{\mathrm{d}t} = \left(2 + H\left(\frac{\min\{A,B\}}{N}, b_C\right)\right) C. \tag{5.6}$$

Here, the growth of C depends on the minimum of A and B that is in the population.

5.3. Results and Discussion

5.3.1. Reciprocal cooperation leads to mixing

We define the strength of the cooperative interaction by the magnitude of the benefit they experience (**fig. 5.1**c). When we evolve the system for varying interaction strengths, we see a clear increase in mixing compared to a non-interacting system (**fig. 5.1**d). This is in line with what we expect from existing literature [6], [13].

5.3.2. COOPERATOR MIXING IS ROBUST TO CHANGES IN PARTICLE SHAPE

To study the effect of the interaction strength on spatial patterning, we measure global and local mixing once the colony reaches a size of 3×10^3 particles. For the global mixing, we simply look at the distribution of the x-coordinates for the different strains (**fig. 5.2**a). In a non-interacting system, A and B will roughly form two patches (bottom row). As soon as the particles start cooperating, these patches mix and A and B will become evenly distributed over left and right. As a measure of local mixing, we take the average fraction of cooperator neighbours, where a value of ≈ 0.58 would mean a perfectly mixed colony (**fig. 5.2**b). We observe minimal mixing where there is no cooperation, and a gradual increase of mixing with increasing benefit. For values of the benefit higher than $\approx 5\ \mu$, the mixing stabilises at a cooperator fraction of around 0.4.

Because the particles in our system are elongated, we expected nematic effects to influence the mixing [9]. However, when we run the simulations for varying particle sizes, there is no observable trend suggesting that longer particles mix better (**fig. 5.2**b). The distribution of the cooperator neighbours is very similar for different aspect ratios with a large spread, but most particles falling into the same range (**fig. S5.2**). This is also the case for non-interacting particles, where most particles have only neighbours of their own kind (benefit = 0).

We also looked at what happens when the two strains are dissimilarly shaped, as previous work has shown that differences in cell shape can lead to phase separation in active systems of non-interacting particles [12]. In our cooperating system however, particles of varying shape globally mix just as well as similarly shaped particles (**fig. 5.2**c). Local mixing seems to be impeded slightly when particles have a difference in shape of about 3 times the diameter, but up until that point, variations in shape have very little effect (**fig. 5.2**d). This shows us that cooperator mixing is robust against the variations in cell shape that are to be reasonably expected in different strains of bacilli.

5.3.3. ASYMMETRIC COOPERATORS STILL MIX

It seems unlikely that cross-feeding interactions in nature are perfectly symmetrical, in the sense that both cooperating species will experience exactly the same benefit from the interaction. Therefore, we looked at populations where the benefit that A experiences is higher than the benefit that B experiences (**fig. 5.3**a, b). We show snapshots for different values of the benefit A experiences (benefit A) and for different values of the difference between benefit A and benefit B, denoted as Δbenefit (**fig. 5.3**c). For each combination we show two snapshots side by side, coloured by species (left) and by growth rate (right). For all combinations of benefits, A and B show more intermixing than would be the case when there is no cooperation.

A difference in experienced benefit does lead to a different make up of the pop-

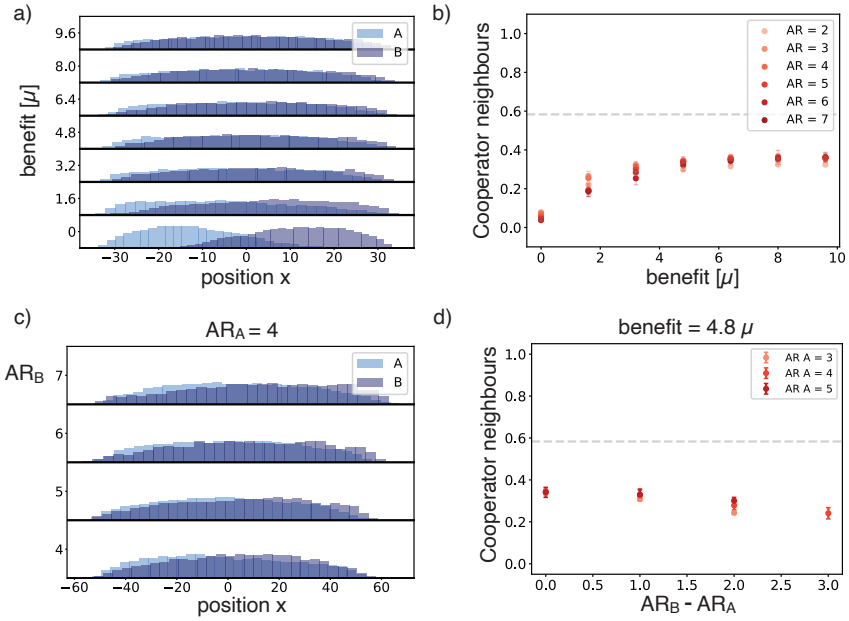

Figure 5.2: **Cooperator mixing is robust to changes in particle shape** a) Distribution of x positions for A and B for different values of benefit. AR = 4. b) Fraction of cooperator neighbours as a function of interaction strength for different aspect ratios. Error bars represent the standard error over 5 runs. c) Distribution of x positions for differently shaped A and B. $AR_A = 4$ and AR_B varies. Benefit is constant at 4.8 μ. d) Fraction of cooperator neighbours for unequally shaped particles, with the difference in AR on the x-axis. Error bars show standard error of 5 runs.

ulation (**fig. 5.3**d). The larger the difference, the more A will outgrow B in the final colony. This effect can be captured quite well with a continuum model of interacting particles which only slightly over-estimates how fast A will outgrow B. The continuum model assumes a perfectly mixed system, which in a spatially structured environment, such as a surface-attached colony, is often not an accurate assumption. Interestingly however, in this system of cooperating particles, because of the self-induced mixing of the particles it becomes a reasonable approximation.

Even though B seems to be outgrown by A for very high values of Δbenefit, B does find itself in more beneficial environments. This because species intermixing is still prevalent, and since the B particles in the colonies are surrounded by A, they can grow at a rate closer to their optimum growth rate (**fig. 5.3**c, e). A, on the other hand, is mostly growing on its background growth rate (**fig. 5.3**c). This process somewhat mitigates the difference in fitness between the strains and evens the playing field to some extent, allowing B to catch up to A, more so than if they would not mix. Local intermixing between species does decrease with larger Δbenefits (**fig. 5.3**e).

5.3.4. COOPERATOR INTERMIXING IS A VIABLE STRATEGY TO KEEP OUT CHEATERS

Because intermixing decreases when cooperation becomes less reciprocal, it begs the question whether this reduced mixing is enough to keep possible cheaters out of a cooperator patch. In order to investigate the effect of cooperator intermixing on competitive dynamics, we introduce a cheater to our symmetric cooperator system (**fig. 5.4**a). This cheater species, C, experiences the same benefit from A and B as the cooperators, however, it does not reciprocate the cooperation. We also assume the cheater species has an overall fitness advantage of μ because it does not have to pay the fitness cost of producing any cross-fed metabolites.

We run simulations where we surround our cooperator pair with 6 cheaters, and let the colony grow to a size of 3000 particles (**fig. 5.4**b, c). When we then record the make up of the population for various values of the benefit, we see that at sufficiently high benefit, the cooperators start out-competing the cheaters (**fig. 5.4**d). This transition coincides with the value of the benefit where we start seeing optimal mixing between cooperators (**fig. 5.4**e). Looking at the fraction of cooperator neighbours for the different species, we see that A and B still intermix in the presence of cheaters, but the cheaters don't manage to intermix with the cooperators. Cheaters are mostly surrounded by other cheaters and are therefore mostly operating on their background growth rate. This is probably because as soon as cheaters mix with cooperators, they grow very fast, however because they don't reciprocate, their cooperator neighbours don't grow as fast. This means that the cheaters soon run out of cooperator neighbours and they get pushed out of a cooperator patch.

The continuum representation of a system containing cheaters that have an overall fitness advantage, consistently predicts cheater dominance for all benefits

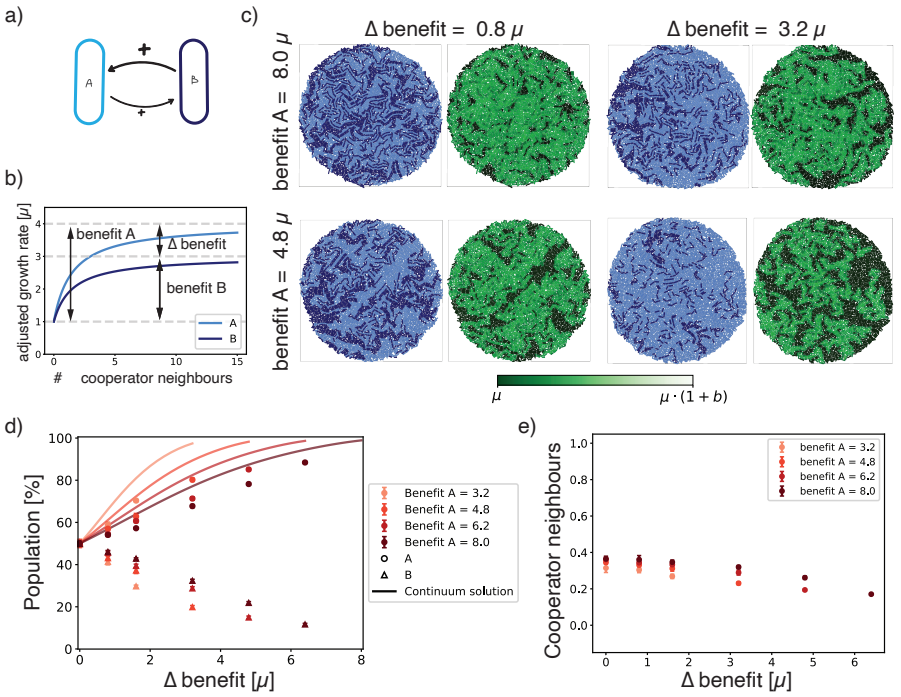

Figure 5.3: **Asymmetric cooperators still mix** a) Schematic representation of an asymmetric interaction, where B benefits A more than A benefits B. b) Adjusted growth rate of A and B for the asymmetric interaction. c) Snapshots of colonies at 3×10^3 particles for two values of the benefit A experiences and two values for the difference between that benefit and the benefit B experiences, denoted as Δbenefit. For each colony, the left figure shows the strains, coloured as in a). The right figure shows individual particle growth rates, coloured in green according to the legend. d) Fraction of the population of A (circles) and B (triangles) as a function of Δbenefit and for different values of benefit A. Error bars show the standard error for 5 runs. The lines denote the solution of the continuum well-mixed model. e) Fraction of cooperator benefit for A (circles) and B (triangles) as a function of Δbenefit for different values of benefit A. Error bars show the standard error for 5 runs.

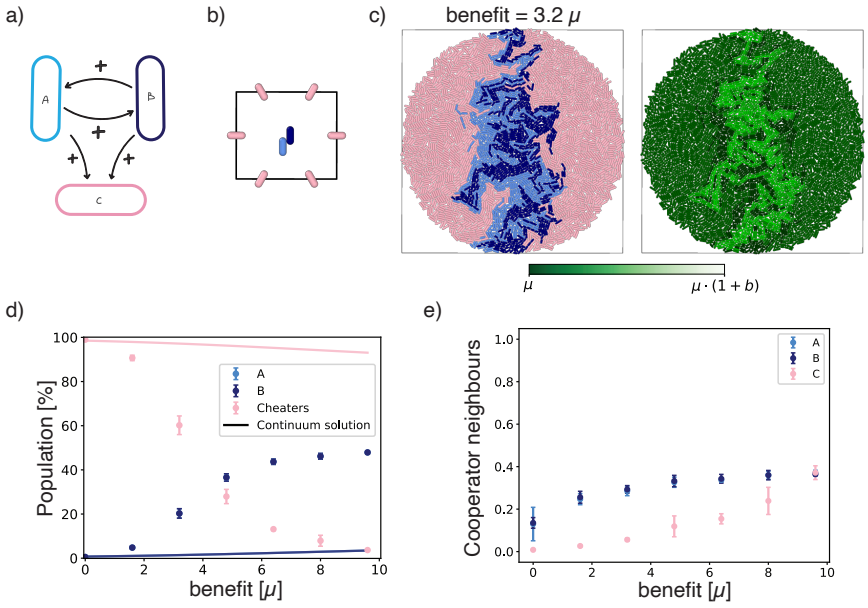

Figure 5.4: **Cooperator intermixing is a viable strategy to keep out cheaters** a) Schematic representation of two cross-feeding cooperators, A and B, and a cheater strain, C, that benefits from the cooperators but does not contribute to the interaction. b) Snapshot of initial configuration of the simulations, consisting of two cooperators, surrounded by 6 cheaters. c) Snapshots of a colony of 3×10^3 particles coloured by species (left), and coloured by growth rate (right). d) Fraction of the population for A, B and C as a function of benefit. Error bars show the standard deviation of 5 runs. e) Fraction of cooperator neighbours for A, B and C as a function of benefit. Error bars represent standard error of 5 runs.

(**fig. 5.4**d). Where our continuum model worked well for the reciprocal system of just cooperators, as soon as there is non-reciprocity, it breaks down completely. This underscores the importance of taking into account spatial structure and physical patterning when thinking about competition.

5.4. CONCLUSION

In this study, we used an individual-based modelling approach to explore the spatial patterning in surface-attached colonies of cooperating bacteria. Our results show that reciprocal cooperation leads to significant mixing within the colonies as previously established [13]. We further show this mixing is robust against variations in particle shape. Both in the general colony and between differently shaped strains, the cooperative interactions consistently resulted in effective mixing. Moreover, even when cooperators were asymmetric in how much they benefit their cooperator counterpart, they continued to mix substantially. We also show

how this self induced mixing excludes non-reciprocal cheaters from the colony, proving an effective competitive strategy. Lastly, we show that in strongly reciprocal systems, continuum models that assume a well-mixed system can be accurate, however, once we introduce non-reciprocity, continuum models do significantly worse.

In summary, our findings show that the strength of cooperation is the most important factor for successful intermixing. The robustness of cooperator mixing to shape variations and its effectiveness in excluding cheaters highlight the importance of these dynamics in the stability and evolution of cooperative behaviours in microbial communities. Taken together, we propose that focusing on strong cooperation is the best strategy to gain advantage over stronger cheaters or other competing species.

BIBLIOGRAPHY

[1] A. R. Pacheco and D. Segrè, "A multidimensional perspective on microbial interactions", *FEMS Microbiology Letters*, vol. 366, fnz125, Jun. 1, 2019.

[2] I. M. Deutschmann, G. Lima-Mendez, A. K. Krabberød, *et al.*, "Disentangling environmental effects in microbial association networks", *Microbiome*, vol. 9, p. 232, Dec. 2021.

[3] E. Frey, "Evolutionary game theory: Theoretical concepts and applications to microbial communities", *Physica A: Statistical Mechanics and its Applications*, vol. 389, pp. 4265–4298, Oct. 2010.

[4] N. I. van den Berg, D. Machado, S. Santos, *et al.*, "Ecological modelling approaches for predicting emergent properties in microbial communities", *Nature Ecology & Evolution*, vol. 6, pp. 855–865, May 16, 2022.

[5] L. Röttjers and K. Faust, "From hairballs to hypotheses–biological insights from microbial networks", *FEMS Microbiology Reviews*, vol. 42, pp. 761–780, Nov. 1, 2018.

[6] W. Liu, J. Russel, M. Burmølle, S. J. Sørensen, and J. S. Madsen, "Micro-scale intermixing: A requisite for stable and synergistic co-establishment in a four-species biofilm", *The ISME Journal*, vol. 12, p. 1940, Aug. 2018.

[7] J. Kayser, C. F. Schreck, Q. Yu, M. Gralka, and O. Hallatschek, "Emergence of evolutionary driving forces in pattern-forming microbial populations", *Philosophical Transactions of the Royal Society B: Biological Sciences*, vol. 373, p. 20 170 106, May 26, 2018.

[8] O. Hallatschek, P. Hersen, S. Ramanathan, and D. R. Nelson, "Genetic drift at expanding frontiers promotes gene segregation", *Proceedings of the National Academy of Sciences*, vol. 104, pp. 19 926–19 930, Dec. 11, 2007.

[9] F. J. Schwarzendahl and D. A. Beller, "Do active nematic self-mixing dynamics help growing bacterial colonies to maintain local genetic diversity?", *Frontiers in Physics*, vol. 10, p. 940 980, Jul. 12, 2022.

[10] A. I. Curatolo, N. Zhou, Y. Zhao, *et al.*, "Cooperative pattern formation in multi-component bacterial systems through reciprocal motility regulation", *Nature Physics*, vol. 16, pp. 1152–1157, Nov. 2020.

[11] S. Gude, E. Pinçe, K. M. Taute, A.-B. Seinen, T. S. Shimizu, and S. J. Tans, "Bacterial coexistence driven by motility and spatial competition", *Nature*, vol. 578, pp. 588–592, Feb. 27, 2020.

[12] W. P. J. Smith, Y. Davit, J. M. Osborne, W. Kim, K. R. Foster, and J. M. Pitt-Francis, "Cell morphology drives spatial patterning in microbial communities", *Proceedings of the National Academy of Sciences*, vol. 114, Jan. 17, 2017.

[13] B. Momeni, K. A. Brileya, M. W. Fields, and W. Shou, "Strong inter-population cooperation leads to partner intermixing in microbial communities", *eLife*, vol. 2, e00230, Jan. 22, 2013.

[14] B. Maier, "How physical interactions shape bacterial biofilms", *Annual Review of Biophysics*, vol. 50, pp. 401–417, May 6, 2021.

[15] E. Pessione, "The less expensive choice: Bacterial strategies to achieve successful and sustainable reciprocal interactions", *Frontiers in Microbiology*, vol. 11, Jan. 20, 2021.

[16] A. Bingham, A. Sur, L. B. Shaw, and H. A. Murphy, "The effect of cooperator recognition on competition among clones in spatially structured microbial communities", *PLOS ONE*, vol. 19, e0299546, 2024.

[17] N. Vallespir Lowery and T. Ursell, "Structured environments fundamentally alter dynamics and stability of ecological communities", *Proceedings of the National Academy of Sciences*, vol. 116, pp. 379–388, Jan. 8, 2019.

[18] S. Xu and J. D. Van Dyken, "Microbial expansion-collision dynamics promote cooperation and coexistence on surfaces", *Evolution*, vol. 72, pp. 153–169, Jan. 2018.

[19] Y. Azimzade and A. A. Saberi, "Geometrically regulating evolutionary dynamics in biofilms", *Physical Review E*, vol. 103, p. L050401, May 18, 2021.

[20] M. Gralka, F. Stiewe, F. Farrell, W. Möbius, B. Waclaw, and O. Hallatschek, "Allele surfing promotes microbial adaptation from standing variation", *Ecology Letters*, vol. 19, B. Blasius, Ed., pp. 889–898, Aug. 2016.

[21] C. D. Nadell, K. R. Foster, and J. B. Xavier, "Emergence of spatial structure in cell groups and the evolution of cooperation", *PLoS Computational Biology*, vol. 6, T. Pfeiffer, Ed., e1000716, Mar. 19, 2010.

[22] R. J. van Tatenhove-Pel, T. Rijavec, A. Lapanje, *et al.*, "Microbial competition reduces metabolic interaction distances to the low µm-range", *The ISME Journal*, vol. 15, pp. 688–701, Mar. 2021.

[23] A. Dal Co, S. van Vliet, D. J. Kiviet, S. Schlegel, and M. Ackermann, "Short-range interactions govern the dynamics and functions of microbial communities", *Nature Ecology & Evolution*, vol. 4, pp. 366–375, Mar. 2020.

5.5. SUPPLEMENTARY FIGURES

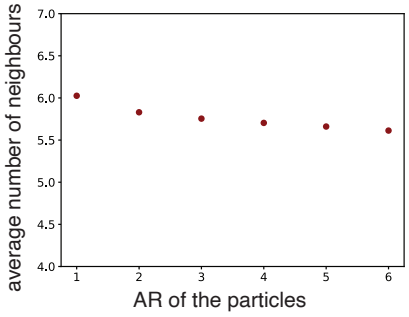

Supplementary Figure 5.1: Average number of neighbours for particles with different aspect ratios.

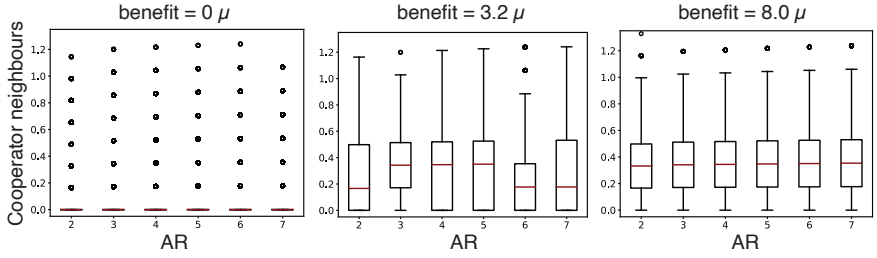

Supplementary Figure 5.2: Distribution of cooperator neighbour fractions as a function of aspect ratio for different values of benefit.

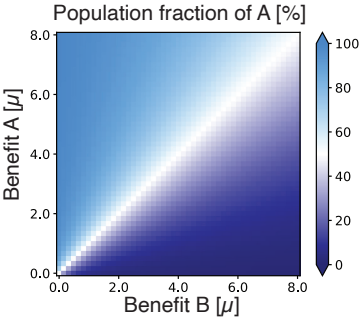

Supplementary Figure 5.3: Continuum solution for different values of benefit A and B.

6

CONCLUSION

In this thesis I have investigated how species interactions play out in a spatially structured environment, providing new insights into the behaviour and optimisation of biofilm-based systems. Using individual-based models, in combination with other computational approaches, and engineered microbial consortia, I explored how tuning mechanical and social factors influences biofilm structure and function. Here, I summarise the key findings and discuss their broader implications for research and industrial applications.

In **chapter 2**, we demonstrated that photoswitchable adhesins can dynamically control bacterial aggregation and biofilm structure. Under pulsed light, bacterial aggregates exhibited liquid-like behaviour, enhancing particle intermixing and quorum sensing activation, while continuous light resulted in more solid-like, dense biofilms. Pulsed illumination improved biofilm growth and *L*-threonine production in co-cultures, showcasing its potential for optimising industrial biofilm applications. Our simulations, specifically, showed that aggregation increased under pulsating light because the off periods allowed for partial disassembly of the clusters, leading to bigger clusters in the end. Depending on the specific bacterial pairs, different light conditions could be tailored to optimise biofilm performance and productivity.

In **chapter 3** we introduce an individual-based model for simulating microcolonies growing on a surface. Varying particle and surface adhesion strengths led to distinct global colony architectures where high surface-adhesion resulted in flat colonies with raised centres, while strong particle adhesion and weak surface adhesion produced dome-shaped colonies. Our individual-based simulations highlighted limitations in capturing different internal structures due to the lack of surface anchoring and isotropic friction in the model. Nonetheless, we show the model is versatile and can produce realistic colony shapes.

In **chapter 4** we aimed to understand what determines cooperator success in

the presence of cheaters. Simulations revealed that the initial placement of microorganisms significantly impacts cooperator success in the presence of cheaters. First contact time between cooperators was a better predictor of success than interaction parameters alone. We engineered an *L. cremoris* consortium representing our cooperator cheater interactions. By altering the starting ratios, we showed that also in a real system, relative distances between cooperators and cheaters were strong determinants of cooperator success. These results, we could closely match with our simulations. We further probed our hypothesis by using antibiotics to inhibit the background growth, which was analogous to increasing cost of cooperation. Again, we could recapitulate the predictions from our simulations in experiments, further strengthening our argument that first contact time between cooperators determines cooperator success in the presence of cheaters.

In **chapter 4**, we already observed strong mixing of cooperators. In **chapter 5** we zoomed in on this phenomenon. We saw that reciprocal cooperation led to significant mixing within colonies, even across different particle shapes and asymmetries in cooperation levels. Strongly reciprocal systems aligned well with continuum models assuming well-mixed systems, but introducing non-reciprocity reduced the accuracy of these continuum models. This highlights the need for incorporating spatial and interaction dynamics in modelling microbial communities. The self-induced mixing effectively excluded non-reciprocal cheaters from the colony, showing that strong cooperation is in itself a good strategy for cheater exclusion.

In conclusion, we have gained better understanding of species interactions in spatially structured environments. These insights will help with designing effective consortia, and help us understand how cooperative behaviour can thrive even when it can be exploited.

ACKNOWLEDGEMENTS

I often say that a PhD is more a certificate for stubbornness than it is for intelligence. This is true at the best of times, but certainly at the time I started, in May 2020. It took two years of working mostly from home and mostly alone, before I got to attend my first conference. Here I found inspiration, met interesting people, and looking back, this was the moment that the science really started for me. It taught me that, if at all possible, one should not attempt to do science alone. It is a human business after all and that is why this section is so important.

Timon, thank you for offering me this PhD position. I have been annoying you for almost a decade now, pestering you with my questions. Thank you for giving me the freedom to make my project my own, and explore my own curiosity. You have always trusted my capabilities more than I did.

Martin, thank you for your advice and mediation when it was really needed. You always look for the way forward which I appreciate.

I would also like to thank the people I worked with. **Rinke**, I approached you a couple years ago with very little idea of what it would turn into but I have so enjoyed working with you. Thank you for always showing your enthusiasm, it is contagious. **Tobias**, it was so great to have someone to high five with when experiments went well (which they did, also thanks to you (and Sagarika)).

Seraphine, thank you for hosting me in your lab for a few weeks. When I was worried that the parameter search was taking too long you assured me that it was always better to get it right. I think it was worth the wait and I appreciate your patience with me. **Juan**, thank you for showing me how you do your experiments and for answering my endless questions.

I'd like to thank my students, **Pam**, **Puck**, **Mike** and **Daniel**. For contributing to my project and teaching me a lot about teaching.

Finally, I would also like to thank the rest of the committee for taking the time to read this thesis and come up with intelligent questions about it.

Besides the people actually doing the science with me, there have been many people in my life that have made this journey much more fun and enjoyable, and who deserve a note of thanks as well.

First of all, I think it is in order to thank **Gijsje**, for putting together the best group of people. You sure have a nose for fun, quirky, and most of all, kind people. Your research group adopted me when I didn't have much of a group myself and it's the single most important reason I stuck it out in the end. So you should get some of the credits.

To my dear paranimphs, or "the Brits", as you are known as, thank you for agreeing to stand by me during my defense, it makes me feel so much better knowing I will have you guys there. Also thank you for many many movie nights and dinners and countless beers. **James**, for your wisdom and infinite kindness, for reminding us nootjes do not constitute dinner, for your curiosity and consideration for other peoples experience. **Iain**, thank you for your quiet charisma, for fact checking everything the minute it comes up, for being kind and attentive, and for teaching me obscure English words.

Thank you to the rest of the GK lab. **Marcos**, for always checking in with me and for being the kindest soul. **SaFyre**, for celebrating my "witchy vibes" before I even dared to. **Anouk**, for sharing your inside thoughts and ranting about what should've been inside thoughts from other people. **Irene**, for sharing your stories and your wisdom and for taking me out dancing. **Sonam**, for being generous with your compliments and for your attention and care for other people. **Gerard**, for making me laugh so many times and for sharing all your controversial thoughts. **Irène**, for being the life of the party. **Jeff**, for always letting me steal your fries. **Fede**, for having impeccable style. **Ivy**, for brightening up the office. **Nikki**, for your contagious laugh. **Mathilde**, for good conversation, giggles, and for confiding in me. **Bert**, for your dry humour. **Christine**, for taking us sailing.

Thank you to my theory friends: **Felix**, for endless coffee hours, for giving me great scientific advice and helping me find my feet. **George**, for sharing your coding wizardry, beers and the good colour schemes. **Hidde**, for being my office pal, where we shared many a laugh, cry (that was mostly me though), rant and whiteboard session. **Kimberly**, for showing me no field switch is too wild. **Pietro**, for being funny, charming and for doubling the group size. **Olivier**, for making sure we don't forget there's math in theoretical physics. **Ireth**, for teaching me Spanish and sharing your life lessons. **Aimee**, for sharing your wonderful artwork. **Marianne**, for helping me think strategically.

Thank you to my other scientific pals, both in Delft and beyond. **Maxim**, ms sunshine, for coffee dates and insightful conversations. **Daniel**, for your encouragement and understanding, which helped me a lot this final year, even though you're a whole ocean away. **Tanja**, for validating my feelings and sharing both frustrations and laughs. **Beatriz**, for your radiant personality and your travel tips. **Sam**, for the random, pretentiously deep conversations about everything and anything. And thank you **Ashmiani, Allard, Nynke, Marieke, Stefan, Jos, Jaïrus, Greg, Swareena, Kasper, Nils, Liedewij, Marijn, Reza, Anna, Stefan,** and many many more lovely colleagues, past and present, who make this such a fun department to do science in.

Thank you to my lovely friends. **Sara**, thank you for your loving support and for sharing your creativity and love for the world with me. **Maren**, my oldest friend, thank you for being there for me for literally my entire life already. Thank you for making me care-packages and understanding every movie reference I make.

Marre, thank you for being my friend for so long, and for always giving me the gods-honest, no bullshit, truth. **Wessel**, for being the adventurous, introspective man you are and for always being there for me when I need it. **Fiona**, for your cheerfulness and for many a GT shared. **Nienke**, for teaching me that I am not, in fact, too much. **Petra**, for all your excitement. **Nicky**, for agreeing to go on this roadtrip with me and doing all the brave things we didn't expect to do.

A huge thank you to my football team(s), **Christa, Nina, Janne, Laura, Lucie, Marre, Bonnie, Kelly, Maike, Chris, Marilse, Nienke, Anne, Manon, Kirsten, Pleuntje, Claudia, Ilse, Lea, Aster, Marijke, Janneke, Elise, Sietske, Hanna, Saimi, Alexandra** and many more amazing women that I had the good fortune of playing with over the years. Thank you for keeping me sane and energised, for all the training sessions (thank you **Nabil**!), matches, 3e helften, and for your unwavering love and support. You gave me the best send-off I could have wished for.

My dear family, thanks **mum and dad** for being proud of me even if I refused to talk about what I was doing. **Megan**, my big sis, thank you for calling me and making sure we see each other even when I prove hard to reach. Thanks **Joost** for sending me funny reels and for psychoanalysing our family members. **Arwen**, thank you for being my room mate for a bit, and for being the coolest little sister one could wish for. **Oma Chris**, thank you for passing on the genes that love science, biochemistry and flowers. And my auntie **Debby**, for giving me great advice that is unfortunately not profanity-free enough to reiterate here.

Jurriaan, even though we didn't make it to the end, you are still such a huge part of the reason I am standing here. Thank you for always believing in me, for being angry for me and for celebrating with me. You took such good care of me and I miss you always.

Lots of love,

Rachel

ANTI ACKNOWLEDGEMENTS

There have unfortunately also been people who have been less than helpful in my journey here. I wanted to acknowledge those too, because I know I am not unique in this experience.

No thank you to the physics study association that made me sing songs about how women couldn't study physics without sleeping with the professor, the day I stepped into university life. No thank you to the 5th year physics student that decided to assign me a 'stripper name' within the first minute of meeting me in the physics coffee corner in my first year. No thank you to the technician that was responsible for onboarding me on the use of the cluster in my third year who raised his eyebrows and asked me if that meant I was some sort of "computer girl". No thank you to the senior researcher that sent me utterly inappropriate texts after a conference, then proceeded to 'apologise' months later by telling me they had not been meant for me anyway so "no hard feelings remain hopefully". And no thank you to him for attending every conference I've been to since. No thank you to the people who told me that it was "surprising" that I was doing a PhD since I was a girl. No thank you to the man who mistook me for a coffee lady at a conference, and after having to correct him two times that I did not work there, responded with "you should consider it". No thank you to the researcher that asked me what I was wearing underneath my outfit during a conference. No thank you to the physicist who declared to a room full of other physicists that biologists "don't know how to design an experiment". No thank you to the people who have called me scary instead of strong and intimidating instead of intelligent. And finally, no thank you to the executive board of the TU Delft, whose knee-jerk reaction to being held up a mirror about the social safety at the university, was to sue the party holding up the mirror instead of looking at the problems they highlighted.

I wish I could tell you this has all made me stronger somehow but in reality it has only shattered my confidence. You have made me feel like I do not belong in science and I cannot forgive you for that.

- Rachel

Curriculum Vitæ

Rachel Los

20-07-1995 Born in Utrecht, Nederland.

Education

2007–2013 Herman Jordan Lyceum, Zeist

2013–2016 Bachelor of science in Nanobiology
Erasmus MC, Rotterdam & Delft University of Technology

2016–2019 Master of science in Nanobiology
Erasmus MC, Rotterdam & Delft University of Technology

2020–2024 PhD. Biophysics
Delft University of Technology
Thesis: Play nice or pay the price
Promotor: Dr. T. Idema

LIST OF PUBLICATIONS

3. **R. Los**, T. Idema, *Cooperator intermixing is an effective competitive strategy against cheaters*, in preparation.

2. **R. Los**, T. Fecker, P.A.M. van Touw, R.J. van Tatenhove-Pel, T. Idema , *Time of first contact determines cooperator success in a three-member consortium*, accepted for publication in ISME Communications.

1. J.J. Quispe Haro, F. Chen, **R. Los**, S. Shuqi, W. Sun, Y. Chen, T. Idema, S. V. Wegner, *Optogenetic Control of Bacterial Cell-Cell Adhesion Dynamics: Unraveling the Influence on Biofilm Architecture and Functionality*, Advanced Science, vol. 11, p. 2 310 079, 2024.